

# APPLIED PHYSICS REVIEWS

## Comparison of technologies for nano device prototyping with a special focus on ion beams: A review

L. Bruchhaus,<sup>1,a)</sup> P. Mazarov,<sup>1,b)</sup> L. Bischoff,<sup>2,c)</sup> J. Gierak,<sup>3,d)</sup> A. D. Wieck,<sup>4,e)</sup> and H. Hövel<sup>5,f)</sup>

<sup>1</sup>*Raith GmbH, Konrad-Adenauer-Allee 8, 44263 Dortmund, Germany*

<sup>2</sup>*Helmholtz-Zentrum Dresden-Rossendorf, Institute of Ion Beam Physics and Materials Research, Bautzner Landstrasse 400, 01328 Dresden, Germany*

<sup>3</sup>*Centre de Nanosciences et de Nanotechnologie, Route de Nozay, 91460 Marcoussis, France*

<sup>4</sup>*Angewandte Festkörperphysik, Ruhr-Universität Bochum, Universitätsstr. 150, D-44780 Bochum, Germany*

<sup>5</sup>*Fakultät für Physik/DELTA, Technische Universität Dortmund, Otto-Hahn-Str. 4, 44227 Dortmund, Germany*

(Received 22 December 2015; accepted 24 October 2016; published online 20 January 2017)

Nano device prototyping (NDP) is essential for realizing and assessing ideas as well as theories in the form of nano devices, before they can be made available in or as commercial products. In this review, application results patterned similarly to those in the semiconductor industry (for cell phone, computer processors, or memory) will be presented. For NDP, some requirements are different: thus, other technologies are employed. Currently, in NDP, for many applications direct write Gaussian vector scan electron beam lithography (EBL) is used to define the required features in organic resists on this scale. We will take a look at many application results carried out by EBL, self-organized 3D epitaxy, atomic probe microscopy (scanning tunneling microscope/atomic force microscope), and in more detail ion beam techniques. For ion beam techniques, there is a special focus on those based upon liquid metal (alloy) ion sources, as recent developments have significantly increased their applicability for NDP. *Published by AIP Publishing.* [<http://dx.doi.org/10.1063/1.4972262>]

### TABLE OF CONTENTS

I. PREFACE .....	2	F. Conclusion .....	14
II. ELECTRON BEAM LITHOGRAPHY (EBL)....	4	IV. ATOMIC PROBE MICROSCOPY (STM AND AFM) DERIVATES FOR NANO PATTERNING .....	14
A. Introduction .....	4	A. Introduction .....	14
B. History .....	4	B. History .....	14
C. Fundamentals .....	5	C. Fundamentals .....	14
1. Fundamental instrument set-up .....	5	D. Examples of applications .....	16
2. Writing strategy .....	6	E. Capabilities for nano device prototyping .....	16
3. Interaction regimes .....	7	F. Conclusion .....	17
4. Processes .....	7	V. IONS .....	17
D. Examples of applications .....	8	A. Introduction .....	17
E. Capabilities for nano device prototyping .....	8	B. History .....	17
F. Conclusion .....	9	C. Fundamentals .....	19
III. SELF-ORGANIZED 3D EPITAXY .....	9	1. Sources and instrument types .....	19
A. Introduction .....	9	2. Ion matter interaction regimes .....	21
B. History .....	10	3. Ion dose .....	23
C. Fundamentals .....	10	4. Resolution .....	24
D. Examples of applications .....	12	D. Examples of applications .....	26
E. Capabilities for nano device prototyping .....	13	1. (Single) ion implantation I .....	27
		2. Si and Au implantation II (surface functionalization/graphene nano ribbon growth) .....	27
		3. Artificial nanopores in dielectric membranes (DNA manipulation—milling of suspended thin films-surface atoms removal) .....	27
		4. Local smoothing of magnetic thin films (small single magnetic domains) .....	31

<sup>a)</sup>Author to whom correspondence should be addressed. Electronic mail: Lars.Bruchhaus@raith.de

<sup>b)</sup>Paul.Mazarov@raith.de

<sup>c)</sup>l.bischoff@hzdr.de

<sup>d)</sup>jacques.gierak@lpn.cnrs.fr

<sup>e)</sup>Andreas.Wieck@ruhr-uni-bochum.de, ResearcherID C-5129-2009, <http://orcid.org/0000-0001-9776-2922>

<sup>f)</sup>heinz.hoevel@tu-dortmund.de

5. A x-ray zone plate.....	32
E. Further exemplary applications.....	33
1. Fluidics.....	33
2. Plasmonics (surface plasmons).....	34
3. Photonics devices, larger than one field of view.....	35
4. Nanopores II.....	35
5. Magnetism II.....	36
6. FIB removal of larger amounts of material.....	36
7. Organic resist lithography (EBL resists).....	38
8. Sample surface swelling.....	39
9. Alternatives organic resist exposure and development.....	39
10. Ligand stabilized Au clusters as unconventional resist.....	40
11. Nano scale modifications of existing features.....	40
12. Implantation III.....	40
13. Surface functionalization.....	41
14. Gas assisted growth.....	41
15. Self-organization under ion irradiation.....	42
F. Capabilities for nano device prototyping.....	43
G. Conclusion.....	44
VI. SUMMARY AND OUTLOOK.....	45

## I. PREFACE

Nanotechnology is a term for analyzing or artificially creating features with at least one physical dimension below 100 nanometer (nm), which is  $1 \times 10^{-7}$  m or 10 millions of a meter<sup>1</sup> down to even the 1 Ångström ( $\text{Å} = 1 \times 10^{-10}$  m) level.<sup>2</sup> The general public can sometimes find it hard to grasp these dimensions. For purpose of “public outreach” consider the examples shown in Fig. 1 below. Fig. 1(a) shows the image of a hair from a typical human head, having a diameter of about 120 micrometers ( $\mu\text{m}$ ) (or  $120 \times 10^{-6}$  m), which is 1200 times larger than the 100 nm height of the triangular-shaped nanostructured object in Fig. 1(b). This same relative, vast difference in scale factor is depicted between the living objects of Figs. 1(c) and 1(d): A giraffe (which can be up to 6 m high<sup>3</sup>) is compared to a Lasius (or moisture ant, about 0.005 m long<sup>4</sup>).

With a resolution of 5 nm, on a 170 mm long human hair, the whole bible could be written (pages in the same quality like an A4 laser printer with 300 dpi, assuming 1000 pages)! A further possibility to visualize atomic, nano, mikro up to our makro world is shown in Fig. 1(e).

Another definition for nanotechnology “is the study of the control of matter on an atomic and molecular scale...”.<sup>8</sup> Ensembles of nanoparticles can display new and extraordinary properties,<sup>9</sup> for example, optical, electronic, and magnetic ones. They depend on the size, period, and elemental composition, which are different from bulk surfaces or discrete nanoparticles.<sup>10–14</sup> The properties are a result of interactions between the excitons, magnetic moments, and surface plasmons of individual nanoparticles<sup>10</sup> and the surface. Nevertheless, care has to be taken not all small

ensembles “... exhibit no unusual properties in the nanoparticle regime...”.<sup>15</sup>

Nanotechnology is a key enabling technology<sup>16</sup> for the following tasks: First, analyzing naturally occurring structures or features on this scale or those created artificially to verify theories, device concepts, or generate new ideas. Second, it can be employed “... to create many... new materials... with wide-ranging applications in medicine, electronics, energy production...”,<sup>8</sup> energy storage, reduction of device energy consumption or higher device speed as well as efficiency (of solar cells<sup>17</sup>), quantum mechanics, optics, or biomimetics<sup>18</sup> (or bionics<sup>19</sup>), so models can be further refined or new ones created. Third, nanotechnology can be used to further study these ideas and theories or to convert them into new devices (machines, ideas, theories...) realizing functionalities. The order of these 3 steps will vary.

In nanopatterning, there exists the differentiation between so called top-down and bottom-up approaches. Bottom-up means placing specific nano components, molecules, or atoms in desired periodicities exploiting atomic forces and growth interactions to get the desired features, without human interaction.<sup>20</sup> “Assembly of small building blocks such as atoms, molecules, and nanoparticles into macroscopic structures—that is, ‘bottom up’ assembly—is a theme that runs through chemistry, biology and material science.”<sup>21</sup> “Bacteria, macromolecules and nanoparticles can self-assemble (SA), generating ordered structures with a precision that challenges current lithographic techniques.”<sup>21</sup>

Top-down or lithography means creating features of a designed shape on the sample surface.<sup>9</sup> Some regard (lateral) pattern definition or lithography on this scale as the most crucial step.<sup>22</sup> It has to be taken into account that feature definition inside organic resists is in many process chains only one step. Especially with increasing requirements as shrinking feature sizes other process steps also can become crucial. Top-down examples are techniques like optical lithography,<sup>23,24</sup> nano imprint,<sup>25,26</sup> or electron beam lithography (EBL).<sup>22,27</sup> They employ a hardware mask/template or a software design to create features on the sample surface directly or via a transfer process. “A key difference from the bottom-up approach is that, in the top-down approach, the parts or chips are both patterned and built in place, so that no assembly step is needed”.<sup>28</sup> “Assembly of nanoparticles as a controlled fashion also provides a link between ‘top-down’ and ‘bottom-up’ strategies for the construction of functional devices as well as flexible scaffolds for the introduction of chemical functionality”.<sup>9</sup>

The scope of this review is to take a look at application results in nano device prototyping (NDP), which is similar to the feature definition in semiconductor volume production (for cell phone, computer processors, or memory). We have categorized these by different fabrication techniques and processes. Accessible feature dimensions shall be smaller than 5 nm (at least in one dimension). R&D is an abbreviation for research and development. The term device is meant literally for any kind of function (electronic, magnetic, optical devices, or surface morphologies (“tribology”<sup>29</sup>) created artificially to fulfil a task. We use prototyping to describe

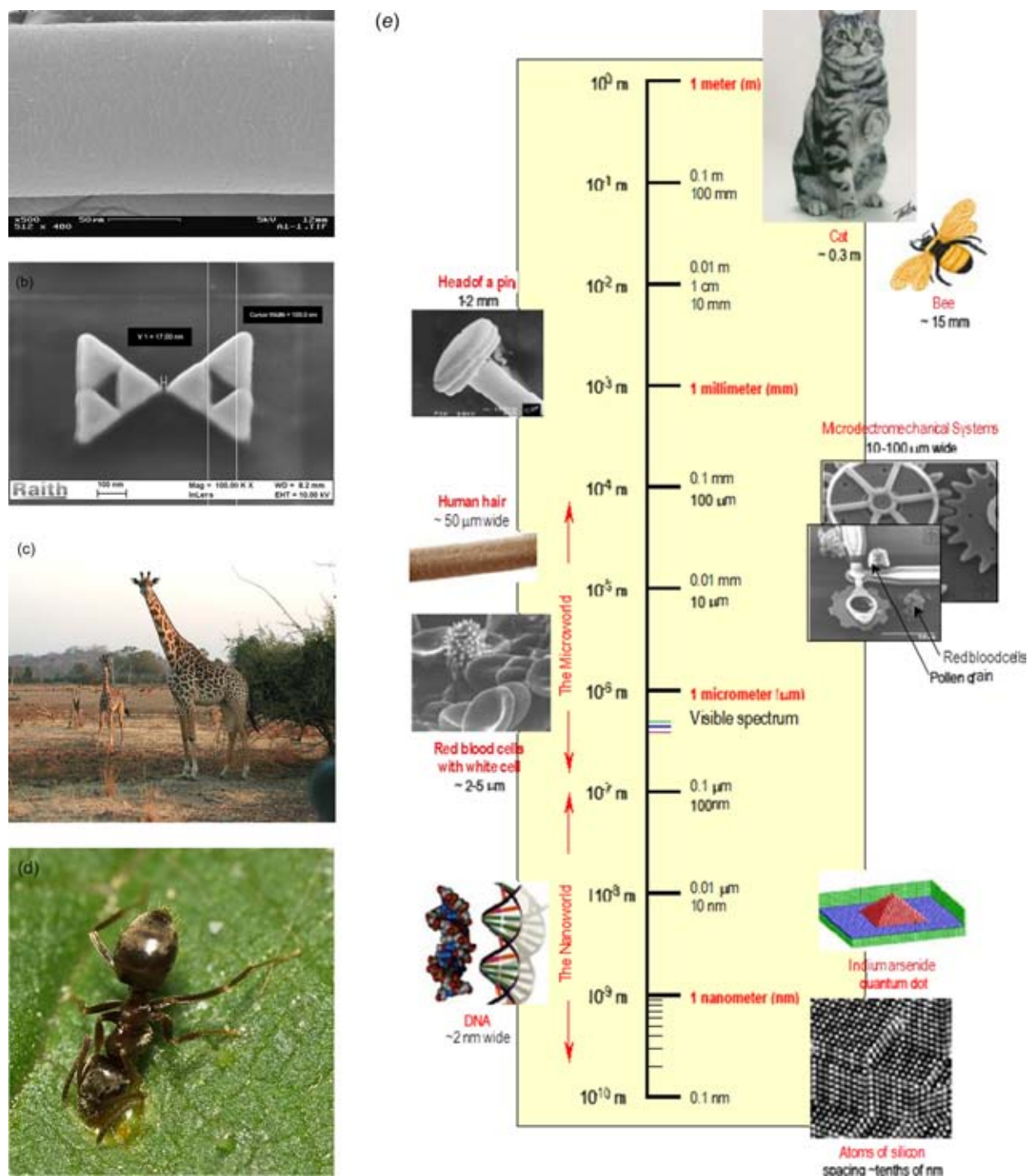


FIG. 1. (a) SEM image of a hair of head (diameter about  $120\ \mu\text{m}$ ). Reprinted with permission from Asian hair, courtesy and copyright University of Rochester/URNano.<sup>5</sup> (b) SEM image of the inner part of a fractal bow tie (about  $100\ \text{nm}$  wide, patterned by a Ga LMIS into  $5\ \text{nm}$  Cr,  $35\ \text{nm}$  Au on a  $\text{SiO}_2$  substrate). Reprinted with permission from A. Elezabi, courtesy and copyright University of Alberta and Application Lab Raith GmbH. More details of this work can be found in Section VE 2. (c) Photograph of a giraffe (height can be up to  $6\ \text{m}$ ).<sup>3</sup> Reprinted with permission from source: PD images John Walker—Images of Africa, taken from German Wikipedia. (d) Photograph of a *Lasius* (moisture ant, length up to about  $5\ \text{mm}$ ).<sup>6</sup> Reprinted with permission from GNU Free Documentation License, courtesy and copyright Sarefo Wikipedia. (e) Sketch: “from atoms, nano, mikro to the makro world,” used with permission and copyright Office of Basic Energy Sciences (BES) for the U.S. Department of Energy.<sup>7</sup>

necessary process steps between the idea and the act of characterizing or measuring the device.

The ability to fabricate tiny features often follows an analytical ability and technique to see things on this scale,<sup>30</sup> e.g., the current possibilities to resolve features on an  $\text{\AA}$  level (such as transmission electron microscopy (TEM), He ion microscopy, or atomic probe microscopy (APM, scanning

tunneling microscope (STM)/atomic force microscope (AFM)). As a result, new analysis techniques can enable next generation fabrication ones. Sometimes they evolve directly from the analysis technique. In addition, analysis and patterning interdependently influence each other. Analysis techniques can be used to (*in situ*) control the patterning or improve theories. Nevertheless, it has to be taken

into account that fabrication usually has different requirements than analysis.

Craftsmen and artists have a need for (complementary) tools as well as processes. So does applied fundamental research and nano device prototyping (NDP), especially as some fabrication processes have become quite complex.<sup>31</sup> Different technologies can be employed for arbitrary shape, high placement accuracy, or lateral nano patterning. Some are parallel (thus fast), like optical lithography<sup>23,24</sup> (routinely employed in the semiconductor industry) and nano imprint.<sup>25,26</sup> However, we think that these are not ideally suited for NDP in our definition, because of their high initial equipment, mask or template costs, the long times needed until first prototype devices are ready for measuring, and their high costs for small device (design) modifications, which belong to the prototyping phase. NDP requires flexibility and cost efficiency taking a small to mid-number of devices into account. For example, a maskless technology has no need for expensive masks/templates, as computer aided design (CAD) designs can be easily and quickly modified. These techniques are often serial (thus too slow for volume production applications), but less expensive and more flexible, so more often used in NDP environments. Some of the techniques presented here are capable of finishing the complete fabrication process in one instrument or even producing devices in only one process step.

A first example is a direct write serial focused charged particle beam technology called direct write electron beam lithography (EBL). Since decades, it is the main tool for lateral nano patterning in research and development. However, for EBL some over all process chains have become quite complex. In addition, some application related requirements are difficult to fulfil (like perfect interfacing to the substrate).

Second, we take a look at two promising additional candidates: Atomic probe microscopy (STM/AFM) based patterning techniques and self-organized 3D epitaxy.<sup>32</sup>

A third detailed example—which is the main focus of this work—is ion beam technologies (with a focus on liquid metal (alloy) ion source techniques). Already in 1959 Feynman announced this vision to use ions for nano fabrication in his talk (“There’s Plenty of Room at the Bottom,” later published in Ref. 33). About 3 years later, Newberry suggested ion beams for micro fabrication.<sup>34</sup> Recent technology breakthroughs in ion beam technologies have significantly improved their applicability for NDP. As the main focus of this review is nano device prototyping applications, further ion beam processes (also industrial ones) like circuit edit, cross sectioning, TEM lamella preparation, and analysis applications will not be discussed.

We will briefly describe historical roots for each technique and involved processes. In addition, the resulting applicability for NDP will be checked for each technology family with respect to the following criteria: the application resolution; minimum periodicities; interfacing to the surface; freedom for arbitrary geometry and shape; producing features at dedicated sample positions/locations, with a high accuracy; 3 dimensional objects; areas of coverage which exceed an instrument’s single field of view; time required to develop a new process; the process know-how accessibility

to the community (“standardization”); process and instrumentation maturity; over all time and efforts necessary to create devices which can be tested and measured (“time to device”); time required for design changes; versatility of the technology for all kinds of applications and material systems; costs from idea to device ready for testing; and the reproducibility for structuring more than a few devices up to the feasibility to run small scale production lines. Table II of Section VI attempts to group and rank these various metrics. Depending on the application, some of these capabilities are necessary during the prototyping phase, when devices and circuitry are often altered.<sup>35</sup>

If a certain application is limited by, or perhaps even impossible to achieve, using conventional processing steps, exploring non-conventional technologies with unique capabilities may be a rewarding alternative. First, we start—as a reference—with the most often applied technique: electron beam lithography (EBL).

## II. ELECTRON BEAM LITHOGRAPHY (EBL)

### A. Introduction

A technology for lateral pattern definition in nano device prototyping (NDP) is Gaussian beam vector scan<sup>36</sup> electron beam lithography (EBL) on organic resists.<sup>27,37,38</sup> Here, at least a sample preparation process step to cover the sample surface with a resist is needed, initially. Further on, a development as well as a pattern transfer process step afterwards is required. The instruments employ acceleration energies from about 20 V to 125 keV Refs. 39 and 40, respectively. Different electron/matter interaction regimes in this energy range take place and further ones could be employed for NDP. Electron beam lithography is well suited for NDP, whereas optical lithography is widely used for semiconductor devices volume production<sup>41</sup> (for cell phone, computer processors, or memory). Both possess a long history (EBL,<sup>42</sup> optical lithography<sup>43</sup>); thus, there exists dedicated instrumentation. They are currently the most commonly used top-down lateral pattern definition techniques allowing feature sizes in the regime of interest in organic resists, for the respective applications.

Now, we will take a look at the history of EBL.

### B. History

Electron beam lithography (EBL) possesses analytical roots to the scanning electron microscopes (SEM) and the transmission electron microscopes (TEM). Early focussing attempts of “cathode rays” (electrons) were carried out by Hittorf (1869) and Birkeland (1869), they applied the rotationally symmetric field lying in front of a cylindrical magnet pole for focusing the rays.<sup>44</sup> In 1924, de’ Broglie discovered the wave nature of the electron.<sup>45</sup> This has been a starting point of the scientific field of electron diffraction (later called charged particle optics, CPO). Already in 1926, Busch has been able to calculate trajectories in an electron ray bundle and found that the magnetic field of a short coil has the same effect on an electron bundle as the convex glass lens with a defined focal length on a light bundle.<sup>44,46</sup> Based

on these calculations, the first lenses have been created by Busch *et al.*, later mentioned in Ref. 44

In 1933, Ruska has managed to overcome for the first time the resolution barrier of an optical (visible light) microscope, employing electrons (magnification of 12 000 with an edge resolution of 50 nm).<sup>47</sup> Almost at the same time, a competing group at AEG research labs in Germany (Brüche, Scherzer, and Recknagel) managed to fabricate a similar electron microscope instrument. Differently to Knoll and Ruska, they have applied electrostatic lenses.<sup>46</sup> Later on, Ruska commercialized the SEM with the company Siemens. More about the history can be found in Refs. 46 and 48–50. At the end of the 1930s, technology advanced quickly due to the similar fundamental technology of electron microscopes, oscilloscopes, and television sets. In 1932, applying de Broglie's theory Knoll and Ruska estimated the resolution limit for a 75 kV electron microscope to 2.2 Å,<sup>51</sup> and this has been reached about 40 years later.<sup>44</sup> Today, leading-edge transmission electron microscopes (TEMs) employing special “correction lenses”—based upon Urban's work<sup>52,53</sup>—can resolve features below 1.6 Å with an acceleration voltage of 1 MV (Ref. 54) or 300 kV.<sup>55</sup> A comprehensive overview about the history of micro and nano patterning is given in Ref. 56.

Already in the 1930s, Carr has studied the electron recording properties of various materials. As a possible image formation process, he suggested the creation of deposited layers.<sup>57</sup> According to Schmallerberg<sup>56</sup> and Owen and Sheats,<sup>37</sup> Buck and Shoulder's paper “An approach to micro-miniature printed systems” is among the first papers suggesting an electron beam patterning process creating devices in 1958. They suggested to locally deposit the gas tetraethoxysilane as siliceous resist.<sup>58</sup> In 1967, Hatzakis and Thornley (researchers from IBM) have published the fabrication of solid state devices employing an organic resist electron beam exposure technique.<sup>59</sup> They have used a resist called poly(methyl-methacrylate) (PMMA, a thermoplastic and transparent plastic),<sup>60</sup> also known under the name of “Plexiglas.” PMMA is a high resolution organic resist which is sensitive to electron exposure and is still used by researchers today. In 1976, Broers *et al.* published remarkable 8 nm feature sizes reached by a deposition lithography process.<sup>61</sup> They deposited layers by extracting molecules from “the process” (sample handling contaminants of earlier process steps, vacuum chamber residuals, ...). Today, dedicated process gases are intentionally and controllably injected by gas injection systems.<sup>62,63</sup> Broers used the deposited layers as etch masks, so the uncovered areas could be etched away and the covered ones remained.

From the resist exposure process fundament by IBM researchers<sup>59,60,64</sup> and the various instrument development branches, electron beam resist lithography started its success story which still continues.

## C. Fundamentals

### 1. Fundamental instrument set-up

Electron beam lithography is either carried out in raster or fixed beam vector scan, variable shaped beam, projection, or mixed modes.<sup>27,36</sup> We will focus here on Gaussian beam

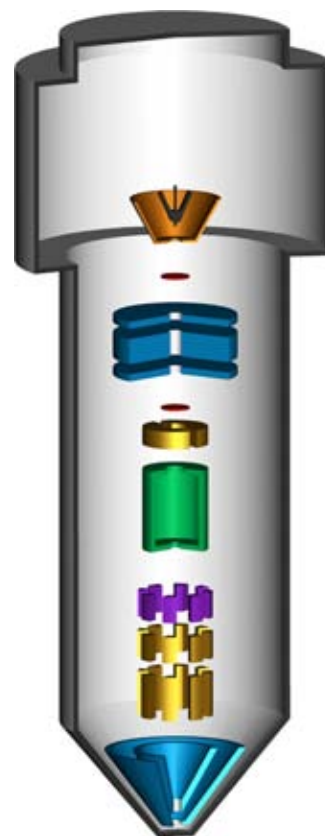


FIG. 2. Schematic of basic focused charged particle column set-up, courtesy and copyright Raith design team.

vector scan electron beam writers and their applications as they are the most commonly used ones in nano device prototyping (NDP).

Scanning electron microscopes (SEMs), focused ion beam (FIB) instruments, vector scan electron beam writers, and vector scan focused ion beam nano patterning instruments all share a similar fundamental instrument and column set-up. Depending on the application, the columns are equipped with different elements. In SEMs, lenses, deflection, and stigmation are usually carried out electromagnetically, since all electrons are indistinguishable and have thus exactly the same mass. EBL writers have usually more than 2 lenses. For ions, this is different; they consist of several isotopes and possess a non negligible energy width. As magnetic fields disperse the momentum of different particle masses, lenses, deflection, and astigmaters are purely electrostatic in FIB—columns. Displayed in Fig. 2 is an ion beam column with such electrostatic lenses, deflection, and stigmation, as all fundamental functions are represented and liquid metal (alloy) ions sources (LM(A)IS) FIBs are the main focus of this review article. A charged particle optics column is assembled on top of a vacuum chamber with, for example, electrons in normal incidence. In an EBL instrument, they are optimized for maximum instrument resolution at reasonable probe currents (<5 nm or guaranteed feature sizes below 10 nm (Refs. 65–69) and large calibrated write-fields (fields of view, deflection fields; illustrated by Fig. 3) with little beam shape and size deterioration away from the optical axis.

Electron sources are optimized for long term beam current stability and the instruments offer a selection of possible probe currents depending on the application, e.g., high resolution patterning. This is usually done with the assistance of an automated beam defining aperture exchanger, allowing us to select the suitable probe current.

The software in EBL instruments has five major tasks: first, an interface to the instrument hardware (adjust lenses, stigmator, vacuum control); second, carry out imaging of the sample surface; third, design basic features; fourth, pattern the features with a predefined dose; and fifth, program and execute complex unattended computer aided design (CAD) based patterning sequences, including the necessary machine parameter control loops (probe current, focus, dose, which were just explained above). Some have the additional capability to design and store CAD patterns. If a pattern design (CAD structure) exceeds one write-field, the instruments can stitch several write fields together. Here, the design is automatically cut into sub structures called write-fields (compare above). Then, the content of the first one will be patterned at the desired position, followed by a sample stage movement to the next position, here a second write-field will be patterned and so on,<sup>41</sup> and alternatively the stage can be moved underneath the beam during patterning. Stage position sensing is usually realized employing a laser interferometer, with high precision. Consequently, complex and unattended batch nano structuring sequences can be programmed, like patterning sequences “over night” or “over week-end;” thus, large areas with small features can be covered, well above one write-field. During the patterning sequence, different tool settings (for instance probe current and size) can be employed suiting different patterning requirements.

In addition, the high positioning reproducibility can be used for multi-level patterning on top of existing patterns, generated also by EBL or other techniques, for example, imprint or optical lithography. Here, the stage is driven to the desired

sample position and an automatic mark recognition sequence including write-field recalibration is carried out.

## 2. Writing strategy

Fixed beam vector scan instruments step the electron beam within a designed geometry employing a selectable exposure grid (step size, “s” in Fig. 3) and dwell time. Between different features, the electron beam is blanked to create well separated, defined features with incident electrons only inside the designed feature frames (for example, a square) Fig. 3 illustrates how example geometries could be written.<sup>36</sup> Here, the circles sketch the digital exposure steps; the electron beam is addressed to and waits here one dwell

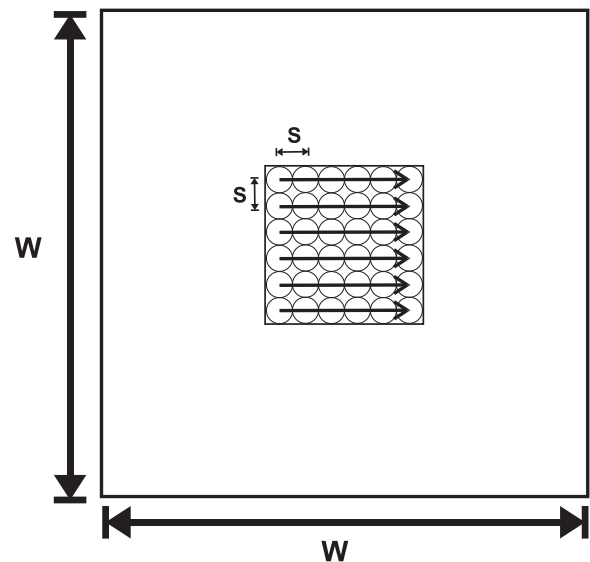


FIG. 3. Sketch of an exposure a write-field of edge length and height  $w$ , a vector scan process for a square, the circles indicate the exposure grid/step size ( $s$ ), and the lines with arrows possible exposure paths (“line mode”).

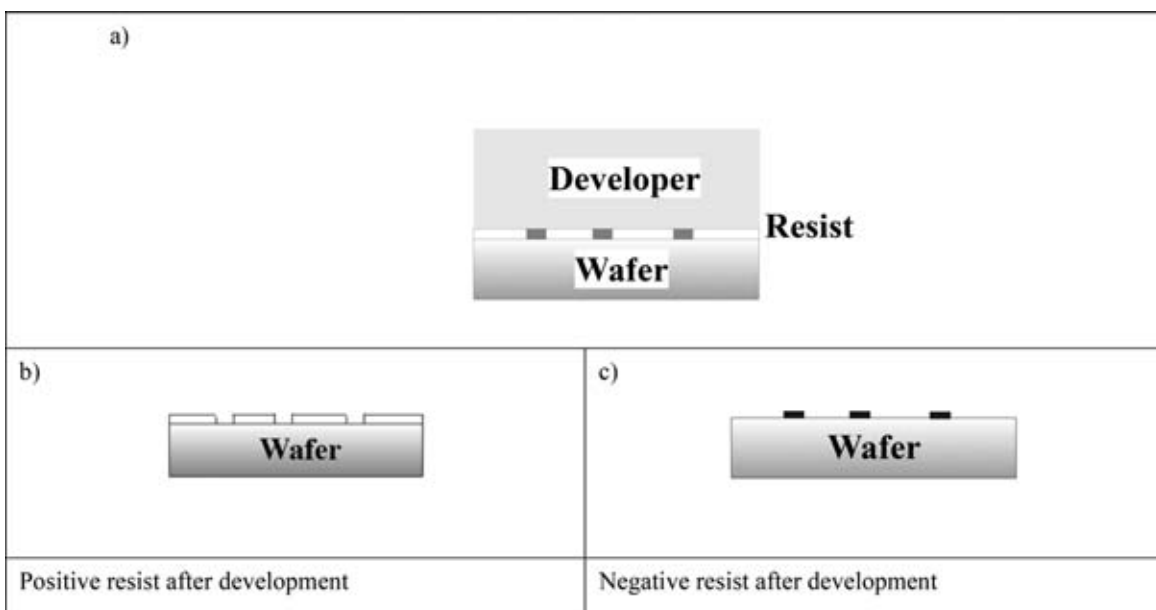


FIG. 4. Sketches (black rectangles ■ indicate irradiated regions) of (a) exposed resist, (b) diluted by the developer in the positive case, or (c) remain after developing in the negative case.<sup>74</sup>

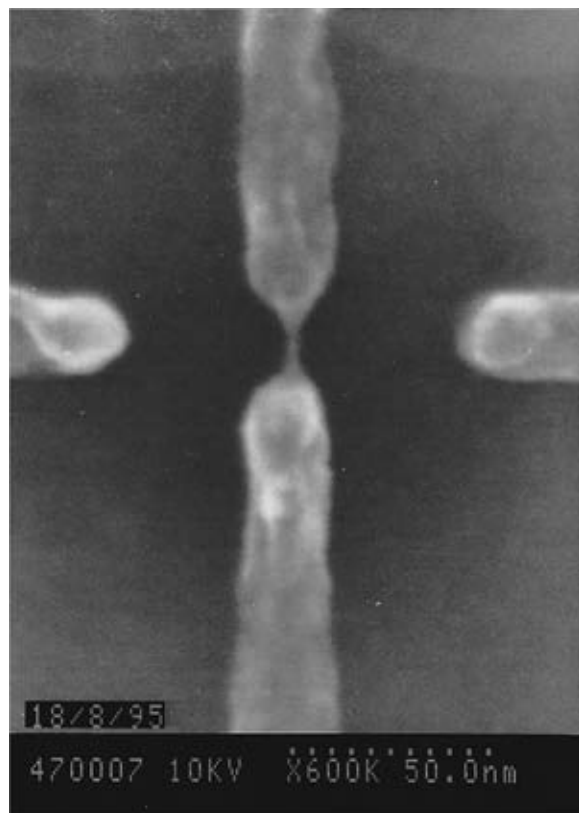


FIG. 5. SEM micrograph of a 3 nm wire close to other structures, Fig. 4 in Ref. 76, Reproduced with permission from Appl. Phys. Lett. 68, 322 (1996). Copyright 1996 American Institute of Physics.

time long, before it is deflected to the next position (usually unblanked). The arrows indicate possible paths (“line mode”) of how the electron beam could be moved along the sample surface within the designed geometry. Obviously, the beam could travel any number of different directions or employ different strategies to effectively “fill in” the geometric shapes. Usually, the stage is moved between different write-fields with the accuracy of a laser interferometer stage.

### 3. Interaction regimes

If electrons accelerated by 30 keV hit the sample surface, then they transfer a momentum of about  $9 \times 10^{-23}$  kg

m/s ( $1.027 \times 10^8$  m/s  $\times 9.1 \times 10^{-31}$  kg, relativistic corrections still being small<sup>41</sup>) and energy to it. This energy and momentum transfer results in different electron matter interaction regimes:<sup>27,70</sup> atoms can be excited, molecules break or cross link, heat can be locally generated, and the energy at the surface can be employed to cause chemical reactions between a precursor gas and the sample surface. These offer fascinating complementary possibilities.<sup>62,63</sup> A gas injection system (gas supply) intentionally injects a precursor gas for a certain time. The energy transferred by the electron beam to the sample surface initiates a chemical reaction of components of the precursor gas with the sample surface. This is, for example, exploited for industrial applications like high end mask repair for optical lithography masks.<sup>71</sup> In addition, the incident electrons can be backscattered out of the sample again.

### 4. Processes

Although different electron matter interaction regimes<sup>27</sup> are exploitable for NDP (nano device prototyping), the most commonly applied application is the exposure of organic resists. The lateral pattern definition inside the resist is followed by a development process step. In addition, sample preparation and pattern transfer technologies are required.<sup>72</sup> Here, the flux of the  $e^-$  deposits energy inside the resist. This can, on one hand, cause more resist molecules to be cut into shorter chains. This “chain scission” is the mechanism behind positive tone resist exposures, see Fig. 4(b)). The shorter molecular chains are more soluble in a developer.<sup>38,73</sup> As a result, exposed resist areas are removed during development. On the other hand, resist molecules can link to form longer molecule chains. This “cross linking” is used to define features in negative tone resists, see Fig. 4(c)),<sup>38,73</sup> rendering the exposed areas insoluble to developers, leading to a removal of the non-exposed areas during development. For some resists like PMMA, the exposure dose defines whether it behaves like a positive tone resist or negative one (in the case of PMMA, a lower dose results in positive behavior and a very large dose to a negative one).

Electron beam resist based patterning techniques possess several limitations. First, in 3D patterning, as the standard

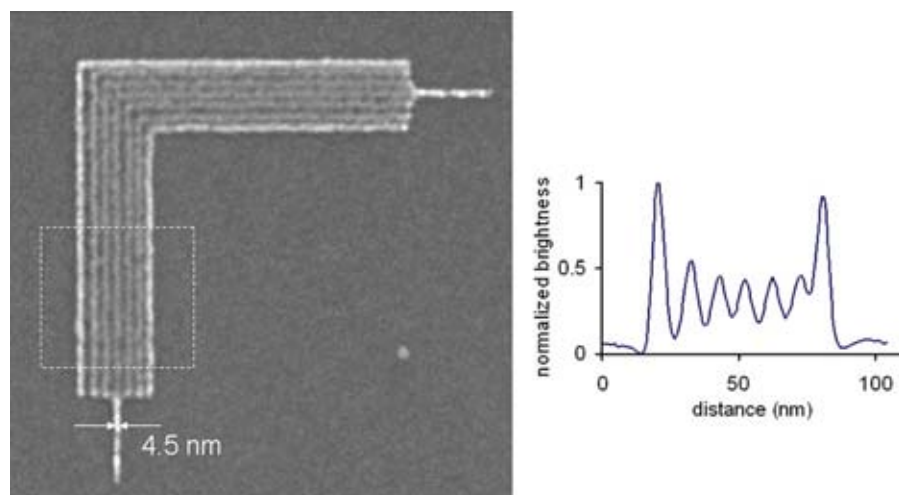


FIG. 6. SEM micrograph of 9 nm pitch structures in 10 nm thin HSQ resist, patterned at 10 kV (b) resulting brightness level averaged lines plot perpendicular to the features inside the dashed box of (a) Fig. 1 in Ref. 77. Reproduced with permission from Yang *et al.*, J. Vac. Sci. Technol. B 27, 2622 (2009). Copyright 2009 American Vacuum Society.

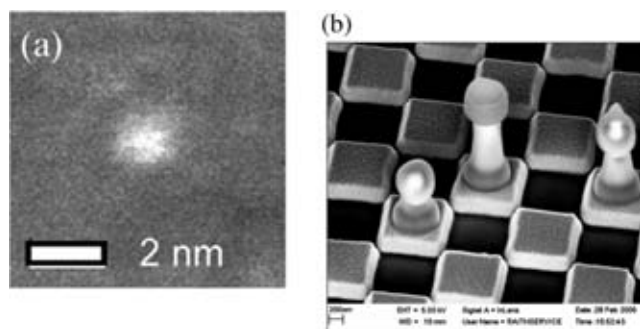


FIG. 7. (a) HAADF STEM micrograph of a dot patterned with a 0.35 nm spot size and  $W(CO)_6$  as precursor, Fig. 10 in Ref. 78. Reproduced with permission van Dorp *et al.*, *Nanotechnology* **19**, 1 (2008) Copyright 2008 IOP Publishing. All rights reserved. (b) SEM micrograph of an electron beam micromachining example employing a  $SiO_2$  precursor, deposited chess pieces on a Au/Si check board sample,<sup>79</sup> courtesy of and copyright Raith Application team.

resist exposure technique is a lateral feature definition one, so 3D patterning requires complex and dedicated processing<sup>75</sup> or exploiting a different electron matter interaction regime like electron beam deposition techniques. Second, electron sample interaction regimes lead to a relatively large interaction volume and electron backscattering, causing the so called proximity effect,<sup>37</sup> making the accurate replication of the design complicated with the necessity for a proximity correction. Third, it is usually an indirect technique with the need for pattern transfer. This can lead to multi step process chains,<sup>72</sup> depending on the application. In addition, creating interface defect free (for details, see Section III C) devices—like quantum dots—can be difficult<sup>14</sup> and it can be challenging to find an appropriate resist for the resolution level or application of interest.<sup>22</sup>

#### D. Examples of applications

First, a resist exposure example applying one of the oldest and still employed resists called PMMA in the positive mode is presented. It has been exposed by a 100 keV TEM, and pattern transfer has been carried out by a lift-off

process.<sup>76</sup> The electron beam has been blanked for a few (7–11) pixels in between the about 30 nm wire to create the necessary energy distribution inside the resist exploiting the proximity effect to reproducibly fabricate a very thin gate,<sup>76</sup> see Fig. 5.

Second, Fig. 6 shows a different example utilizing a promising, much younger, negative tone resist called hydrogen silsesquioxane (HSQ). In this case, exposure was carried out with a 10 keV electron beam. Similar feature sizes have been reached by exposing the features classically, without the blanking pixels technique described above. There they applied a special development process: 4 min in aqueous 1 wt. % NaOH, 4 wt. % NaCl.<sup>77</sup>

Third, as mentioned above electron beam induced deposition can be used as a complementary patterning technique. An exemplary high resolution result by Dorp *et al.* is displayed in Fig. 7(a). It has been created utilizing a 200 keV scanning transmission electron microscope (STEM, spot size of about 0.35 nm) with  $W(CO)_6$  as the precursor. It has been imaged within the same instrument utilizing the high angle annular dark field (HAADF) mode.<sup>78</sup> An exemplary result for direct 3D micro patterning is shown in Fig. 7(b), using a  $SiO_2$  precursor.<sup>79</sup>

Another focused electron beam-induced-deposition (FEBID) result is shown in Fig. 8: magnetic 3D structures.<sup>80</sup> In addition, it displays a sketch of the experimental configuration and magneto-optic Kerr effect (MOKE) hysteresis loops from a 3D wire.<sup>80</sup> The MOKE configuration shown in Fig. 8(g) used on a tilted nanowire (NW) as displayed in Fig. 8(e) gave evidence of a 3D magnetic functionality of the nanowire by square hysteresis loops (see Fig. 8(h)). A deformation of the nanowire by laser-heating during the MOKE experiment (Fig. 8(f)) could be reduced by focusing the laser on the nanowire base close to the substrate.<sup>80</sup>

#### E. Capabilities for nano device prototyping

Focused electron beam analysis tools can be upgraded to patterning capabilities at moderate costs, if an adequate

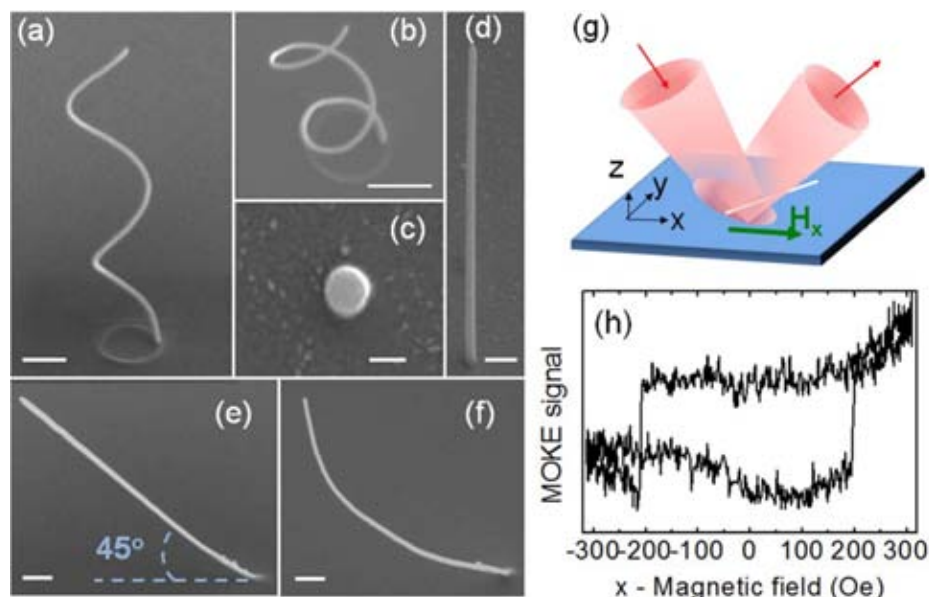


FIG. 8. “3D magnetic nanostructures grown by FEBID. (a)–(f) SEM micrographs, the scale bar is 500 nm in all images, except for (c). (a) and (b) Different views of a double-loop nanospiral. (c) Top-view of a straight NW, scale bar 100 nm. (d) and (e) Lateral view of NWs grown at 0° and 45°, respectively, to the substrate plane. (f) Curved NW after MOKE measurements. (g) Sketch of the experimental configuration used to obtain MOKE hysteresis loops of 3D-NWs at 45°. (h) Magneto-optic Kerr effect (MOKE) hysteresis loop of a 3D wire,” Fig. 1 in Ref. 80. Reproduced with permission from Fernández-Pacheco *et al.*, *Sci. Rep.* **3**, 1492 (2013). Copyright 2013 Authors, licensed under a Creative Commons.

transmission or scanning electron microscope is available in the lab. They can be used for dedicated patterning applications, for example, on the few devices, single field of view (FoV) level, without the requirement for high precision sample manipulation. Dedicated EBL writers have reached an unprecedented level of stability and maturity; thus, they are expensive.

It has to be taken into account that (electron) beam resist lithography usually covers only one process step in a device fabrication process. The developed resist pattern inside an organic resist has to be transferred, which can be challenging and time consuming depending on the application. In addition the realizability of interface defect free (for details see Section III C) features depends on the other process steps.

If the other necessary process steps are fast and only a few nano devices needed, the overall time to device can be adequate for NDP; however, EBL is a rather slow technology compared to optical projection lithography, so not suitable for volume production.

Large area patterning for prototyping applications is possible with high end instruments which offer: stability, placement accuracy, and reproducibility. As a result, features <10 nm can be patterned over large areas (>cm<sup>2</sup>) or at different dedicated sample locations. In addition, future device characteristic research can be carried out in semiconductor R&D sites, with instrument stage travel ranges of 200 mm (with 12 in. wafer handling capability) or larger.<sup>81</sup> This is in conformance with the current semiconductor fabrication process and thus gives the opportunity to partially pattern R&D wafers with this instruments and otherwise process them in the normal semiconductor production line.<sup>81</sup>

As it is a top-down lithography technique which employs SW designs (no need for masks), the features can be easily and quickly altered; however, the rest of the process to get finished devices has to be repeated. Little design modifications can only be realized expeditiously, if the rest of the process has not been changed.

EBL possesses significant advantages: its high resolution capabilities, half a century of usage and thus technology evolution with a resulting wide spread standardized process know-how, instrumentation as well as process maturity, a large technology flexibility by applying different pattern transfer techniques<sup>82</sup> and versatility for many applications, also utilizing different electron matter interaction regimes applicable to NDP. Although challenges applying EBL exist (examples given in Section II C 4), it is since decades the most commonly applied technology in nano device prototyping and for some special applications also for small scale production.

As the electron beam is a charged beam, the charge has to be removed from the sample surface, and thus charge removal is necessary either by a somehow conducting sample, by the resist surface, or by other means. Most applications and material systems can accommodate this, as many substrates are (semi) conducting and for high resolution small beam currents are required.

The techniques' capabilities for nano device prototyping will be summarized and compared with the others—covered in this article—in Table II.

## F. Conclusion

With about 50 years of instrument and process development as well as evolution,<sup>83</sup> the EBL technique and instrumentation have reached a high level of maturity (stability, pattern placement accuracy, resolution down to the sub 10 nm regime<sup>77</sup>).<sup>82</sup> As a result, the electron beam writer is the main lateral nano patterning tool in R&D and an essential part of many nano structuring activities. It is the first choice for nano device prototyping (NDP),<sup>35</sup> and for photo mask generation (however, employing usually a different type of electron beam lithography, than Gaussian beam vector scan).<sup>84</sup> These masks are necessary for optical “stepper” instruments in the semiconductor industry (for cell phone, computer processors, or memory). It is ideally suited for a large range of complex lateral batch nano patterning tasks directly from CAD designs. It is capable of delivering the necessary resolution for many applications. Electron matter interaction regimes are mostly non-destructive to inorganic sample materials. The instrumentation gives flexible process control and can be realized with a high automation level for unattended batch nanofabrication. It is possible to select from a variety of commercially available EBL equipment solutions from attachments for SEMs/TEMs to dedicated >200 mm travel range Gaussian beam vector scan electron beam writers, suitable for a large range of applications; however, these are not adequate for full 12 in. wafer exposure tasks. Challenges can occur if (pattern transfer) processes get too complicated or interface defect free features (for details, see Section III C) are required. However, it is well suited for many R&D type nano device prototyping applications, which is the scope of this article. In addition, many successfully applied processes in many different labs around the world are routinely applied; some of them with sub 5 nm resolution capabilities.<sup>77</sup>

We now take a look at applications carried out by alternative techniques, starting with self-organized 3D epitaxy.

## III. SELF-ORGANIZED 3D EPITAXY

### A. Introduction

A nano patterning technique—with fascinating potential—is a solid film crystalline growth process called self-organized 3D epitaxy. This bottom-up approach is a very efficient and parallel thus quick way of nanopatterning. Epitaxy is one important root of nanotechnology.<sup>85</sup> Epitaxy can be used to fabricate sharp monolayers—but initially it has not been used for lateral pattern definition. As a high quality layer deposition technique, it is a central part of the standard process for semiconductor device fabrication already for decades. These high quality films are employed to produce: solid state electronics, optoelectronics (light emitting diodes, LEDs), photonic devices<sup>14,86</sup> like quantum wells or lasers, discrete bipolar transistors,<sup>87</sup> high frequency transistors,<sup>20</sup> random excess memory (RAM),<sup>87</sup> candidate for metal oxide semiconductor (CMOS) ICs,<sup>87</sup> and thermoelectric modules.<sup>14,20,88</sup> “...The field spans the subnano to the macro-scale, and covers both equilibrium and far-from-equilibrium

systems with timescales that can vary from microseconds or less, to many years....”<sup>15</sup>

If certain process parameters are applied, regular three dimensional features can evolve, instead of thin films. This is called self-organized 3D epitaxy. Self-organized 3D epitaxy is a bottom up lateral pattern definition process, and thus very different from commonly applied top-down nano patterning techniques.

Thin layer creation as well as self-organized 3D epitaxy can allow the realization of dedicated, and sometimes even unique physical properties. In the last two decades, a prominent application for ordered nano structures with lattice matched growth and feature sizes smaller than 10 nm in three dimensions has evolved: The growth of interface defect free quantum dots, with many potential device applications, for example, opto electronics,<sup>89</sup> including lasers,<sup>15,90</sup> and single-electron transistors.<sup>20</sup> Quantum dots feature sizes have to be around 10 nm,<sup>14</sup> so the charge can be confined in 3 dimensions,<sup>14</sup> leading to 0-dimensional electronic systems. These can be charged via tunnel processes with a small and well defined number of electrons or holes. Thus, they are often referred to as “artificial atoms.” Here, the charge carriers occupy quantum states like in atoms, following the same Aufbau-principle in shells nominated s-, p-, d-shells and so forth.<sup>91</sup>

## B. History

This technique is a pure patterning one, without analytical roots. Early successful thin layer deposition experiments with controlled crystal growth have already been published in 1836 by Frankenheim.<sup>92</sup> He studied liquid phase epitaxy (LPE) of sodium nitrate on calcite. First, sputter metal deposits have been reported by Grove employing a glow discharge plasma in 1853.<sup>93</sup> Four years later, Faraday evaporated thin films by “...exploding fuselike metal wires in an inert atmosphere...” which is a different deposition technique.<sup>93</sup> From 1877, early applications have been to coat mirrors by sputtering.<sup>93</sup> A long time later, at the end of the 1960s, evaporation became also a wide spread deposition technique.<sup>93</sup>

In 1938, Stranski and Krastanov published a theoretical paper about seed formation and nucleation during oriented growth processes;<sup>94</sup> this is the theoretical fundament of the aforementioned self-organized 3D epitaxy. Since this time, the parallel progress in vacuum technology (surface quality), epitaxy equipment and analysis techniques (like *in situ* control of the growth process), or improved models for layer quality have

altogether contributed to today’s remarkable growth layer quality.<sup>86,93</sup> In 1952, Welker of Siemens company extended the elementary—periodic table group IV—semiconductors by compound ones from group III and V, for example, GaAs.<sup>95</sup> At that time, these have been created by melting the elements together and opened a huge application field for epitaxy. In 1970, Esaki and Tsu suggested to tailor electronic band structures by creating epitaxial layers (1D layer growth).<sup>96,97</sup> This led to the possibility of “bandgap-engineering” employing epitaxy, which is today a common way to create heterostructures, quantum wells, and quantum well lasers, pioneered by Kroemer<sup>98</sup> and Alferov.<sup>99</sup> In 1978, Störmer invented the discipline of modulation doping. Here, a heterostructure is exclusively doped in the higher band gap layer, yielding a transfer of the mobile carriers into the adjacent lower bandgap layer.<sup>100</sup> This allowed—for the first time in semiconductor history—a spatial separation of mobile carriers from their ionized (“parent”) impurities, atoms otherwise limiting the mobility by Coulomb scattering. In this way, the room temperature mobility was enhanced by typically a factor of 2 and at low temperatures, this enhancement exceeded a factor of 1000.<sup>101</sup> This opened the path to exciting research in fundamental transport physics, leading to the discovery of the integer quantum Hall effect (1980 Klitzing, initially on Si<sup>102</sup>) and the fractional quantum Hall effect (1997, by Tsui *et al.*,<sup>103</sup> as well as Laughlin<sup>104</sup>). In 1985, Goldstein had been among the first to describe growth parameters (substrate temperature, arsenic pressure, and film thickness) at the transition between 2D and 3D growth and showed examples for both. In addition, they analyzed the 3D nucleation by x-ray diffraction, STEM, and photoluminescence for 2D quantum wells and 3D clusters.<sup>105</sup> Around 1990, more and more researchers started to grow islands as a potential 3 dimensional lateral nano patterning technique.<sup>14</sup> During the last two decades, many different multidisciplinary techniques to synthesize nano particles and new materials have evolved.<sup>15</sup> In 1995, operational quantum dots have been successfully fabricated and their optical response proven by Shchukin, see Fig. 11,<sup>90,106</sup> or Ge quantum dots have been deposited by strain engineered Ge vapor phase epitaxy (VPE) on Si (001).<sup>107</sup>

## C. Fundamentals

Epitaxy is a form of controlled phase transition leading to single crystal solid layers.<sup>86,108</sup> A new crystalline phase (called “epilayer” or “crystallization interface”) is created on

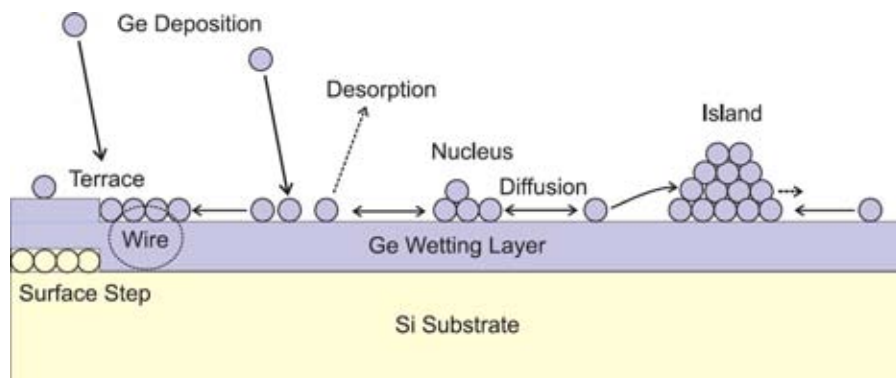


FIG. 9. Sketch of involved processes in a Ge or SiGe layer on Si MBE growth process (substrate temperatures  $T > 400^\circ\text{C}$ ), including step flow, accumulation of SiGe as wires and dots, gathering of material at steps and nucleus, Fig. 1 in Ref. 96. Reproduced with permission K. Brunner, Rep. Prog. Phys. 65, 27 (2001). Copyright 2001 IOP Publishing. All rights reserved.

top of the substrate surface.<sup>86</sup> The substrate surface serves as seed crystal.<sup>87</sup> The atoms of the next atomic layer (epilayer) adapt to the crystal structure of the surface of the substrate.<sup>86</sup> When the first monolayer is formed, atomic ordering takes place. The epilayer crystal quality normally does not exceed that of the substrate surface, often it is inferior.<sup>87</sup> However, thick buffer layers can lead to a reduction of the lattice defect density which is particularly important if there is no (nearly) lattice-matched substrate available. This is the case for GaN on sapphire, widely used in the light emitting diode industry today. Epitaxy is a surface kinetic process and depends on the structure and the chemical activity of the substrate surface.<sup>86</sup> A thermodynamic description of growth is given in Ref. 108. In general, to give a chance to find the lowest possible energy and thus build up an epitaxial layer, the mobility of the adatoms must be enhanced. For this purpose, the substrate is usually heated to temperatures between about 300 °C and 1000 °C, so, for example, the hexagonal (atomic) lattice ordering can be reached, representing the highest density packaging, depending on the material. Another way to enhance the surface mobility of the adatoms to form epitaxial layers is to shine very intensive light on the wafer instead of heating. Photons close to the visible spectral region of some eV are able to transfer enough energy to surface atoms, to move them, so adatoms find a regular lattice position. In some cases, a mass transport from the substrate to the growing epilayer takes place (“segregation”).<sup>86</sup> This is often an unintentional phenomenon, since the growth of thick buffer layers should lead to a dilution of the unintentional impurity density during growth and thus to gradually cleaner epitaxial layers. Segregated atoms have a statistical tendency to stick at hetero-interfaces. That is why, short-period superlattices (SLs) with some ten periods (like 2 nm GaAs/2 nm AlAs, for example) are often grown to filter out segregating atoms. These SLs are called “couches poubelles” (French for “garbage layers”) and often precede the growth of a thick ( $\approx 1 \mu\text{m}$ ), further cleaning buffer layer.

Assembling nanoparticles in a controlled manner by epitaxy is a kind of a link between “top-down” and “bottom up.”<sup>9</sup> “Self-assembly (SA) is the process in which a system’s components—be it molecules, polymers, colloids, or macroscopic particles—organize into ordered and/or functional structures without human interaction”<sup>109</sup> (bottom up definition can be found in the preface, Section I). “This can be referred to as guided (self-) assembly.”<sup>20</sup> This technique allows precise control of physical properties like doping profiles, tailored band gaps, conductivity, and magnetic properties. Some are different from the ones of the substrate and some cannot be created by other techniques.<sup>87</sup>

Different techniques can be applied to carry out epitaxy. They can be classified based on the involved physical or chemical processes<sup>110</sup> or other means.<sup>10</sup> An exemplary overview can be found in Refs. 108, 111 or 86. Layers can grow from amorphous solid deposits (solid phase epitaxy), liquid phases (solution, melt, liquid phase epitaxy), or vapor/gas (vapor phase epitaxy).<sup>86</sup> We will describe three sub-groups and for two of them we present examples of successfully created 3D nano features. Liquid phase epitaxy (LPE)<sup>86</sup> techniques have been employed for 3D nano feature creation. This

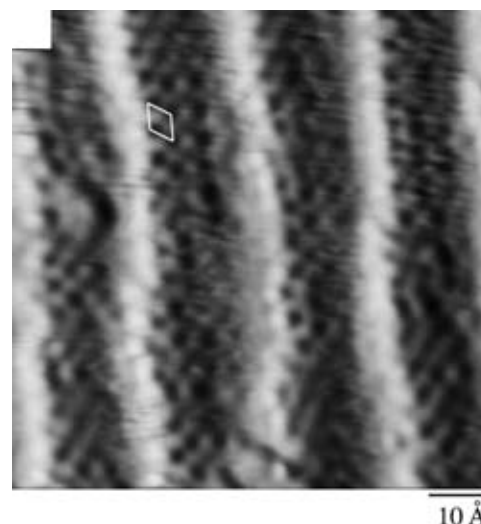


FIG. 10. “STM images recorded after deposition of 0.2 ML Ni on Pt(997) at different temperatures. Step down direction is from right to left... (c)  $T = 300 \text{ K}$ ;  $I = 0.9 \text{ nA}$ ,  $V = 24 \text{ mV}$ . The... image is displayed in  $\partial z/\partial x$  mode to enhance the contrast on the terraces. The solid line represents a  $(2 \times 2)$  unit mesh,” Fig. 1(c) in Ref. 119 (“(c)” removed). Reproduced with permission from P. Gambardella and K. Kern, *Surf. Sci. Lett.* **575**, L229 (2009). Copyright 2009 Elsevier.

is historically the first epitaxy technique and possesses a potential for low cost and large area nano patterning. In addition, colloids or dry ligands with different geometries can be added to the liquid, as a tool to influence the geometry of the resulting self-organized features. Another popular technique is called molecular beam epitaxy (MBE), which is the cleanest epitaxy technique, and two self-organized 3D epitaxy application examples are described below. MBE is not a vapor phase technique because it operates in the extreme ballistic limit. In contrast to vapor or a gas, the evaporated particles do not interact in between them. The residual gas pressure  $p$  of, for example,  $10^{-12}$  mbar yields to an mean free paths for  $\text{N}_2$  (air) of about  $l = 0.07 \text{ cm}/p(\text{mbar}) = 7 \times 10^8 \text{ m}$  for purpose of “public outreach,” which is two times longer than the distance to the moon (!) and much larger than the dimensions of the ultra high vacuum (UHV)-vessel. Of course, formally also a ballistic molecular beam could be considered as a “gas” or “vapor.” However, this ballistic beam is totally non-interacting, neither in between its own particles nor with the residual gas particles and thus not a gas in thermal equilibrium. In MBE, the source material is evaporated<sup>87</sup> in an ultra-high vacuum instrument and directed in a ballistic path to the sample surface, employing Knudson cells or electron evaporation. Today’s instruments have reached a high level of maturity. They generate thin layers of very high purity and ultra-high crystalline quality; dedicated process parameter control and in situ analysis are possible. The sample is positioned facing all cells in the working distance (WD) and in that way the epitaxial layer grows on its surface.<sup>113</sup> Examples of the mechanisms between the sample surface (Si) and the epilayer (Ge) during a MBE growth process can be as follows: material is deposited on the sample surface, nuclei are formed, islands evolve, and atoms desorb into the vacuum chamber and diffuse on the surface (as illustrated in Fig. 9).

The most applied technique in industry is MOVPE (metal organic vapor phase epitaxy) or, more generally, the MOCVD (metal organic chemical vapor deposition). It works at a slight underpressure (close to atmospheric pressure) and with a relatively high throughput of carrier gases whose molecules transport the desired atoms to the heated substrate wafer. There, the gas molecules are cracked into even more volatile fragments, leaving on the wafer the desired atoms which arrange themselves to make up the epitaxial layer. With this technique, most of the blue GaInN-LEDs are fabricated today.

Different growth types can be differentiated, three of which will be summarized here, depending on the crystal/lattice properties of the epilayer and the “crystalline phase” (substrate). First, homoepitaxy (“isochemical phases”) takes place, if the epilayer consists of the same material as the substrate,<sup>86</sup> which is the ideal epitaxial situation because there is a natural perfect lattice match. The surface adatoms fit perfectly on the substrate, making up their own crystalline lattice (for example, GaAs on GaAs). They arrange themselves with the same lattice constant on the substrate surface as the one of the substrate itself. This is then called lattice matched growth, which we call “defect free interface to the surface,” since the crystalline lattice of the host material (substrate) matches the one of the adatoms. In addition, two techniques with different chemical components from the epilayer exist:<sup>86</sup> heteroepitaxy and graphoepitaxy. Second, in heteroepitaxy, the crystal of substrate surface and the epilayer differ<sup>86</sup> and microscopic factors dominate (monoatomic steps, etc.<sup>86</sup>). Third, graphoepitaxy is based on macroscopic factors (macrosteps, macro particles, etc).<sup>86</sup> Hetero- and grapho epitaxial growth have much in common: the described effects can act simultaneously during growth and the mechanisms can have the same nature.<sup>86</sup>

Self-organized 3D epitaxy resulting in regular nano features can be realized by heteroepitaxy (strain engineering). Self-assembly in heteroepitaxial growth can evolve due to topographical conditions, stressor guidance or vertical organization,<sup>20</sup> as islands preferably nucleate at steps or on amorphous areas.<sup>86</sup> Both kinetic and thermodynamic effects can lead to ordering.<sup>86,114,115</sup>

Regular ripple formation is an effective strain relaxation mechanism.<sup>14</sup> In strain engineering, natural lattice constant differences can be exploited (for example, between Si/Ge). Strain engineering of Ge growing on Si has many advantages and the subsequent feature forming sequence can be observed within a MBE process. The process parameters (like the Ge deposition rate and/or the Si substrate temperature) can be found to generate nanostructures and to control the size and position distribution.<sup>14</sup> Alternatively, an intentionally tailored parameter (for example, employing alternating III/V semiconductor layers) can be employed for nano patterning feature growth. Possible geometries, if Ge is evaporated onto Si, are pre-pyramids, hut clusters, pyramids, domes,<sup>116</sup> and ripples.<sup>115</sup> In different material systems, 3D crystal growth has been reviewed, for example, in Ref. 10. Many applications for these epitaxial grown nano features have evolved: injection lasers (InAs/GaAs),<sup>14</sup> magnetic nano features (by evaporation from a target<sup>117</sup>), sensors (exploiting changes in the plasmonic wavelengths of metal

nanoparticles, changes in the photoluminescence of semiconductor nanoparticles, or variations in the magnetic relaxation of magnetic nanoparticles in different chemical or biological environments), nanoscale thermometers, and pH meters, summarized in Refs. 10 and 9. However, it has to be taken into account that self-organized 3D nanoparticles do not grow automatically and they require external support.<sup>15,118</sup> For example, nanoparticles are not thermodynamically stable and can disintegrate into elongated hut clusters.<sup>114</sup> Intermolecular and interparticle forces in nanoparticle assemblies are particularly complex. Because of this complexity, the processes are still not completely understood; most of the advances have been empirical. In addition, dots can, for example, have a random distribution, which is sufficient and adequate for some application.<sup>20</sup> Nevertheless, the recent advances in synthesis and characterization of nanoparticles show that more and more aspects are understood now.<sup>15</sup>

#### D. Examples of applications

During the last two decades, interesting regular nano features have been created. Three exemplary ones will be mentioned here created on vicinal substrates, by hetero or strain epitaxy employing: electron evaporation, MBE, and colloid LPE. Gambardella grew two monolayers of Ni on Pt(997), a vicinal surface of (111) terraces, resulting in an impressive period of about 2 nm ( $T = 300\text{ K}$ ;  $I = 0.9\text{ nA}$ ,  $V = 24\text{ mV}$ ), which can be seen in Fig. 10.<sup>119</sup> Vicinal steps are created by miscut and followed by an annealing process. Then, the lines are formed by step bunched factors.<sup>32</sup> “Ni was deposited by means of an e-beam evaporator. After evaporation, the sample was cooled to 77 K; all STM images have been recorded at this temperature.”<sup>119</sup>

Further periodic pattern examples from vicinal substrates are: Men *et al.* grew  $\text{CaF}_2$  on Si(111) (64 nm period);<sup>32</sup> Rohard *et al.* grew a Co nanodot array on Au(788) (3.8 nm/7.2 nm array);<sup>120</sup> and ViolBarbosa *et al.* grew Fe on “alternate parallel stripes of Cu(111) terraces and (110) oxidized facets...” (4 nm period).<sup>121</sup>

An example for the creation of pyramidal shaped quantum dots by epitaxy with a narrow size distribution is displayed in Fig. 11 (a typically dot has a size at the base of  $12 \pm 1\text{ nm}$  and a height of 4–6 nm).<sup>90</sup> A fraction of the dots could be excited by spatially and spectrally resolved cathodoluminescence, proving the operational capability.<sup>90</sup> A series of ultrasharp lines has been measured (FWHM  $< 0.15\text{ meV}$ ), each originated from a separate single InAs quantum dot.<sup>90</sup> Further examples of successful quantum dots fabrication employing MBE are Refs. 114 and 107, in addition the spin locking of electron spin coherence has been analyzed.<sup>122</sup>

Langmuir–Blodgett films are a promising LPE pattern creation technique from pre-existing nanoparticles in a solution. It possesses low cost and high throughput potential, at high resolution.<sup>10</sup> Complex regular feature geometries can be created by self-assembly from colloidal solutions from  $\text{LaF}_3$  triangular nanoplates and Au nanocrystals, an example is displayed in Fig. 12(a).<sup>21,118</sup> Another fascinating example is employing DNA as “dry ligand.”<sup>123</sup> In a dewetting process, Au nanoparticles surrounded by DNA result in regular features<sup>123</sup> here an example can be seen in Fig. 12(b).

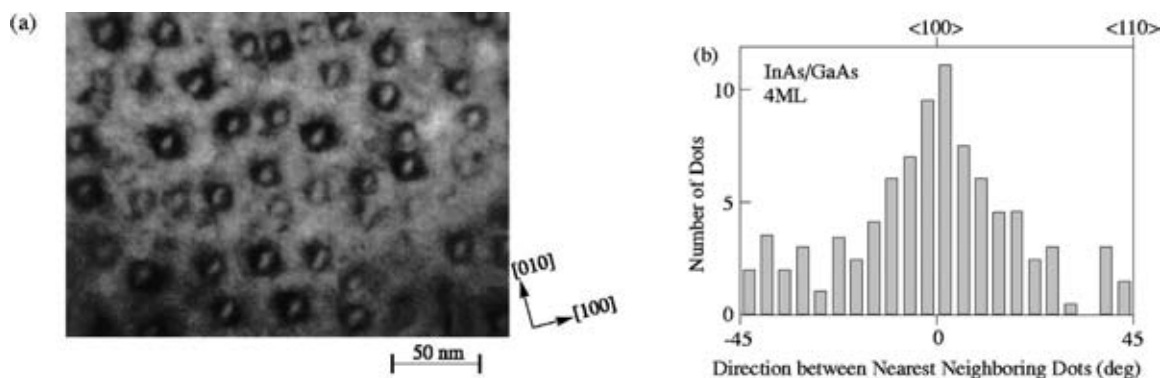


FIG. 11. 3D-MBE, “Ordering of quantum dots: (a) plan-view transmission electron microscopy (TEM) micrograph of a single sheet of InAs dots grown in molecular beam epitaxy by four-monolayer deposition of InAs. Dots are preferentially aligned in rows parallel to  $\langle 100 \rangle$ . (b) Histogram of the direction between the nearest neighboring dots,” Fig. 18 in Ref. 106. Reproduced with permission from Reuter *et al.*, *Rev. Mod. Phys.* **71**, 1125 (1999). Copyright 1999 American Physical Society.

### E. Capabilities for nano device prototyping

Self-organized 3D epitaxy is suitable for many nano patterning applications. Liquid phase derivatives allow nano feature creation at very low overall costs.<sup>21,118</sup> However, if dedicated ultra high vacuum (UHV) equipment and sophisticated *in situ* layer grow process control techniques are required, then the necessary equipment is similar in expense to dedicated electron beam lithography (EBL) writers. Initial process development time (i.e., overall time to result) as well as design modifications can be a challenge and take a long time compared to SW design based top-down techniques. Some processes have the potential to produce operating devices in one single process step.<sup>124</sup> It is a bottom-up parallel, therefore fast growth technique which can cover large areas ( $>1 \text{ cm}^2$ ).<sup>14</sup> Consider one monolayer on a 3 inch wafer with a surface of about  $180 \text{ cm}^2$ : every  $\text{cm}^2$  of almost any solid contains in its first monolayer about  $10^{15}$  atoms, which makes  $3 \times 10^{17}$  atoms on a 3 inch wafer. If we would like to position all these atoms with a speed of typically 1 atom/s,

we would need  $3 \times 10^{17}$  s (equalling about  $3.5 \times 10^{17}$  days or  $9.5 \times 10^9$  years). This demonstrates the power of massive parallel, self-organized 3D growth, in which one monolayer is epitaxially deposited in typically 1 s, thus  $3 \times 10^{17}$  faster than by direct and sequential manipulation of single atoms. It means that epitaxy is the only way to create macroscopic crystal layers in practice, taking profit of the power of self-organization. This is possible at the resolution level of interest (see for example, Fig. 12) and with the potential for interface defect free features (for details see Section III C).<sup>87</sup> In addition, 3D features with  $<10 \text{ nm}$  lateral resolution are naturally possible. Vertically even down to monolayer height control is possible, at least to the UHV growth techniques.

State of the art periodicities are possible; on vicinal substrates, periods down to 2 nm have been reached, see Fig. 10.<sup>119</sup>

However, feature placement at very specific locations with high positioning accuracy is difficult to realize on the level known from EBL writers. Self-assembly processes

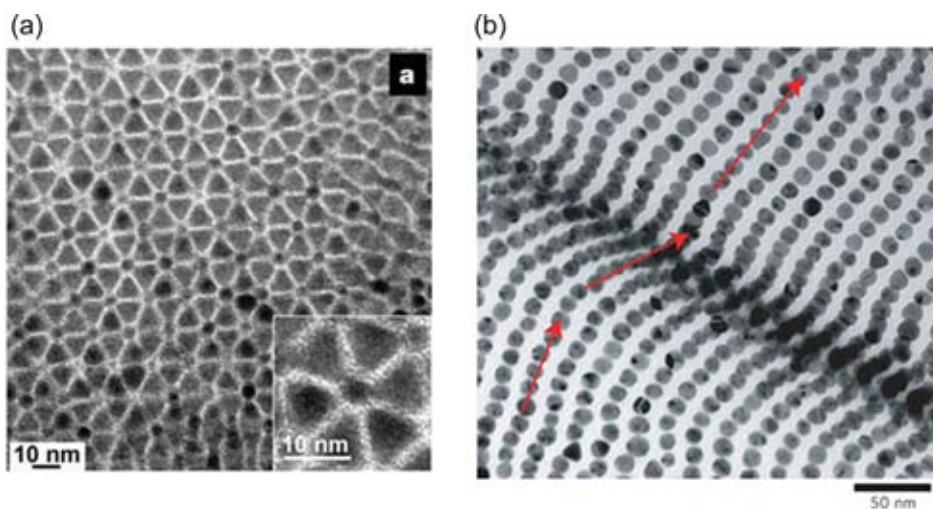


FIG. 12. (a) “TEM images and proposed unit cells of binary superlattices self-assembled from triangular nanoplates and spherical nanoparticles. Self-assembled from  $\text{LaF}_3$  triangular nanoplates (9.0 nm) and 5.0 nm Au nanoparticles.”<sup>21</sup> The structure shown is formed on a silicon oxide surface, Figure 4(a) in Ref. 21. Reprinted by permission from Shevchenko *et al.*, *Nature* **439**, 55 (2006). Copyright 2006 Macmillan Publishers Ltd. (b) “Crumpled, nanoparticle superlattice sheet. High-resolution TEM micrograph of a ridge in (a), showing that nanoparticles remain aligned even when the sheet is bent.”<sup>123</sup> Figure 3(b) in Ref. 123. Reprinted with permission from Cheng *et al.*, *Nat. Mater.* **8**, 519–525 (2009). Copyright 2009 Macmillan Publishers Ltd.

have emerged that appear capable of satisfying these needs, at least to some extent.<sup>20</sup> In addition, regular periods in one direction can be realized, an example being aligned stripe patterns<sup>125</sup> and for two different materials.<sup>21</sup> This is sufficient for many applications. There does not yet exist one single epitaxy technique for 3D nano patterning, with commonly applied recipes. Currently, there exist many different techniques—where different instruments are sometimes required. However, the large variety of epitaxy techniques leads to a large versatility but not usually in one single instrument.

Progress has been made in particle size and shape control;<sup>125</sup> however, it is still a challenge<sup>126</sup> compared to top-down techniques. Special arbitrary shapes are difficult to realize. Features grow/evolve because of the materials and process conditions (stress, kinetics), which cannot be tailored in a way as SW designs, masks or templates in top-down techniques. However, different kinds of shapes can be realized by adding adequate geometry colloids, “dry ligands” in LPE (an example is shown in Section III D, Fig. 12(b)), special sample cutting followed by annealing or by combined processes with top-down methods, such as local substrate pretreatment. These allow controlled feature placements and periodicities in the substrate plane.<sup>125</sup>

The techniques’ capabilities for nano device prototyping will be summarized and compared with the others—covered in this article—in Table II.

## F. Conclusion

“Self-assembly provides a simple and low-cost method for producing ensembles of nanoparticles in a controllable manner,...,”<sup>10</sup>; “low-cost” for some liquid vapor derivatives. The technique possesses reproducible and fast parallel large area processing capabilities. In addition, it can create features with a perfect interface to the substrate (for details, see Section III C) and tailor physical properties, some not obtainable by other techniques.<sup>87</sup> However, although better understanding of the fundamentals and tighter process control has managed to narrow the size and height distribution<sup>14</sup> results are not yet as reproducible as by conventional top-down techniques within their resolution limits. Thus, “At present,... most nanoparticle-based optoelectronic components are made with top-down nano fabrication techniques rather than bottom-up self-assembly approaches.”<sup>10</sup> For high placement accuracy, arbitrary shapes or specific periodicities top-down techniques might be more feasible.

Design modifications can take quite long. In nano device prototyping, the design has to be often altered and other techniques (with software designs) might be more suitable. However, once the process is established the same features can be reproduced over and over again easily.

Currently, self-organized 3D epitaxy is not so frequently used as nano patterning technique in nano device prototyping (NDP), except for quantum dot applications. The research is mainly focused on developing potential techniques for large area mass production applications with moderate feature uniformity and no pattern placement requirements. Self-organized 3D epitaxy is a promising technique for applications with large area but not so strict feature shape and

position requirements, like adding regular nano features to solar cells to enhance their efficiency.<sup>124,127</sup> Finally, using a combined process the sample surface can be locally functionalized or sacrificial features can be placed at dedicated sample positions, with desired periodicities and outer shapes (geometries), before the self-organized 3D epitaxy step. Then, mediated growth due to intended local surface modifications (“defects”) can take place at these locations, leading to the required results.

Next, we take a look at applications and methods carried out by atomic probe techniques.

## IV. ATOMIC PROBE MICROSCOPY (STM AND AFM) DERIVATES FOR NANO PATTERNING

### A. Introduction

Atomic probe nano feature creation<sup>2,28,128–130</sup> is a versatile nano patterning field with remarkable resolution and placement accuracy capabilities. On one hand, atomic probe patterning can be a human interaction induced bottom-up single atom manipulation or on the other hand it can be used as a top-down one like low voltage electron beam resist exposure with the apex of the tip acting as field emitter. Also mixtures of both are possible. These techniques are very different from epitaxy. They all allow, within their specific capabilities, tailoring nano feature shapes and dimensions similar to EBL by transferring SW designs onto the sample surface.

### B. History

These patterning techniques possess analytical roots. Already in 1929, an instrument called “stylus profiler” has been used to image sample surface topography.<sup>131</sup> In 1972, Young published the usage of a similar set-up. He developed it as non-contact instrument, detecting the field emission current between the tip and the sample calling this instrument the “Topographiner.”<sup>132</sup> Later on, in 1982, Binnig, Rohrer, Gerber, and Weibel published their invention the “scanning tunneling microscope” (STM). The STM can visualize atomic lattices of some conducting surfaces, in an ultra-high vacuum environment.<sup>133</sup> A few years later Binnig and Quate<sup>134</sup> have published results from a similar technology, capable of operating also on insulating surfaces at ambient conditions. It is called the atomic force microscope (AFM) and senses surface forces. Today, many derivatives exist and are employed also at ambient conditions. Then, researchers started to employ these techniques also for patterning.

### C. Fundamentals

Most atomic probe microscopy techniques are equipped with a very accurate piezo electric positioning stage which moves a tip or probe along the sample surface. These piezo crystals allow positioning down to the sub Å level and travel ranges up to about hundred μm if not combined with, for example, an encoder stage, so employing them alone larger travel ranges are not possible, like those available in EBL writers. In addition, they allow sub Å vertical positioning or sensing capabilities. The inverse piezo effect is employed for positioning (certain ceramics expand if a voltage is applied).

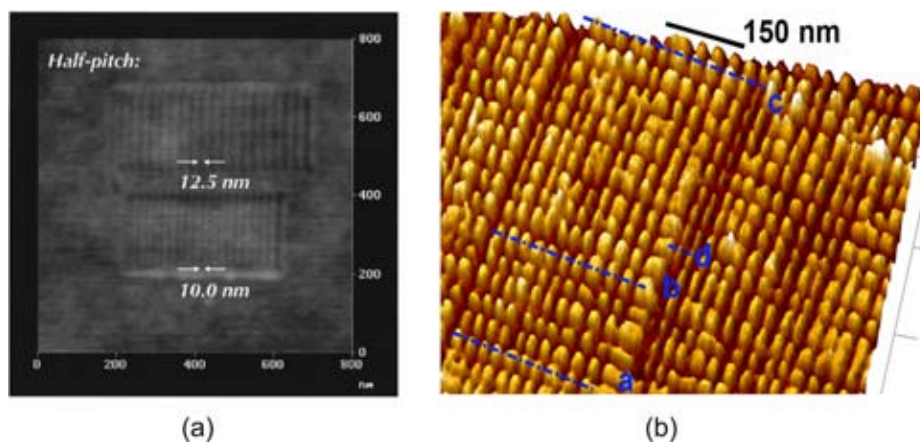


FIG. 13. (a) AFM scan of gratings written with a tungsten tip in PMMA. Grating half pitches are 12.5 and 10.0 nm in the upper and lower gratings, respectively, Fig. 7 in Ref. 142. Reproduced with permission from Cheng *et al.*, J. Vac. Sci. Technol. B **8**, 519 (2009). Copyright 2009 American Vacuum Society. (b) “AFM topography image (proving 7 nm resolution)... demonstrating the patterning of small features into 9.5 nm thick C-MC4R resist with an electrochemically etched tungsten tip,” Fig. 6 in Ref. 143. Reproduced with permission from M. Kaestner and I. W. Rangelow, J. Vac. Sci. Technol. B **29**, 06FD02 (2011). Copyright 2011 American Vacuum Society.

However, the expansion is not linear to the applied voltage; therefore, position measurement can be used to correct this.

In addition, atomic probe microscopy techniques either sense the tunneling current between the apex of the probe and the sample surface (STM) or the deflection of a cantilever (AFM) to control the tip sample distance. An AFM detects surface forces by measuring the deflection of a cantilever with a laser diode or by self-actuated piezo resistive cantilevers.<sup>135</sup> The piezo resistive method can be employed if laser alignment is difficult in the desired set-up or space is limited. In atomic force microscopy, different atomic forces are involved: long range mostly attractive van der Waals (down to about 4 Å apex sample distance), short range forces mostly repulsive (short distances <4 Å). In addition, capillarity-, Coulomb-, and further forces are involved.<sup>136</sup> Under certain conditions, it is possible to visualize surface atom lattices.<sup>137</sup> The surface force serves as feedback loop to keep the distance constant, while rastering the sample surface. Two fundamental modes are differentiated: the non-contact regime (mostly attractive forces) and the contact mode (repulsive forces). Forces (mostly repulsive) can be described by the Lennard Jones potential  $\Phi$

$$\Phi(r) = 4 \cdot \varepsilon \left( \left( \frac{\sigma}{r} \right)^{12} - \left( \frac{\sigma}{r} \right)^6 \right). \quad (1)$$

Equation (1): Lennard Jones potential  $\Phi$ ,  $r$  being the distance between the apex of the tip and the surface.<sup>138</sup>

In the STM analysis case, the tunneling current between an atomically sharp tip and a conducting sample surface is used for detecting the sample topography, often in an ultra-high vacuum (UHV) environment. The sensitivity allows resolving atomic lattices.

Today, many additional derivatives of this fundamental surface analysis methods (STM and AFM) exist: magnetic force microscopy (MFM, sensing magnetic fields); scanning near field optical microscopy (SNOM, here evanescent electromagnetic fields, often in the visible spectrum, as created by a sub-wavelength diameter probe, the transmitted or

reflected electromagnetic field can be detected); scanning thermal microscopy (SThM, the tip is either used as a nm sized resistor thermometer or thermocouple) and many other variants.

A possible classification scheme for patterning applications has been suggested by Stauffer.<sup>129</sup> It differentiates four different quantities exploitable for patterning: energy flux, forces, energy quanta, and potential barriers. These can be directly regulated by control parameters like electron/ion beam current, the applied electric fields as well as additional environmental ones like gas/fluid supply or additional external energy sources (radiation).<sup>129</sup> This large variety of possible interaction regimes and techniques results in many different exploitable processes for nano patterning.<sup>2,128,130,139–141</sup> The techniques can locally modify the sample by: exposing resists (serve as emitter<sup>2</sup>), mechanical machining, depositing, treating the sample thermally, decomposing organometallic gases,

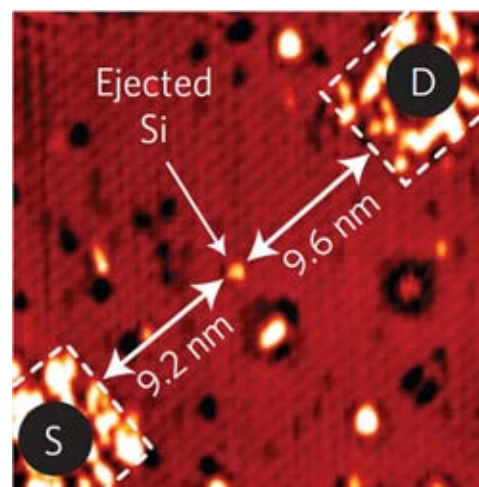


FIG. 14. “Single-atom transistor based on deterministic positioning of a phosphorus atom in epitaxial silicon.... STM image... of the inner device area..., where the central bright protrusion is the silicon atom, which is ejected when a single phosphorus atom incorporates into the surface,” Fig. 1(b) in Ref. 146. Reprinted with permission from Fuechsle *et al.*, Nat. Nanotechnol. **5**, 502–505 (2012). Copyright 2012 Macmillan Publishers Ltd.

manipulating molecules and atoms, carrying out electrochemical and photo-electrochemical processes, transferring material,<sup>140</sup> or etching with the assistance of ions and electrons.

#### D. Examples of applications

Most sub 10 nm results have been published utilizing STM or AFM so far, some exemplary results will be briefly described here. With basic environmental requirements, AFM can nanofabricate sub 10 nm features.<sup>142,143</sup> With a converted commercially available AFM,<sup>142</sup> Moon *et al.* imprinted ultra-sharp tungsten and carbon like tips into poly(methyl methacrylate, PMMA) reaching down to the sub 10 nm resolution level (an example is shown in Fig. 13(a)). Here, they worked in the repulsive (contact) mode and locally displaced the resist by applying the appropriate forces. In addition, they have suggested a nano meter precision pattern registration technique for this set-up.<sup>142,144</sup> Another group exposed a molecular resist (calixarene derivative C-Methylcalix<sup>4</sup> resorcinarene (C-MC4R, C<sub>32</sub>H<sub>32</sub>O<sub>8</sub>, Sigma-Aldrich) by the energy delivered by electrons and successfully patterned <10 nm pits, and the result is displayed in Fig. 13(b)).<sup>143</sup> They employed the following exposure parameters: tip bias voltages <20 V and a dose of 1  $\mu\text{C}/\text{cm}$ .<sup>143</sup> Further on, Wilder *et al.* have analyzed different resist exposure mechanisms taking place in EBL and atomic probe microscopy exposure.<sup>145</sup>

In a second example, a STM has been used to create single electron transistors by quantum dot fabrication,<sup>146</sup> employing hydrogen resist lithography.<sup>147–150</sup> “Patterning occurs when electrons field emitted from the probe locally desorb hydrogen, converting the surface into clean silicon.”<sup>147</sup> In this way, the source (S) and Drain (D) electrodes as well as the small dot in the center were structured, as can be seen in Fig. 14. After PH<sub>3</sub> dosing and annealing, phosphor atoms are incorporated in the surface. A single phosphorous atom in the centre shows up with the single Si atom ejected

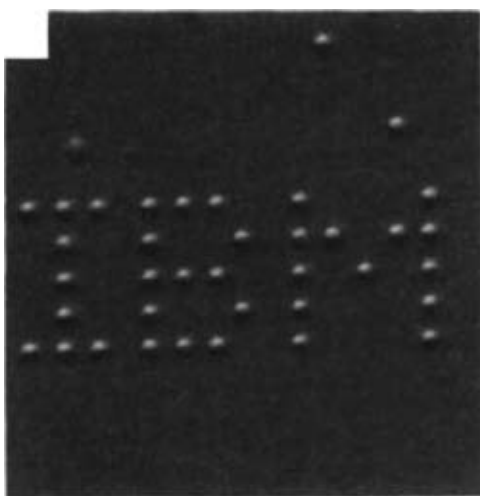


FIG. 15. STM image of individual Xe atoms on Ni (110), arranged to write “IBM,” Fig. 1(f) in Ref. 151 (“(f)” removed). Reprinted with permission from D.M. Eigler and E.K. Schweizer, Nature 344, 524 (1990). Copyright 1990 Macmillan Publishers Ltd.

in the incorporation process. Here, energy flux in the form of electrons from the tip is the exploited interaction regime.

A third example is individual atom manipulation. It has been demonstrated already in 1990 by Eigler and Schweizer.<sup>151</sup> They managed to position individual Xe atoms on a Ni surface using a STM and afterwards read out the results with the same instrument, displayed in Fig. 15.<sup>151</sup> The STM tip exchanges mainly van der Waals and electrostatic forces with the sample surface, which could also be delivered by a conducting AFM tip. These forces can be tailored by the distance and the applied voltage. The actual tunnelling current is often negligible in view of the acting forces;<sup>152</sup> it is only employed as a feedback loop to keep the distance constant. Usually, less force is needed to move an atom along a surface than to extract it from the surface.<sup>153</sup> As a result, the Xe atoms could be moved along the surface and positioned to dedicated locations. Here, manipulation forces are larger than the lateral forces of the Xe atoms to the surface.

Later on, Eigler together with Heinrich *et al.* have managed to position large assemblies of CO molecules to create operating devices. They acted as a three-input sorter that uses several AND gates and OR gates.<sup>154</sup>

Nevertheless, single atom manipulation is currently only possible in very specific material systems and mostly under UHV and cryogenic temperatures.<sup>2</sup> In another technique employing electric fields with an STM feature sizes down to the 1 nm level<sup>148</sup> can be reached at room temperature. In addition, a few nm feature sizes can be patterned with an AFM at ambient conditions,<sup>155</sup> increasing the usability of the technology family for more applications. Individual molecule placement has also been carried out in a room temperature environment.<sup>156</sup> However, the selection of the molecule is important, as the binding energy must be larger than the ambient thermal energy (“kT about 25 meV”) conditions and small enough that it can be moved.<sup>157</sup>

#### E. Capabilities for nano device prototyping

The fascinating capability of tailoring individual atoms and molecules is about the ultimate resolution and pattern placement accuracy we can think of today. Already individually, but especially in combination this resolution, pattern placement accuracy, and resulting shape tailoring capabilities are unique.<sup>2</sup>

In the case of pattern placement accuracy, for new features with respect to existing ones already on the sample, it can be realized on 3 different levels: down to the atomic level by placing an individual P dopant atom,<sup>149</sup> on the 1 nm level by an interferometric special phase imaging technique,<sup>142,144</sup> or on similar levels as accessible for EBL writer. This is possible, because the placement accuracy of the piezo positioning stage can be quite high and reproducible.<sup>158</sup> The master is usually a design in software, so modifications can be carried out quickly and at low costs, in addition the feature shape can be controlled pretty well.

For individual atom arrangement, patterning has been shown only laterally so far, as one atom thick features. 3D patterning similar to self-organized 3D epitaxy or top-down

techniques is so far only accessible to other atomic probe microscopy patterning techniques. A nano device interface to the sample surface depends on the technique, individual atom placement can create perfect interfaces (for details see Section III C), and for other AFM based techniques, a perfect interface can be difficult to realize (similar to EBL).

Many SPM techniques are available in low to mid-price regimes.<sup>2</sup> However, dedicated cryogenic UHV (STM) with patterning adequate positioning stage travel ranges and sample preparation devices are similar in expense to dedicated SEM lithography attachment solutions with laser stages or entry level EBL writers. With the large variety of different techniques and accessible interaction regimes,<sup>2</sup> atomic probe microscopy derivatives are very versatile nano patterning techniques. They can be used for many nano patterning applications. However, this is usually not possible within one single instrument. In addition, dedicated process know-how, especially of the leading edge results, is not very wide spread yet (not “standardized”) inside the community. This might be because of the existence of so many different (competing) techniques and the necessity for different instruments. As a result, it can take quite long to develop a new process for a specific application, so the initial process development time (i.e., overall time to device) depends strongly on the technique and how well the associated process is known.

Creating nano features over larger areas is not feasible employing individual SPMs (because of the limited raster/scan area).<sup>159</sup> Employing a single AFM tip, “... SPM methods are very time consuming and not suitable for large-scale assembly of nanostructures.”<sup>12</sup> The patterning speed for larger areas can be increased if it is combined with other techniques or by the idea to employ parallel techniques with more than one active tip,<sup>2,135</sup> for data storage.<sup>160</sup> Only with the parallel versions, the speed limitations can be overcome and the technology advantages kept. Thus, the technology family is currently not so well suited for setting up a R&D nano patterning production line. However, large area patterning speed contributes only partially to the overall process time in nano device prototyping (NDP) and is not required for the creation and studying of ultra-high resolution proof of concept devices.<sup>154</sup>

The techniques’ capabilities for nano device prototyping will be summarized and compared with the others—covered in this article—in Table II.

## F. Conclusion

Atomic probe microscopy derivatives are well suited for NDP, because of the combination of currently unprecedented feature shape fidelity, pattern placement accuracy, and resolution. Creating a few ultra-high resolution devices, the rather slow pattern definition step is tolerable, as the capabilities are currently not accessible via other techniques and contribute only as one part to the over-all time to device. Thus, the necessary time to result in NDP can still be quick to moderate if only the ultra-high resolution step is carried out applying one of these techniques. In addition, further non-conventional techniques exist like dip pen lithography<sup>161</sup> and further commercial developments Zyvexlabs<sup>162</sup>

and SwissLitho.<sup>163</sup> Further on, its mid-price availability of some derivatives make it accessible to many research groups.

Next, we take a look at applications and methods carried out by ions.

## V. IONS

### A. Introduction

Ion beam implantation has been for decades a crucial fabrication step in the semiconductor industry, where silicon regions are doped p-type or n-type, altering the electrical properties<sup>164</sup> to allow the manufacturing of diodes and transistors. Nano device prototyping is the scope of this review article, so this classical ion beam implantation and standard applications of point ion source instruments like circuit edit, cross sectioning, and TEM lamella preparation are not described here, examples can be found in Refs. 166–170. Already, in 1959, Feynman in his famous talk (“There is plenty of room at the bottom”) at Caltech<sup>33</sup> and 3 years later Newberry<sup>34</sup> published the ideas that ions can be used for patterning of small things. Later on, Townsend summarized its unique power to create materials “not obtainable by normal thermodynamic processes.”<sup>165</sup> Today, we know a large variety of ion matter interaction regimes, which are exploitable for nano patterning. Ion matter interaction regimes can be applied utilizing different instrument types.

Recent technology breakthroughs improving the instrument performance for focused ion beam nano patterning are:

- improved liquid metal ion source (LMIS, including beam current stability),<sup>171</sup>
- gas field ion sources (GFIS) for lateral high resolution analysis applications,<sup>172</sup>
- improved plasma sources<sup>173,174</sup>
- (single) focused ion beam implantation<sup>175–182</sup>
- dedicated nano patterning instruments based upon an electron beam writer instrument architecture<sup>41,183</sup>

We will summarize the fundamentals, explain techniques employed so far, take a look at five example applications in detail, and briefly introduce further ones, proving their applicability as complementary (lateral) nano patterning technique by different ion beam instrument types. If an application is limited by conventional processing, exploring one or the other ion matter interaction regime with unique capabilities may be a rewarding alternative.

### B. History

Ion beam technologies possess analytical roots. A few years after Ruska and Knoll (compare to EBL history in Section II B) in 1937 Müller invented the field emission microscope.<sup>184</sup> First, he had used electrons for a special kind of projection imaging of a sharp tip surface material. In 1955, he has been able to visualize individual atoms and the tip metal high index net planes by employing the “Field Ion Microscope,” with a resolution of 2.3 Å.<sup>184</sup> Drummand *et al.*<sup>185</sup> have realized a scanning ion microscope with 20 keV Ar ions focused to a 1 μm probe and a beam current density of 0.6 A/cm<sup>2</sup>. They also cut a grid to image it and

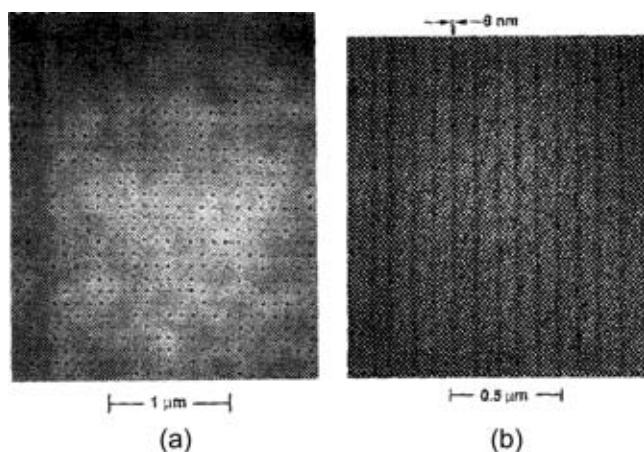


FIG. 16. SEM micrographs (a) down to 7 nm dots (in 60 nm PMMA, 50 kV Ga, 8 nm spot, 8  $\mu$ s dwell time), Fig. 6(b) in Ref. 204; (b) 8 nm thin lines (in 30 nm PMMA, 50 kV Ga, 8 nm spot,  $2.4 \times 10^{-7}$  Ga<sup>+</sup>/cm), Fig. 5(a) in Ref. 204. Both reproduced with permission from R. L. Kubena *et al.*, *J. Vac. Sci. Technol. B* 9, 3079 (1991). Copyright 1991 American Vacuum Society.

estimated the sputter rate. In addition, they have noticed that the cutting "...is considerably slower than obtainable by electron beam techniques, but the use of ions has the advantage that, for reasonable current densities, the process is non-thermal...".<sup>185</sup> However, their source technology suffered from a low beam current inside a dedicated (small) spot size; thus, the beam brightness of the available ion source has not been high enough.<sup>186–188</sup> Fifteen years later, Levi Setti published first results from a scanning transmission ion microscope using hydrogen ions from a field ionization source.<sup>189</sup> Further details about ion beam techniques and ionization processes can be found in Ref. 187. The first reported applications of ion beams for the fabrication of small things have been carried out by Kanaya *et al.* in 1965,<sup>190</sup> according to Schmollenberg.<sup>56</sup> The paper title is "Micro color recording, etching and machining by means of high voltage ion beams." They cut a 20  $\mu$ m diameter hole into a thin Ni sheet and discussed possible advantages of ion beams over electron beams due to their smaller particle wavelength and higher momentum. In the 1960s, a brighter and promising source technology called liquid metal ion source (LMIS) was starting to be used, for the historical background see for example, Refs. 41 and 191–194. It became applicable for FIB applications in the 1970s.<sup>195</sup> During the 1980 and 1990s, further groups evaluated focused ion beams employing LMIS for patterning, Massachusetts Institute of Technology (MIT, USA),<sup>196</sup> Nippon Electric Company (NEC, Japan),<sup>197</sup> and Hughes research lab (HRL, USA)<sup>198</sup> They summarized and tested various techniques and applications and reached state of the art results like those visible in Fig. 16. In 1983, LaMarche *et al.*<sup>199</sup> showed that FIB Ga implantation into Si acts as an etch-stop for an anisotropic potassium hydroxide (KOH) etching at elevated temperatures. This process has been used to fabricate sensors or MEMS (Microelectronic Micromechanic Systems) structures.<sup>180,200</sup>

At the beginning of the 1970s, Seliger and his team<sup>201,202</sup> added an "Einzel lens" to an ion implantation system. The instrument was capable to create ions by different techniques, radio frequency plasma, surface ionization, sputtering, or

electron bombardment.<sup>187</sup> They doped a Si sample by a boron focused ion beam and exposed an electron beam lithography resist (PMMA, described in the EBL fundamentals Section II C) using 60 kV He ions. The 300 keV instrument applied during these experiments is described in Ref. 187. They reported a beam diameter of about 3.5  $\mu$ m. In addition, they employed LMIS technology which showed a significantly higher beam brightness of  $3.3 \times 10^6$  A/cm<sup>2</sup>sr than the formerly used plasma ion sources (up to 100 A/cm<sup>2</sup>sr); thus, the probe current in the fine beam is significantly higher.<sup>186</sup> At about the same time, Orloff and Swanson studied a field ionization source and performed micro etching.<sup>203</sup> In 1991, Kubena *et al.* succeeded to pattern sub 10 nm features (see Fig. 16) in poly(methylmethacrylate, PMMA), an electron beam lithography organic resists (for more details see EBL history Section II B). The resist film (60 nm thin) has been patterned using an acceleration voltage of 50 kV, employing Ga LMIS technology.<sup>204</sup>

Although "...the potential elegance of the technique was clear then....,"<sup>196</sup> challenges have been encountered like:

- Organic resist related ones: discontinued lines (exposure process, shot noise, limited angular intensity LMIS.),<sup>196,204–207</sup> as well as lower penetration depth ones (of Ga ions compared to electrons) like: thick resist is only exposed at the surface<sup>82</sup> and marks are not visible for the ion beam.<sup>208</sup>
- The employed incident ions are deposited into the sample surface and might cause unwanted contaminations to the sample material system.<sup>82,209,210</sup>
- Unintended damage to the area that has been patterned, because of imaging/milling coincidence.<sup>209</sup>
- LMIS resolution degrades significantly for high beam currents<sup>211</sup>
- The lack of stability and adequate automated control and feedback mechanisms for nano patterning without user interaction even during long sequences.<sup>82</sup> For example, in 2004 Marrian has compared ultra-high resolution vector scan electron beam lithography (EBL) instruments (explained in Section II) with flexible ion/electron beam combined instruments available at that time, the conclusion has been: "...But, and perhaps most telling, the available tooling for electron beam lithography (EBL) is much more sophisticated, which is perhaps the single-most reason it is much more widely used."<sup>82</sup> "Sophisticated" with respect to (unattended) nano patterning requirements. More details can be found in Ref. 41.

Today, almost all of these challenges can be overcome by the summarized technological breakthroughs (explained in Section V A). For organic resist exposure, there exists one drawback which might limit applications: discontinuous lines (caused by shot noise or the different nature of the exposure process).<sup>207</sup> If this is limiting an application, we suggest to employ a different technique or process (examples will be given in Section V D or V E). Since pure resist exposure by ion beam lithography (IBL) is still a relatively new technique compared to the significantly longer history and experience of EBL resist processing, it will (for now) not be on equal footing especially as FIB organic resist exposure experiments have not revealed significant advantages compared to EBL, yet. Further challenges reported for organic resist exposure can also be



spread, virtual source size, angular intensity, beam brightness, source life time, source stability (last two<sup>41</sup>), and a choice between different ion species.<sup>230</sup> Especially for fine spot sizes the source emission stability is an important parameter for the usability, if more than a few nano features requiring the same dose (number of ions per pixel) shall be created. The lifetime has to exceed at least the time to carry out the patterning job. More details about ion beam generation mechanisms can be found in Refs. 187, 192, 213, and 231–235.

3. The recently commercialized ultra-high resolution ion microscope, equipped with a gas field ion source (GFIS).<sup>172,213,214,231</sup> It can become a complementary patterning technique with <1 nm potential instrument resolution capability. Early 10 nm and below patterning results in resists—used also for electron beam lithography—have been published by Sidorkin<sup>236</sup> and Winston,<sup>237</sup> exemplary results can be found in Sections VE 4 and VE 7. Gas field ion sources are based on the field ionization process. It takes place at high electric fields ( $\geq 10$  V/nm). Around 1940, Müller employed this ion generation technique in his field ion microscope<sup>184</sup> (as described in Section VB). The tip is operated in a noble gas environment applying electric extraction fields.<sup>172</sup> GFIS is capable to resolve sub nm features in imaging<sup>214</sup> and to pattern sub 5 nm minimum feature sizes.<sup>238</sup> The source possesses a small virtual source size (0.3 nm), high reduced beam brightness ( $1 \times 10^9$  A/(sr m<sup>2</sup> V)),<sup>172</sup> calculated from an angular intensity of 2.5  $\mu$ A/sr).<sup>172</sup> The energy spread was estimated to 0.25–0.5 eV.<sup>172</sup> More details about the operation principle can be found in Refs. 172, 192, and 231. Available ions for this technology are He and Ne, currently employed,<sup>239</sup> further possible ones are: H<sub>2</sub>, N<sub>2</sub>, Ar, Kr, and Xe,<sup>194</sup> as illustrated by “♥” in Fig. 17.
4. Instruments utilizing a new generation of inductively coupled plasma (ICP) ion sources,<sup>41,214,216</sup> as well as Electron Cyclotron Resonance (ECR) ion sources<sup>240</sup> have entered resolution regimes so far only accessible to LMIS, with much higher beam currents. In these ion sources, the ions are extracted through a small aperture. The virtual source size can be altered by selecting different beam defining apertures. The polarity of the emitted ions can be selected by the polarity of the extraction electrodes.<sup>231</sup> Typical parameters for Xe are a few eV energy spread,<sup>217</sup> a spot size depending on the beam current from 50 nm to about 1  $\mu$ m and a reduced beam brightness of  $10^4$  A/(sr m<sup>2</sup> V)<sup>217</sup> with mostly single charged (ionised) ions in the beam.<sup>217</sup> The described plasma ion sources are well suited for  $\mu$ m scale milling applications. With larger beam currents of more than 1  $\mu$ A Xe ions, this technique is up to 50 times faster for milling applications than liquid metal ion sources using Ga (an example application can be found in Sec. VE 6).<sup>217</sup> Available species for this technology are: inert gas ions, such as He, Ne, Ar, Xe and in addition O<sup>-</sup> or O<sub>2</sub><sup>+</sup>,<sup>194,214</sup> as illustrated by “♦” in Fig. 17. An exemplary application result is given in Section VE 6.

Instruments employing liquid metal ion sources (LMIS) are well suited for a large range of applications. Since about the 1980s, this ion source technology is dominating focused ion

beam (FIB) applications.<sup>216</sup> They are wide spread and routinely used in a large number of nanotechnology labs, mostly as two beam and columns workstations, consisting of a Ga LMIS FIB and a SEM column (the instrument description is given by type 6 below). As a result, many ion beam nano patterning experiments are currently carried out in these labs employing LMIS. From a broader point of view, we take a look at the fundamentals (applicable also to other ion instruments), necessary processes development steps and application results for different instrument types, because some promising interaction regimes currently apply different fundamental instrument set-ups (here the instrument description is given under type 1 and 2 above). With additional and beneficial capabilities some of these interaction regimes can also be tried employing point ion source technologies. Although (Ga) LMIS possesses a mid-range reduced beam brightness of  $2 \times 10^6$  A/(sr·m<sup>2</sup>·V)<sup>241</sup> and energy spread (few eV),<sup>242</sup> it is a well matured source technology<sup>214</sup> and spans a wide range of applicable beam currents [0.1 pA; 50 nA] at competitive resolution, for some applications below the 5 nm level.<sup>243</sup> Starting with their invention at the beginning of the 1960s, with its more than 50 years of evolution,<sup>83</sup> they are very well suited for high resolution patterning applications, especially with the improvements described in Ref. 171. For LMIS, a large variety of incident (process) ions are available, red marked elements in Fig. 17.<sup>194</sup> In the case of LM(A)IS instruments, three further fundamental instrument types can be differentiated:

5. Automated and dedicated ones for a single (industrial) application like mask repair or circuit edit.<sup>244</sup>
6. Versatile ones sometimes equipped with two charged particle optics (CPO) columns, one with electrons usually from the top (electrons hit the sample surface with normal incidence) and the other one with Ga ions for patterning and analysis applications, at an angle. These SEM/FIB or FIB/SEM systems are often employed for analysis, cross sectioning, or TEM lamella preparation applications<sup>166,167</sup> and can also be used for patterning, a recent overview can be found in Ref. 245.
7. A dedicated one for nano patterning (NanoFIB, LPN CNRS, Marcoussis France jointly developed within an EC growth project<sup>246</sup>). It is equipped with the improved LMIS technology mentioned above,<sup>171,194</sup> and optimized for long time (>12 h (Ref. 72)) patterning processes. In addition, it has been realized inside a lithography instrument architecture<sup>41</sup> with a sample stage controlled by a laser interferometer positioning signal, which can be employed, for write-field (for details see Sections IIC 1 and IIC 2) calibration, absolute stage positioning information and automated drift correction, using a dedicated SW. Thus, unattended batch nano fabrication jobs are possible. Patterning process reproducibility is obtained by the stable probe current<sup>171</sup> (stable dose), in combination with automatic correction and control schemes. Sub 5 nm lateral resolution patterning has been proven utilizing this instrument (this is shown in Section VD 3).<sup>247</sup> A recent overview is Ref. 218. The technology has been commercialized<sup>219</sup> and offers a choice of liquid metal alloy ion sources. An ExB filter is available.<sup>248</sup> In addition,

processes can be catalysed by inserting gases into the process chamber<sup>62,63</sup> or an annealing process can be added. All this can be selected from a large variety of ion matter interaction regime processes. Thus, desired interaction volumes and ion matter interaction regimes fitting the application and material system (fundamentals described in Section VC 2) can be selected by the incident ion types, cluster types, and charge states of the particles. Both will be further explained in the following section.

## 2. Ion matter interaction regimes

Ga ions accelerated by 30 keV hitting the sample surface transfer a momentum of about  $3 \times 10^{-20}$  kg m/s ( $1.16 \times 10^{-25}$  kg, resulting speed 288 km/s, i.e., non relativistic<sup>41</sup>). In addition, they hit the sample surface with a higher energy density<sup>249</sup> than electrons of the same energy. As a result, (Ga) ions offer a large variety of ion matter interaction regimes, which are accessible to ion beam processing (analysis and patterning), thus also to vector scan point ion instruments. For Ga<sup>+</sup> (and ions of a similar mass), a so called linear cascade regime has been defined (accessed by acceleration voltages from 5 to 50 kV);<sup>228</sup> the majority of the available Ga FIB instruments inside nano patterning labs operate in this regime. As a result, many researchers have access to them and carry out nano patterning experiments with them. Ga possesses a low melting temperature (303.05 K which is equivalent to 29.9 °C) and—depending on purity and environmental conditions—a large undercooling behavior down to about  $-8$  °C.<sup>250</sup> As a result, it is liquid at room temperature inside the instrument and can emit<sup>251</sup> if heated before. During operation no steady heating is required. In addition, Ga LMIS produces mainly single charged ions (>99%).<sup>193,252</sup> This means that each ion carries the elementary charge of  $1.6 \times 10^{-19}$  As (or Coulomb).

Interaction mechanisms—as a first approximation<sup>253</sup>—can be analyzed separately, as elastic (nuclear) and inelastic (electronic) interactions, because of the large mass difference between the incident ions or surface atoms with respect to electrons<sup>227</sup> and the resulting different response times to impacting ions.<sup>254</sup> Ions interacting with other atoms cause elastic and nuclear interactions often referred to as radiation “damage.”<sup>227,228</sup> Following Townsend, we will employ the term radiation interaction instead; “One should repeat that the prejudice invoked by the words damage or defects is unfortunate since the changes in structure produced by the passage of fast ions enables us to make materials which were not obtainable by normal thermodynamic processes. It is also true that the “damaged” material may have superior properties to the original solid.”<sup>165</sup>

Incident ions transfer momentum to target surface atoms and loose initial kinetic energy until they come to rest, within the so called collision cascade region<sup>228</sup> or interaction volume. The interactions with the surface depend, for example, on the acceleration energy, mass of the incident particle, and mass of the substrate. Most theoretical work has been carried out so far for Ga<sup>+</sup> as these are most commonly used; if light incident ions like He, Ne, or

Si are employed, the interactions are significantly different. For example, lighter ions like Si would result in an interaction volume significantly larger than that of Ga<sup>+</sup> ions, but still significantly smaller than electrons. Employing an instrument with an ExB filter, ions with different charges can be separated, so, for example, Si<sup>++</sup> ions will be accelerated faster than Si<sup>+</sup> ions employing the same acceleration voltage (in the same instrument), thus resulting in an even larger interaction volume.

The extension of ion matter interaction regimes, called collision cascade region, can be modelled by Monte Carlo computer programs like “SRIM” (The stopping and range of ions in matter) by Ziegler *et al.*,<sup>254,255</sup> which simulates statistical interaction events. SRIM takes direction changes due to binary collisions into account together with nuclear and electronic energy loss. If the energy deposit into the target is small enough, Monte Carlo simulations predict experimental results quite well.<sup>227</sup> In SRIM, only amorphous substrates are taken into account, so an effect like channeling is neglected. Exemplary interaction volumes for 40 keV Ga<sup>+</sup> ions impacting into an amorphous silicon substrate have been simulated by SRIM as well as for electrons by Casino (details about the Casino SW can be found here<sup>41</sup>). For 40 keV kinetic energy, the interaction volumes have been simulated:

The SRIM simulation results of primary Ga ions are displayed in Fig. 18(a); they induce radiation interactions in the range of a few tens of nanometers in 3 dimensions (approximated by an ellipse with  $a = 44$  nm (about  $8 \mu\text{m}$  for electrons) and  $b = 48$  nm (about  $6 \mu\text{m}$  for electrons). The interaction volume is  $3.9 \times 10^{-22}$  m<sup>3</sup> or  $0.00039 \mu\text{m}^3$  (without backscattering and collision cascade effects, which would enlarge the interaction volume for Ga ions). Further interaction volumes for different atom and ion species can be found in Refs. 256, 229, and 230. For electrons, the interaction extension for all three dimensions is each about two orders of magnitude larger than for Ga ions. Although the interaction volume is much larger than for ions, the surface imaging or pattern definition resolution can be higher than for ions. This can be estimated from the high particle density entrance channel in Fig. 18(b) near the surface (at the top).

Ion interaction regimes with electrons of the target atoms are called inelastic or electronic interactions (see for example, Refs. 226–228). This process can be regarded as a continuous viscous drag between the incident ions and the sea of electrons.<sup>226</sup> The nuclear contribution usually dominates the stopping power<sup>226</sup> in the linear cascade regime. At higher ion acceleration voltages, the electronic stopping power increases too and is usually observed at energies of several hundred keV. In addition, channeling can occur,<sup>228</sup> it describes incident ions travelling along a low particle density trajectory inside a sample crystal lattice. Here, ion interaction regimes with the surface atoms are the same as in the non-channeling case, at sub surface crystal layers they have less interactions with the crystal and thus travel longer.

Possible interaction regimes are visualized in Fig. 19. Incident ions can interact as described above with the surface atoms and electrons as well as groups of surface atoms (molecules). In addition, they can participate in chemical

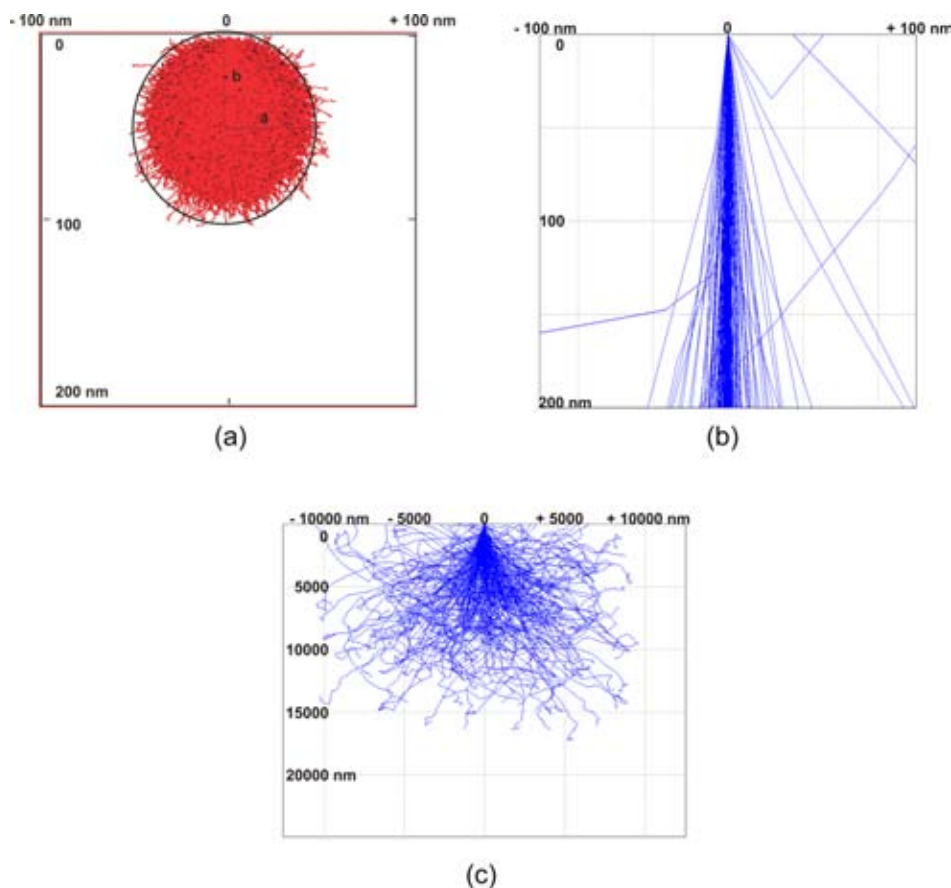


FIG. 18. (a) Ga ions simulated interaction volume (40 kV, Si sample, SRIM, 1 000 000 trajectories), (b) electrons upper part, same scale as for the Ga ions (40 kV, Si sample, Casino, 1000 electrons, 200 displayed), and (c) complete interaction volume for electrons (40 kV, Si sample, Casino, 1000 electrons, 200 displayed); for details, see Ref. 41.

reactions with either surface atoms or precursor gas molecules.<sup>62,63,257</sup> Table I gives an overview about matter interaction regimes for ions and electrons.

The interaction regime called atom intermixing or chemical alloying is mentioned in Table I and illustrated by “Table II” in Fig. 19. It can place atoms from a layer below a thin surface layer into the latter. This atom transport from a lower substrate layer into the thin surface layer takes place at the interface between them.<sup>212,226</sup> This effect can be exploited as complementary patterning/implantation processes. First, to achieve a larger concentration of impurity atoms in a thin surface layer than possible by direct implantation, which is limited by the steady state condition.<sup>226</sup> Second, thin magnetic films can be locally separated by the formation of domain walls already at a low ion dose and with high resolution capabilities (an example is given in Section VD4).

Interactions between incident ions and inorganic materials like milling (or sputtering), ion implantation, and thin layer atom intermixing have been successfully applied for nanopatterning (here application examples are described in Sections VD and VE). In addition, organic resist exposure has been studied already from the very beginning (as explained in the history Section VB); however, the definite exposure process is not completely understood yet.<sup>207</sup> Further routinely employed techniques are employing additional process gases. They can be initiated into the vacuum chambers resulting in many additional capabilities; a comprehensive overview about precursor gases for deposition and etching with focused ion and electron

beams is given in Refs. 62 and 63. The gas can interact directly with the incident ions and the sample surface (initiate gas assisted processes by the incident energy), both listed in Table I.

In addition to the ion matter interaction regimes described in Table I another fascinating mixed ion matter effect exists. It is initiated by broad ion sources (type 1 in Section VC1) with large beam currents eroding a surface area in a way that self-organized regular nano structures evolve<sup>227</sup> (an application example is given in Section VE15). These 3D nano features arise, on amorphous semiconductor surfaces and can be explained by similar processes on metal surfaces: “...in metals, the surface curvature dependence of the sputtering yield and the presence of an extra energy barrier whenever diffusing adatoms try to descend step edges, produce a similar surface instability, which builds up regular patterns.”<sup>89</sup> In addition, rapid amorphization (surface diffusion<sup>159</sup>), mass redistribution, and modifications to the surface curvature contribute.<sup>258</sup> The feature size can be influenced, for example, by the acceleration energy<sup>259</sup> and angle of incidence. Here, different areas (different components) of the surface are milled with different speeds. Further details can be found in Refs. 260, 228, 227, and 261. Although the large variety of ion-matter interaction regimes opens fascinating patterning opportunities and Seliger has proven the practical feasibility of resist exposure already in 1973,<sup>201,202</sup> still only two  $\text{Ga}^+$  ion matter interaction regimes are routinely employed: milling and gas assisted processing.

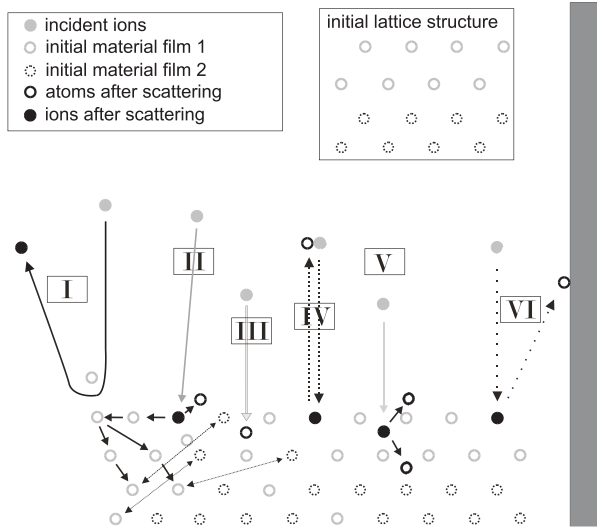


FIG. 19. Overview of exemplary ion matter interaction regimes. Incident ions are: (I) backscattered, (II) implanted at lattice sites (and cause further interaction regimes like atom intermixing with a 2nd material layer), (III) implanted at interstitial sites and come to a rest, (IV) target atoms are milled out of the sample, (V) implanted at interstitial sites, influencing the original crystal structure, and (VI) target atoms are milled out of the sample and redeposit at a surface in the vicinity. From Ref. 41, modified.

In the next section, another important parameter that can influence ion matter interaction regimes and interaction volumes will be briefly described.

### 3. Ion dose

Together with other research groups, we explore non-conventional patterning applications. Especially for these applications the dose plays a significant role. In addition to varying the incident ion species and acceleration energy, the dose is another parameter that can be used to alter ion matter interaction regime (results) and interaction volumes. Dose is the quantity of particles absorbed by a medium within a certain area.<sup>228</sup> Dose is proportional to the probe current ( $I_p$ ) and point dwell time ( $T_D$ ) and inversely proportional to the square

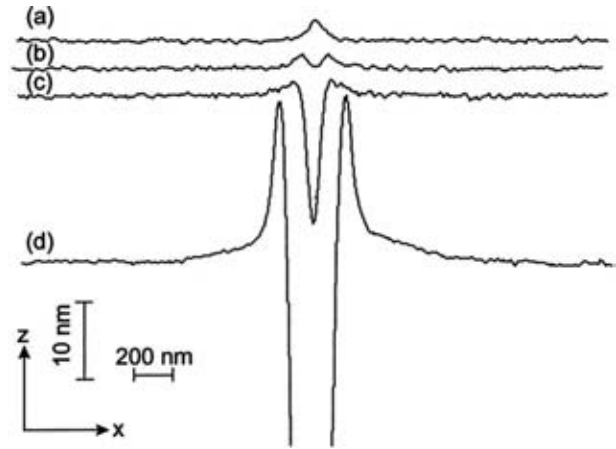


FIG. 20. Left: Cross sections of a Si (100) surface applying different doses ( $50\text{ keV Ga}^+$  ions) (a)  $1.3 \times 10^{15}$ , (b)  $8.6 \times 10^{15}$ , (c)  $8.6 \times 10^{16}$ , and (d)  $1.7 \times 10^{19}$ , Fig. 1 from Ref. 262. Reproduced with permission from B. Basnar *et al.*, *J. Vac. Sci. Technol. B* **21**, 927 (2003). Copyright 2003 American Vacuum Society. Right: definition of dose regimes following Ref. 183.

of the “step size” (as illustrated by Equation (2)). Depending on the process, a definition of area or line dose is used.

$$D = \frac{I_p \cdot T_D}{s^2}, \quad D_L = \frac{I_p \cdot T_D}{s}. \quad (2)$$

Equation (2): Area and line dose.  $D$  is the area dose,  $D_L$  is the line dose,  $I_p$  is the probe current,  $T_D$  is the point dwell time (time the beam rests at a point of the discrete patterning grid), and  $s$  is the distance between two points in the discrete patterning grid (“(exposure) step size”).

Fig. 20 shows experimental cross sectional AFM results from different ion doses irradiated onto silicon (100) wafer surfaces; surface bumps and milling are visible, due to local amorphisation and surface modifications.<sup>262</sup>

The ion dose can be classified into three regimes: low/medium/large (for  $\text{Ga}^+$  ions in the linear cascade regime), causing different surface effects,<sup>253</sup> which can be exploited for different applications (implantation, amorphisation, and milling).

TABLE I.  $\text{Ga}^+$  and electron matter interaction regimes (Roman numerals, refer to those in Fig. 19). Adapted from Ref. 41

$\text{Ga}^+$ ions can	Electrons can
Cut/crosslink organic molecules	Cut/crosslink organic molecules
Excite atoms	Excite atoms
Generate heat	Generate heat
Be backscattered (these become charge neutralized at the surface, becoming an atom, and get re-ionized leaving the surface again, making them the same as the incident ions) (I)	Be backscattered
Initiate gas assisted processes	Initiate gas assisted processes
Participate in gas assisted processes	...
Implant at interstitial (III, V) or lattice places (II, IV, VI) in crystalline or into amorphous surfaces (get charge neutralized at the surface, thus become atoms)	...
Cause surface modifications, move surface atoms to other positions (II, V), these can also be ones from a buried layer below, which can then intermix with ones in a thin surface layer, giving access to unique concentration profiles	...
Remove surface atoms (“milling”), these atoms can either “redeposit” (VI) at surfaces in the vicinity or escape into the vacuum chamber (IV)	...

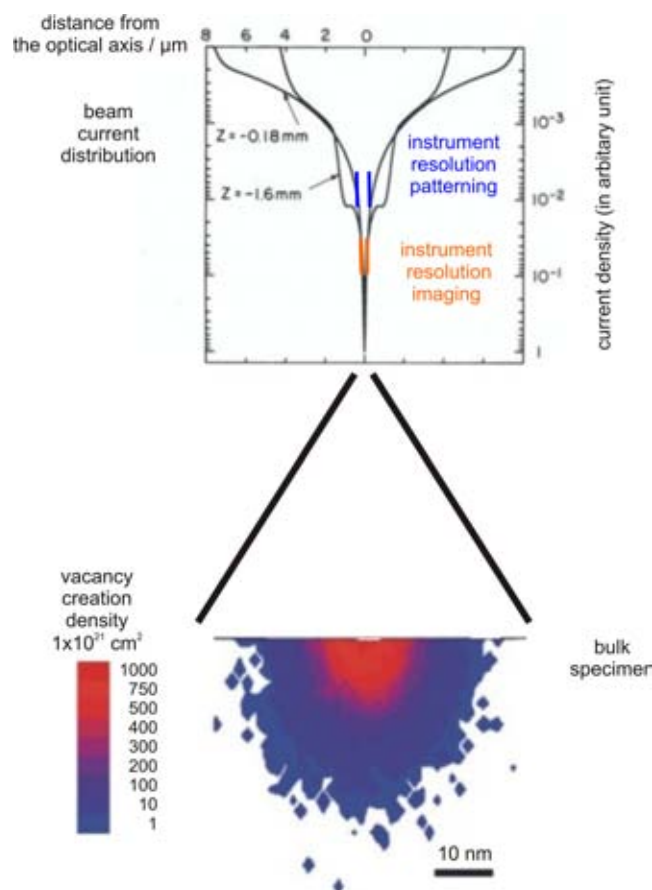


FIG. 21. Combining a modified calculated beam current distribution plot for two objective lens excitations ( $Z = -0.18$  and  $Z = -1.6$ ), with suggested possible patterning and imaging resolutions for certain applications and material systems modified Fig. 2 in Ref. 252. Reproduced with permission from J. Orloff *et al.*, *J. Vac. Sci Technol. B* **9**, 2609 (1991). Copyright 1991 American Vacuum Society with a modified TRIM simulation of the energy deposited by the ion beam and the collision cascades of a 35 keV Ga beam with a bulk target showing the damage localization, Fig. 3(a) in Ref. 243 (modified). Reproduced with permission from J. Gierak *et al.*, *Ultramicroscopy* **109**, 457 (2009). Copyright 2009 Elsevier.

In the low ion dose regime ( $10^{11}$ – $10^{15}$  ions/cm<sup>2</sup>), the surface damage generation dominates. The crystal to amorphous transition is initiated at the surface (few monolayers); the global crystallographic order of some materials (metals, metal alloys, and oxides) will not be modified. Stress is accumulated and afterwards relaxation occurs, resulting in “bumps.” If ions hit solids with covalent bonds, the surface phase can be rendered locally into the amorphous phase and if they hit amorphous oxide surfaces they may become locally crystalline.<sup>253</sup> The depth concentration profile of implanted ions can be characterized by a Gaussian distribution around the projected range  $R_p$ .<sup>226</sup> Significant milling does not take place in this dose regime, but other effects like atomic lattice modification, atom mixing, phase transitions, surface cleaning,... occur.

Fig. 20 illustrates that in the medium ion dose regime (intermediate,  $10^{15}$ – $10^{17}$  ions/cm<sup>2</sup>) milling effects progressively take place, “volcano crater shape” features evolve. If the dose is further increased, multi-dimensional atomic lattice modifications and complex configurations can be generated.<sup>228</sup>

The high dose regime ( $>10^{17}$  ions/cm<sup>2</sup>) milling and redeposition of sputtered material effects are dominant; thus,

material ejection is limited and also the aspect ratio for a small hole. It is usually applied for material removal applications; however, the other effects are still present. Milling effects in the linear cascade and the high dose regime can be modelled with the linear cascade model and the binary collision approximations.<sup>254</sup> It is a quite well understood and studied regime, because of the commercial interest of the semiconductor industry, for applications like circuit edit.<sup>244</sup> However, the medium and low-dose regime has so far been relatively little studied and applied for patterning applications.

In Sec. VC4, we take a look at different concepts for resolution.

#### 4. Resolution

Resolution can describe, on one hand, the minimum distance between two objects in analysis or imaging, which can still be differentiated.<sup>263</sup> On the other hand, in fabrication other concepts are more adequate like the minimum distance (period) between two artificially created objects or the smallest feature size, which can be intendedly created. The smaller the resolvable features or periods are, the higher the resolution.

In the fields of charged particle optics and ion matter interaction regimes, some aspects of resolution can be modelled, resulting in numbers for the beam diameter, current distribution, or lateral scattering (primary and collision cascade effects).

Four different inter-related fundamental resolution concepts can be differentiated: beam diameter (instrument resolution), beam profile (current distribution), interaction volume (collision cascade regimes), and application resolution.

A first resolution concept, the instrument resolution, can be simulated (beam diameter calculations: finite elements methods, trajectories analysis, Barth Kruit formula,<sup>264</sup> wave optics,...) based upon charged particle optics (CPO) theory.<sup>46,49,265–267</sup> At the beginning of this field first analytical and nowadays numerical models have been developed based upon experimental verifications.<sup>265</sup> The value for the beam diameter is often advertised by instrument manufacturers and proven on special selected and ideal samples. Today’s point liquid metal ion source (LMIS) optical systems are mainly limited by spherical and chromatic aberrations<sup>260</sup> as well as charge effects.<sup>261</sup> Which one of these actually dominates depends on the “column operation mode.”<sup>193</sup> For patterning applications with large write-fields, aberrations due to the deflection of the beam away from the optical axis have also to be taken into account.

A second resolution concept is called ion trajectories or beam current distribution. It is also studied in the field of CPO theory which allows us, for example, to simulate the beam diameter in the surface plane.<sup>252,264</sup> The ion trajectories, the current distribution and the beam profile, and thus the application resolution can be influenced by the position of the sample surface in the image plane (working distance (WD)), which can be influenced by the objective lens excitation or the vertical sample position, as illustrated in Fig. 21). There exists a specific working distance for the optimum imaging resolution the Gaussian plane and a different value is needed to mill the smallest features the plane of least

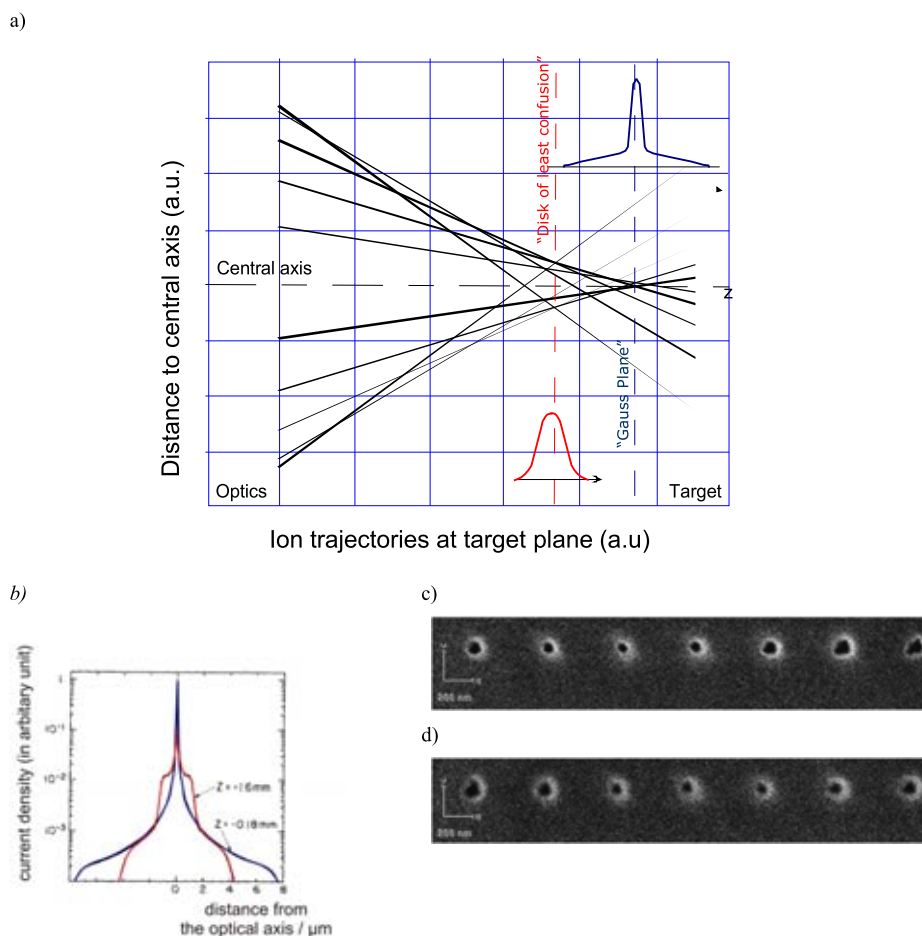


FIG. 22. (a) “Schematic representation of the trajectories of ions at the exit of an electrostatic lens with aberration. (1) Geometrical plane of the “Gauss optimum” with a profile presenting not only a narrow peak but also side wings. (2) Optimum plane for FIB writing experiments (“circle of least confusion”) giving a bell-shaped profile for the current distribution.”<sup>269</sup> Fig. 3.12 in Ref. 269. From Gierak *et al.*, *Nanofabrication Handbook*, edited by S. Cabrini and S. Kawata. Copyright 2012 CRC Press. Reproduced with permission from Taylor and Francis Group, LLC, a division of Informa plc. (b) Calculated current density distribution profiles for the case of large aberrations (at different focus positions  $Z$ , Spherical aberration referred to image side  $C_{si} = 20000$  mm, Chromatic aberration referred to image side  $C_{ci} = 240$  mm (Ref. 268)), modified (colors matched to Fig. 22(a)) Fig. 2 in Ref. 252. Reproduced with permission from J. Orloff *et al.*, *J. Vac. Sci Technol. B* 9, 2609 (1991). Copyright 1991 American Vacuum Society. (c) Part of an ion SE micrograph (scale bar has been copied into this part of the image from the original), taken with a lens setting for optimum image focus ( $\Delta WD = 0 \mu\text{m}$ ), the holes have been drilled with different WDs, starting with the left one:  $-40 \mu\text{m}$ ,  $-20 \mu\text{m}$ ,  $0 \mu\text{m}$ ,  $+20 \mu\text{m}$ ,  $+40 \mu\text{m}$ , sharp image and the smallest hole is one left to the centre at  $-20 \mu\text{m}$ . (d) Part of an ion SE micrograph (scale bar has been copied into this part of the image from the original image), taken at lens setting for optimum patterning focus ( $\Delta WD = -20 \mu\text{m}$ ), the holes have been drilled with different WDs, starting with the left one:  $-60 \mu\text{m}$ ,  $-40 \mu\text{m}$ ,  $-20 \mu\text{m}$ ,  $0 \mu\text{m}$ ,  $+20 \mu\text{m}$ , unsharp image and smallest hole in the center at  $-20 \mu\text{m}$ .

confusion, which is illustrated in Fig. 22(a). This results in different beam current distributions or beam profiles illustrated in Fig. 22(b), Orloff *et al.*<sup>252</sup> In addition, it has to be taken into account that “...the spherical aberration coefficient increases rapidly with working distance (as the fourth power), a short working distance will decrease the amount of current carried in the tail of the distribution.”<sup>252</sup> Figs. 22(c) and 22(d) illustrate these different optimum foci for the two cases.

A third resolution concept, interaction volumes, can also be modelled, in this case by Monte Carlo particle scattering simulations<sup>254,255</sup> or molecular dynamics<sup>227,270</sup> (more details can be found in Section VC 2). Ion matter interaction regime processes are usually complex many body interactions, so being able to model certain aspects for some applications is essential for users and mandatory for opening new application fields. The interaction volume can be influenced by the selected ion species, probe current, angle of incidence, and acceleration voltage.

The fourth resolution concept, application resolution, effective interaction volume or voxel is well suited for practical applications.<sup>193,271</sup> It includes the ones above, the achievable signal to noise ratio<sup>260</sup> in imaging, contrast creating or structuring mechanisms,<sup>260</sup> as well as the chemical or physical processes including their corresponding process sensitivities, interaction volumes (ranges), and contributions from the environment (vibration, electromagnetic fields,...).<sup>261</sup> Application resolution is a result-oriented concept and has to be figured out experimentally for each application. Imaging or patterning “ideal” material systems which can proof the instrument resolution is very different from using such an instrument to fabricate certain structures or devices in the material system of interest. Since the end of the 1970s, liquid metal ion source (LMIS) instruments carry out patterning as well as analysis applications, both rely on and influence each other. Acceleration energies between 5 and 50 keV in Ga LMIS point source ion beam instruments

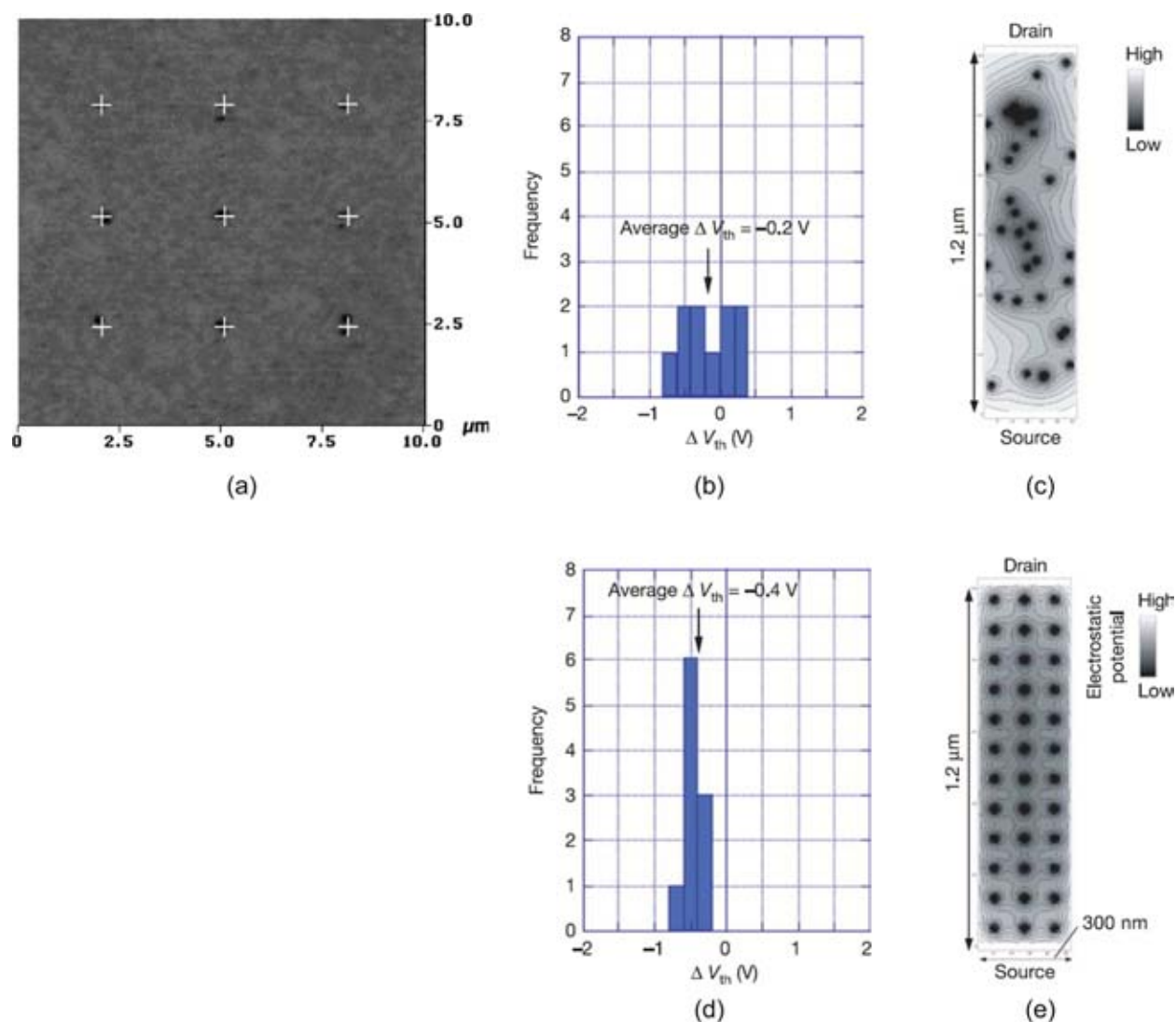


FIG. 23. (a) AFM image of etch pits created in CR39 by single-ion incidence. Histograms of  $V_{th}$  shift ( $\Delta V_{th}$ ) before and after single-ion implantation from 10 resistors and calculated contour maps of the Coulomb potential in the channel. Fig. 4(a) in Ref. 175, adapted from APEX/JJAP (b), (c) conventional random dopant distribution (d), (e) ordered dopant distributions. The Gaussian fitting curves of the  $V_{th}$  shifts in the ordered dopant distribution shows a standard deviation of only 0.1 V, which is three times smaller than the random dopant distribution, Fig. 4 in Ref. 176. Reprinted with permission from Shinada *et al.*, Nature 437, 1128–1131 (2005). Copyright 2005 Macmillan Publishers Ltd.

induce near surface processes with a few tens of nm penetration depth/interaction volume. A high “instrument resolution” enables small lateral spot sizes (a few nm). However, if the interaction volume for the target application is of the order of a few tens of nm or more this will dominate the effective usable resolution.

In high resolution imaging, all interaction processes have to be taken into account. An incident ion matter interaction phenomenon is called milling or “sputtering” (as described in Section VC2). The relatively large material removal rate for 5–50 keV  $\text{Ga}^+$  ions limits the resolving capability of an ultra-sharp edge, because the edge is removed/smoothed out during the imaging process: “For extended small features (like layered structures), rearrangements, redepositon, and differential milling rates may limit the resolution in some cases.”<sup>260,272</sup> For high dose ion matter interaction regimes, the resulting patterning application resolution can be lower than for low-dose ones, due to the beam current distribution of the ion beam.<sup>218</sup> In addition, features without interface defects produced by the ion impact can also be realized by ion

beam nanopatterning (similar to that in the self-organized 3D case, Section III C), for example, by selecting the incident ion species according to the sample material system, sometimes an additional annealing process is required.

For some applications, ion beam imaging/structuring can be more suitable than electron beam imaging/patterning although the instrument resolution is often lower (LMIS). Clever processing can allow to pattern with an application resolution better than the actual instrument resolution (a nanopore application example is given in Section VD3).

#### D. Examples of applications

The prevalent FIB instruments (almost every nano patterning and analysis lab is equipped with one) are more and more used to evaluate a large variety of patterning applications (ion matter interaction regimes), also beside the two main stream ones (milling and gas assisted processing). In this first section, a modified version of the versatile FIB instrument

(No. 6 in Section VC1) as well as the dedicated nano patterning ones (described under point 7 in Section VC1) have been used to create leading edge application results. These are thought to stimulate testing of further ion matter interaction regimes for all kinds of applications. Some of them can create operating devices (or preliminary stages of them) already within one process step. Different possibilities to categorize them exist by: ion matter interaction regimes, material systems, instrument technology, or application fields.

At five application results, we take a closer look: (single) ion implantation for local doping, preparation for graphene nanoribbon growth, nanopores for DNA manipulation, small magnetic domains, and the fabrication of an X-ray zone lens. This will be done with a focus on:

- ion matter interaction regimes exploitable for nano patterning
- precision
- process times/(instrument) stability
- resolution
- the current nano application challenges in this specific application field.

### 1. (Single) ion implantation I

Single ion events represent the minimum dose (1 ion) and in combination with the ion matter interaction regime implantation give access to small interaction volumes and thus, a high possible application resolution. Classical ion implantation used in the semiconductor industry (instrument type 2 in Section VC1) reaches dopant atom distribution homogeneity challenges on the scale of future devices. This is because device sizes approach average distances between impurity atoms. Single ion implantation employing FIB and secondary electron detection<sup>273</sup> can improve this by tailoring the number of dopant atoms and thus the dopant concentration and their exact position.

The dopant atom position can be defined very accurately employing dedicated LMAIS instrumentation (a modified type 6 in Section VC1). Shinada *et al.* showed pattern placement capabilities of the technique by implanting individual Si<sup>++</sup> ions (60 keV, LMAIS, modified tool type 2 in Section VC1 has been employed) into Polyallyldiglycolcarbonat (PADC or CR-39), within a diameter of 100 nm,<sup>175</sup> the results are shown in Fig. 23. The same group placed phosphorous atoms—in a different experiment—into a transistor channel region (30 kV)<sup>176</sup> and analyzed the electrical devices afterwards. Fig. 23 shows the larger transistor threshold voltage ( $V_{th}$ ) shift compared to the undoped case ( $\Delta V_{th}$ ) and a lower statistical distribution (tighter confined bell curve) of  $\Delta V_{th}$  than conventionally fabricated ones.<sup>176</sup>

These remarkable results prove the successful application of single ion event LMAIS FIB for semiconductor doping altering the electrical properties of FETs.

### 2. Si and Au implantation II (surface functionalization/graphene nano ribbon growth)

Another nano fabrication challenge is the reproducible fabrication of graphene at specific sample locations in the desired material quality to integrate it into devices.

As described in Refs. 177 and 178.

Graphene can have exceptional optical, chemical, mechanical, and electrical properties like, e.g., very high carrier mobilities. In addition, it is compatible with planar processing technologies developed for silicon and it is a candidate for metal oxide semiconductor (CMOS) devices. It can be grown onto different substrates by different techniques such as mechanical exfoliation, chemical vapor deposition (CVD), and thermal decomposition. The mechanical exfoliated one is described as the purest graphene possessing a high electron mobility. However, because of the current size limitations of the flakes, they are not used in commercial devices. Employing CVD or thermal decomposition wafer scale graphene sheets can be synthesized. Trying to transfer CVD graphene onto a dedicated substrate can degrade its electrical properties. Graphene can be formed on insulating or semiconducting of silicon carbide (SiC) by thermal decomposition, and thus be integrated into devices. A low-dose LMAIS FIB process with a high potential application resolution is achievable by combining ion implantation or multi-ion beam lithography and thermal or pulsed laser annealing (PLA) to selectively synthesize graphene only where ions have been implanted.<sup>177,178</sup> Regions where Au, Cu, Ge, or Si ions have been implanted show a lower processing temperature than crystalline SiC (c-SiC), so thermal annealing can be used to initiate local graphene growth.<sup>177</sup> There is also evidence that the implanted species affect the needed PLA fluence for the formation of graphene.<sup>178</sup> A multispecies LMAIS instrument has been used for the implantation (type 7 in Section VC1).<sup>177,178</sup> Direct patterning with nanometer resolution can be achieved without using conventional lithography techniques, see Fig. 24. By controlling the ion beam lithography and annealing conditions, single or a few layers of graphene can be synthesized.

In addition, Raman spectra have revealed that graphitization is stronger for incident ions Au and Cu (CVD catalytic species, than Ge and Si (isoelectronic), compare the intensity of the relevant bands D, G and 2D in Fig. 25).

A combination of LMAIS FIB (“35 keV Au ions... fluence  $5 \times 10^{16}$  ions/cm<sup>2</sup>”) and pulsed laser annealing (PLA) in air is shown in Fig. 26. Here “a periodic micro-ribbon array composed of five lines, each 2  $\mu$ m wide and 10  $\mu$ m long, separated by 2  $\mu$ m was patterned.” Fig. 26 shows “the Raman map of the 2D-band intensity... of this area” which “shows graphitization only where the SiC was implanted”. Thus, LMAIS FIB implantation into c-Si locally lowers the temperature or fluence in PLA needed for graphitization, so graphene nano ribbon growth can be locally initiated.

### 3. Artificial nanopores in dielectric membranes (DNA manipulation—milling of suspended thin films-surface atoms removal)

DNA manipulation—employing holes, channels, apertures, or nanopores with diameters <10 nm is a promising technique. A single molecule detector can be created by electrically monitoring the current variation flowing through an orifice. If nanoparticles, colloids, or DNA is added to the solution, current variations are observed resulting from the

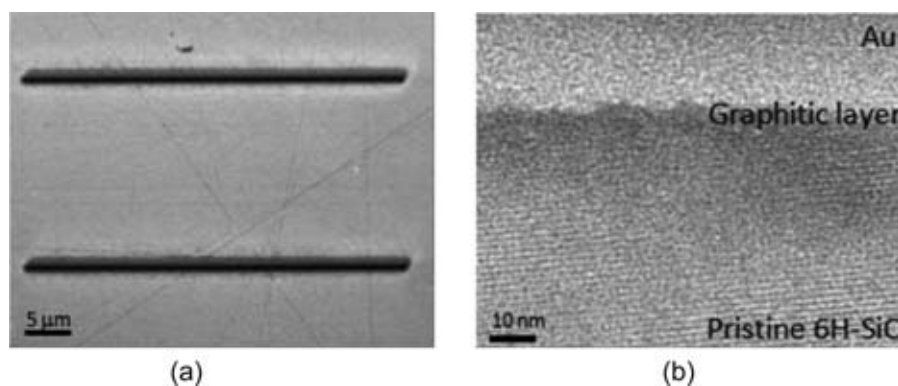


FIG. 24. (a) “...SEM images taken on... graphene nanoribbon surfaces... where the width of the two parallel nanoribbons (dark lines) is on the order of 200 nm...” Figure 3(c) in Ref. 177 (“(c)” removed). Reproduced with permission from Appl. Phys. Lett. **100**, 73501 (2012). Copyright 2012 American Institute of Physics (b) “...TEM images taken across the Au/graphene/6H-SiC...” “...shows the underlying 6HSiC’s structural perfection...” Figure 3(d) in Ref. 177 (“(d)” removed). Reproduced with permission from Appl. Phys. Lett. **100**, 73501 (2012). Copyright 2012 American Institute of Physics.

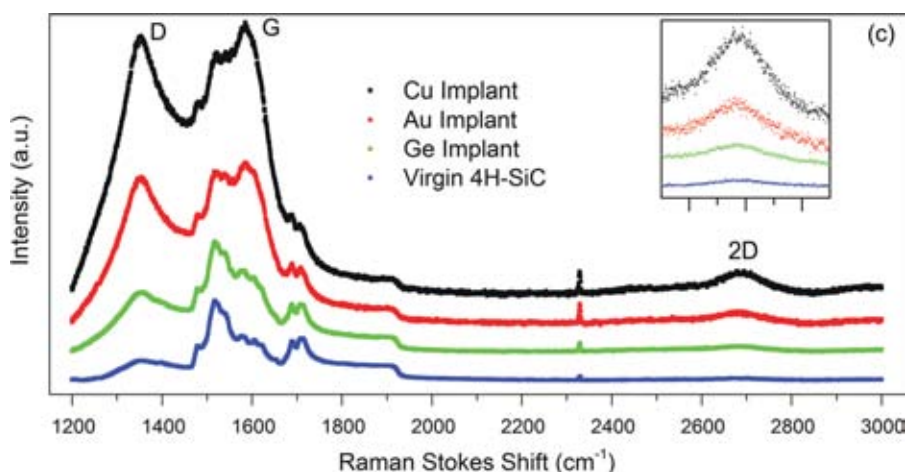


FIG. 25. “Raman spectra for each implant condition annealed at  $1 \text{ J/cm}^2$  and 50 pulses. The spectra are normalized by the shoulder at  $1920 \text{ cm}^{-2}$  to avoid interference with the large convoluting G-band. Inset: Magnified plot of the 2D-bands,” Fig. 2(c) in Ref. 178. Reproduced with permission from Appl. Phys. Lett. **100**, 73501 (2012). Copyright 2012 American Institute of Physics.

passage of the nano-objects through the orifice. This is done by applying a voltage between two electrodes in a conductive solution and measuring the resulting current. If a molecule passes the nanopore the current decreases, this effect is called “current blockade”. Current changes indicate molecule compositions for *in vivo* virus analysis or DNA manipulation.<sup>274–276</sup>

The current nano patterning challenge is to reproducibly create nanopores in a range from 5 to 30 nm diameter. Such



FIG. 26. “Growth of FLG with nanoscale features by Au-ion beam lithography and PLA...” (c) Raman 2D-band map of the metamaterial array.” Scale bar is  $2 \mu\text{m}$ , Part of Fig. 3(c) in Ref. 178. Reproduced with permission from Appl. Phys. Lett. **100**, 193105 (2012). Copyright 2012 American Institute of Physics.

nanopores can be fabricated by various techniques like EBL (electron beam lithography) and subsequent reactive ion etching (RIE).<sup>277</sup> The current leading technique aims at directly drilling nanopores in a membrane using a highly focused and dense electron beam in a TEM, before it was also found very convenient for fine-tuning pore sizes to smaller sizes.<sup>278</sup> These methods allow ultra small pore fabrication but require one-by-one nanopore processing. A FIB sculpturing process<sup>279</sup> on the other side allows batch patterning of multiple devices since specimen size limitations are not an issue for FIB machines. Advantages of EBL (Section II) are: it is an established, wide spread, and well understood process technology. However, challenges exist for reproducible sub 5 nm holes creation: the resist resolution limit in combination with the required aspect ratio for the RIE process step.<sup>280</sup> A sculpturing technology can reproducibly create sub 5 nm holes;<sup>279</sup> however, it is a rather slow and manual process (first mill larger holes and close them again in a second process step).

Simple direct milling of nanopores is not possible, as ion solid interaction regimes and lateral scattering of the primary beam limit the resolution.<sup>274,280</sup> However, high dose milling ion matter interaction regime combined with clever processing can result in a high application resolution, even below the instrument resolution. A refined process is required and a Ga LMIS FIB has been used (NanoFIB, type 7 in Section VC 1): Bianco *et al.*<sup>274</sup> took a SiC membrane (30 or 10 nm thick)

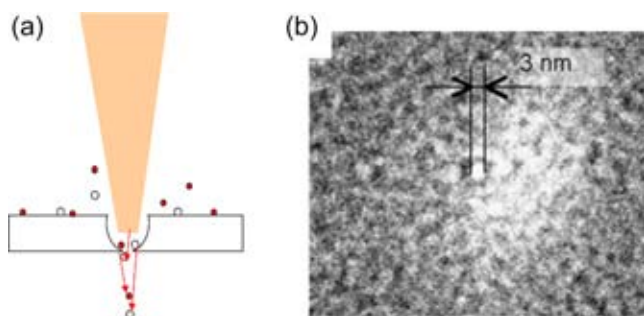


FIG. 27. Patterning process and result schematic of the membrane engraving processes. (a) Entry side milling, milled until the nanopore is opened at the rear side, Fig. 3(c) in Ref. 243. Reproduced with permission from J. Gierak *et al.*, *Ultramicroscopy* **109**, 457 (2009). Copyright 2009 Elsevier. (b) TEM micrograph of a resulting nanopore drilled by a Ga beam into a 20 nm thick SiC membrane with around  $2.5 \times 10^7$  ions/point, “(d)” removed, Fig. 5 (left) in Ref. 243. Reproduced with permission from J. Gierak *et al.*, *Ultramicroscopy* **109**, 457 (2009). Copyright 2009 Elsevier.

instead of bulk material (thickness in the range of the projected range of the impinging ions). This results in direct patterning of sub 5 nm holes (“application resolution”) on the rear side of a membrane. The process exploits the lateral extension of the interaction volume (described in Sections VC2 and VC4) at the membrane rear side, when patterned from the top.<sup>247</sup> As a result, some of the displaced atoms are directly ejected at the rear side of the membrane. This “forward scattering” almost eliminates redeposition effects.<sup>247</sup> The membrane is patterned from one side and stopped as soon as a small diameter opening is created on the rear side<sup>247</sup> (as shown in Fig. 27(a) and the result in Fig. 27(b)).

Fig. 28(a) shows a molecule measurement set-up<sup>281</sup> and (b) an ionic current variation measurements induced by  $\lambda$  DNA molecules passing through or inserted in a Si<sub>3</sub>N<sub>4</sub> nanopore.<sup>275</sup>

The results achieved so far are competitive to those reached by other patterning techniques. The advantage is

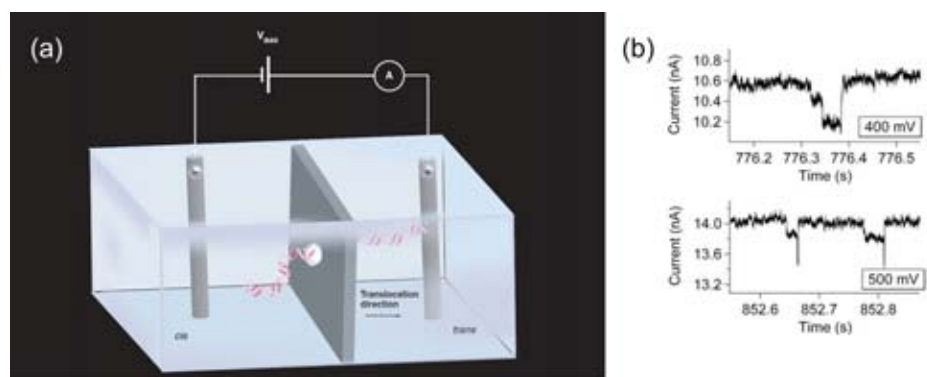


FIG. 28. (a) Molecule measurement concept employing nanopores Fig. 1 in Ref. 281, Reproduced with permission from Healy *et al.*, *Nanomedicine* **2**(6), 875–897 (2007). Copyright 2007 Future Medicine. (b) Ionic current variation measurements induced by  $\lambda$  DNA molecules passing through or inserted in a Si<sub>3</sub>N<sub>4</sub> nanopore, Fig. 3(b) in Ref. 275. Reproduced with permission from *Microelectron. Eng.* **87**, 1300 (2010). Copyright 2010 Elsevier.

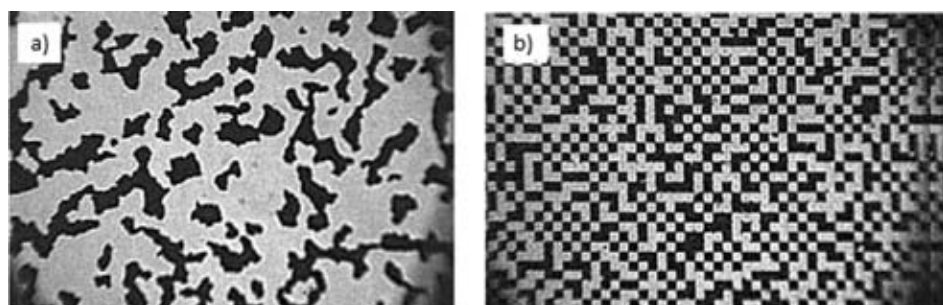


FIG. 29. Magneto optical image of a thin line array patterned by Ga: (a)  $2 \times 10^{13}$  ions/cm<sup>2</sup> not sufficient for the formation of domain walls and (b) with  $2 \times 10^{16}$  ions/cm<sup>2</sup> Figs. 2(a) and 2(d) (enumeration modified) in Ref. 286. Reproduced with permission from R. Hyndman *et al.*, *J. Magn. Magn. Mater.* **240**, 34 (2002). Copyright 2002 Elsevier.

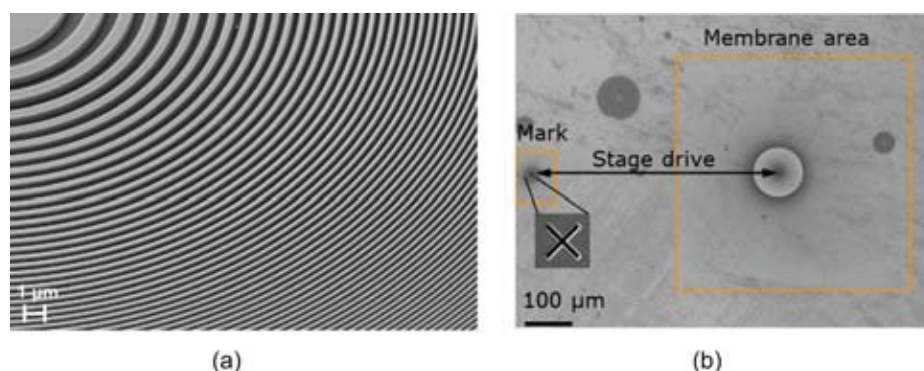


FIG. 30. SEM micrographs (a) showing a 45° tilted view of the zone plate: inner zones, Fig. 3(a) in Ref. 72. Reproduced with permission from A. Nadzeyka *et al.*, *Microelectron. Eng.* **98**, 198 (2012). Copyright 2012 Elsevier. (b) The silicon nitride membrane with active area including gold zone plate and position of reference mark for automatic positioning correction on bulk sample, Fig. 1 in Ref. 72. Reproduced with permission from *Microelectron. Eng.* **98**, 198 (2012). Copyright 2012 Elsevier.

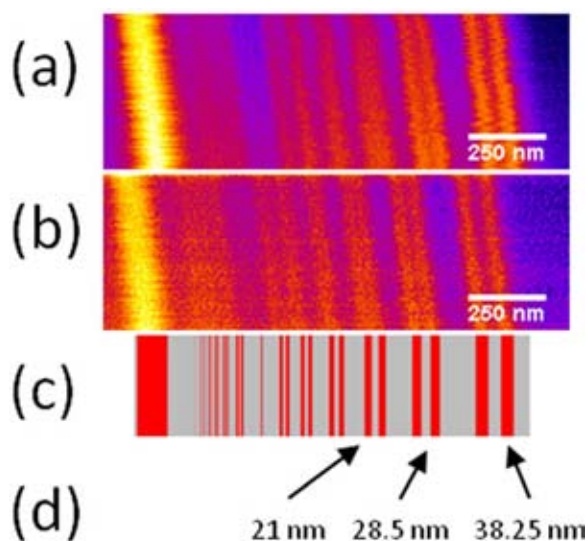


FIG. 31. “Scanning X-ray microscopy image of a certified commercial test sample (BAM L200) recorded at 1200eV (a) image acquired in the 2nd order focus of the FZP with a pixel size of 5 nm and a dwell time of 10 ms, (b) image acquired in the 3rd order focus of the FZP with a pixel size of 5 nm and a dwell time of 15 ms, (c) schematic representation of the certified test object, and (d) width of the features (half pitch),” Fig. 5 in Ref. 31. Reproduced with permission from K. Keskinbora *et al.*, *Opt. Express* 21, 11747 (2013). Copyright 2013 OSA Publishing.

that it is a one process step technique. Each hole is patterned in a few tens of ms (typically 20), because of its size and the thin sample (membrane), thus only a tiny material volume has to be removed for each hole allowing precise dose calibration and a high reproducibility. However, the process (milling) belongs in the large dose regime ( $2.5 \times 10^6$  ions/point equaling  $1 \times 10^{19}$  ions/cm<sup>2</sup> calculating with the 5 nm spot size as given in Ref. 247), thus the resulting lower application resolution can be overcome by clever processing. Fig. 28(b) shows exemplary ionic current variations, caused by the insertion of DNA molecules passing through a

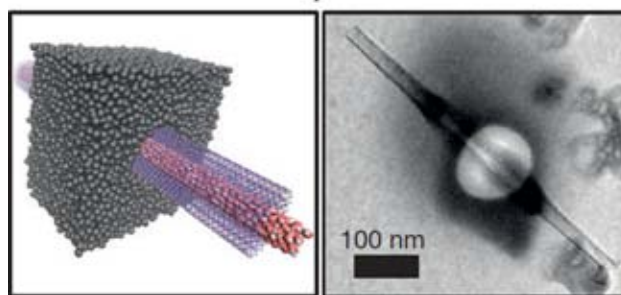
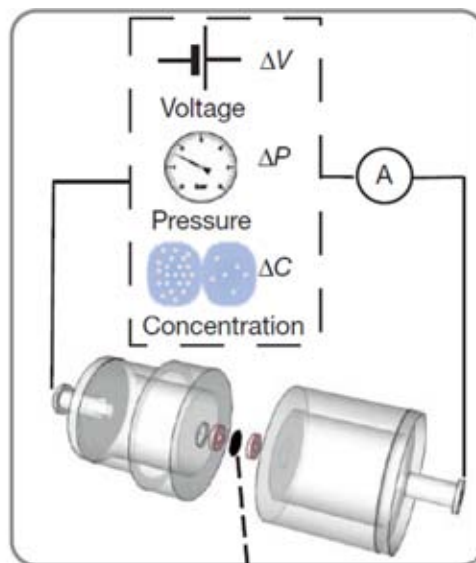


FIG. 33. (Top) Measurement set-up schematic for a single transmembrane BNNT, lower left: concept, lower right: TEM micrograph of a result, Fig. 1(b) in Ref. 290. Reprinted with permission from A. Siria *et al.*, *Nature* 494, 455–458 (2013). Copyright 2013 Macmillan Publishers Ltd.

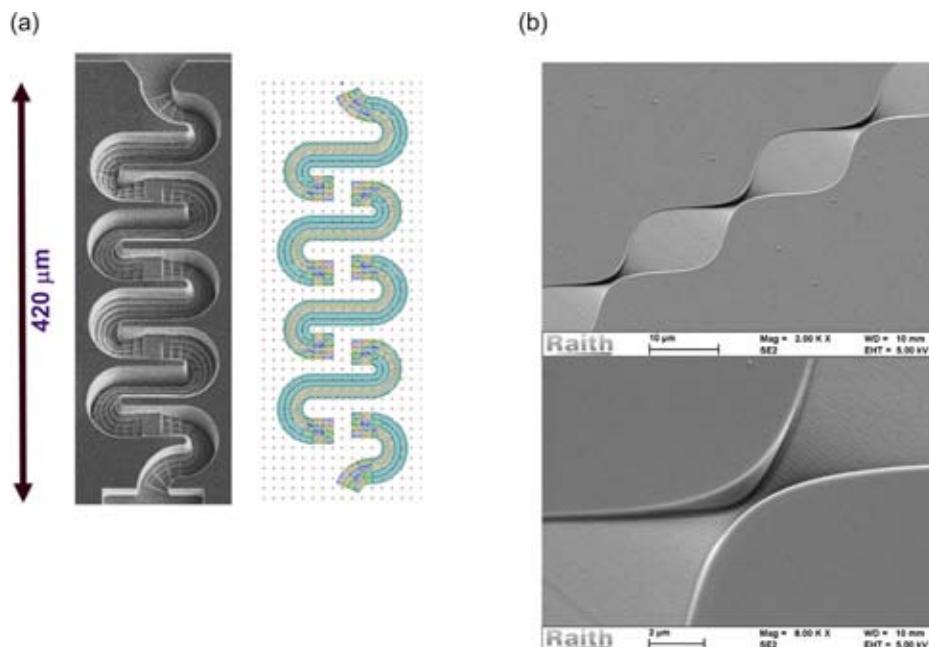


FIG. 32. SEM micrographs of exemplary microfluidic devices created by focused ion beam microfluidic devices (a) “View of CAD data used for making the 3D serpentine mixer. Data consist of curved polygons that have no cuts through the entire length of the device,” Fig. 8 in Ref. 288. Reproduced with permission from L. E. Ocola and E. Palacios, *J. Vac. Sci. Technol. B* 31, 06F401 (2013). Copyright 2013 American Vacuum Society. (b) With complex 3D microfluidic geometry Fig. 10 in Ref. 289 (“(a)” and “(b)” removed). Reproduced with permission from E. Palacios *et al.*, *J. Vac. Sci. Technol. B* 28, C611 (2010). Copyright 2010 American Vacuum Society.

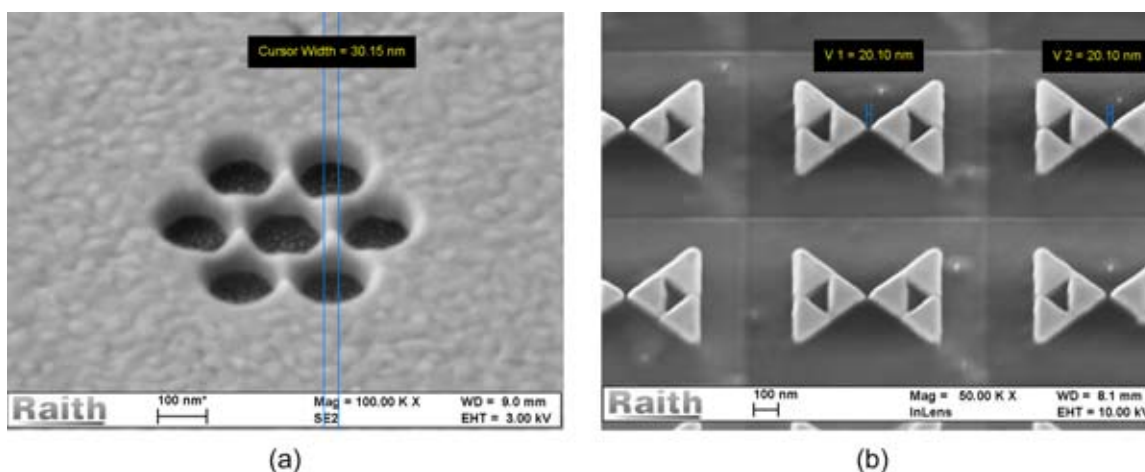


FIG. 34. SEM micrographs of exemplary optical devices created by Ga LMIS focused ion beam milling (a) a single base feature consisting of 6 circles (“oligomere”), where 12 000 of them have been created within a  $100\ \mu\text{m} \times 100\ \mu\text{m}$  area (35 kV Ga LMIS FIB milled into 80 nm Au on a  $\text{SiO}_2$  substrate)—courtesy and copyright H. Giessen University of Stuttgart and Application Lab Raith GmbH; (b) other base features are triangles (“fractal bow tie,” 35 kV Ga LMIS milled into Cr (5 nm) Au (35 nm) on a  $\text{SiO}_2$  substrate, probe current 5.3 pA, process time 25 h to pattern  $144 \times 144$  bow ties over about  $100\ \mu\text{m}$ )—courtesy and copyright (a) Elezzabi University of Alberta and Application Lab Raith GmbH.

nanopore used as a dividing wall, which has been detected at different voltages 400 and 500 mV.<sup>275</sup>

#### 4. Local smoothing of magnetic thin films (small single magnetic domains)

Small single magnetic domain regions are created to study their thermal stability and their coupling effects between dots organized in matrixes. Thus, nano patterning processes are required to fabricate small single magnetic domain areas which allow us to overcome<sup>282</sup> the so-called superparamagnetic limit as 2D discrete media with perpendicular anisotropy.<sup>283</sup> This can be done by conventional lateral nano patterning techniques like EBL (Section II) followed by a pattern transfer<sup>284</sup> or self-organized 3D epitaxy<sup>285</sup> process. An advantage for EBL is the freedom in feature shapes and position on the sample, whereas a disadvantage is the process complexity (pattern transfer). For self-organized 3D epitaxy (Section III), the advantages are the reported feature sizes down to 3 nm and the potential

patterning speed for volume production purposes. Ion irradiation can locally alter magnetic properties of ultra-thin magnetic films, down to the nm scale.<sup>286</sup> Depending on the ion dose, the surface properties can be tailored from ferromagnetic with reduced coercivity to paramagnetic.<sup>282,286</sup> In the presented results, the ion beam has been employed to create domain walls (displayed in Fig. 29(b)), using a Ga LMIS FIB (NanoFIB, type 7 in Section VC 1). The ion-matter interaction regime responsible for this is called atom intermixing resulting in a magnetic “smoothing” effect.

The fabrication challenge of magnetic layer smoothing here is to reduce reproducibly the size of the fabricated magnetic cells. This can be done by the low to medium dose combination of the ion implantation and atom intermixing ion matter interaction regime. The employed dose for this application ( $6.3 \times 10^4$  ions/point or  $2 \times 10^{16}$  ions/cm<sup>2</sup>, assuming 20 nm effective beam size) is in the medium dose regime resulting in a medium potential application resolution.

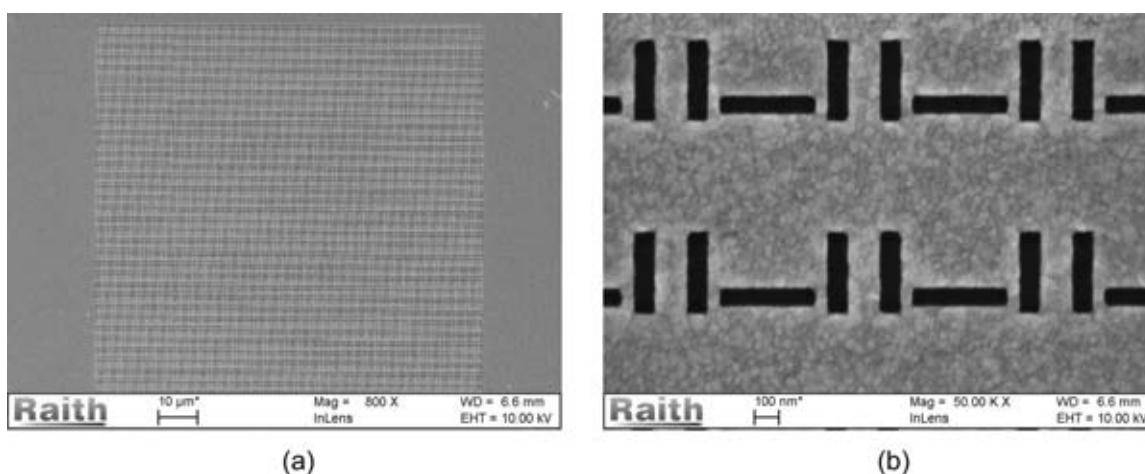


FIG. 35. SEM micrographs of Si and Ga milled feature in Au on  $\text{SiO}_2$  (35 kV, LM(A)IS) (a) overview at an instrument magnification of 800 and (b) a few elements at an instrument magnification of 50 000, both courtesy and copyright Giessen University of Stuttgart and Application Lab Raith GmbH.

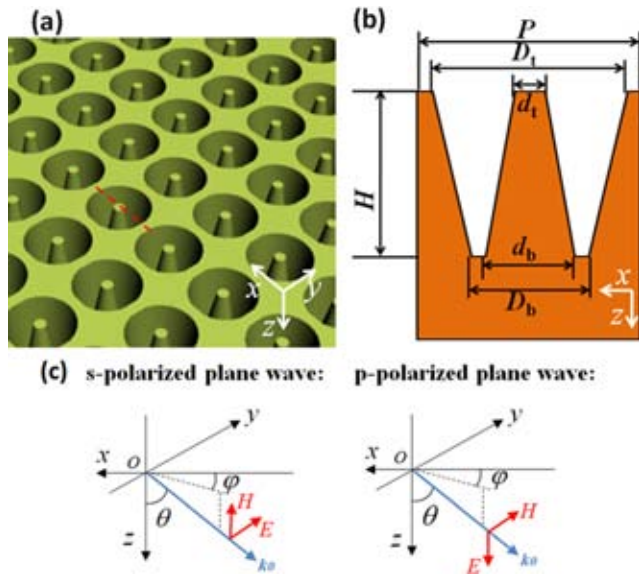


FIG. 36. (a) “Three-dimensional schematic diagram of PTCH-based absorber... with all the structural parameters illustrated.” (b) “Cross section of one unit cell in the  $xz$  plane along the red dashed line in (a)” (c) “s- and p-polarized plane waves are considered as the light source incident from the top,” Fig. 1 in Ref. 291. Reproduced with permission from L. Mo *et al.*, *Opt. Express* **22**, 32233 (2014). Copyright 2014 OSA Publishing.

During the ion irradiation, atoms from the substrate and a few incident  $\text{Ga}^+$  ions are mixed into the thin magnetic film. This alters locally the magnetic properties. The material composition has been: Pt(3.4 nm)/Co(1.4 nm)/Pt(4.5 nm) grown on a transparent  $\text{Al}_2\text{O}_3(0001)$  substrate.

Advantages of this technique are the process simplicity (only one process step), the freedom in feature shape as well as position, and the extreme sensitivity (only a few Ga ions per pixel are necessary for feature creation). For volume production requirements, the overall process is slower than, for example, self-organized 3D epitaxy (Section III); however, these remarkable direct patterning results open fascinating opportunities for magnetic nano device prototyping.

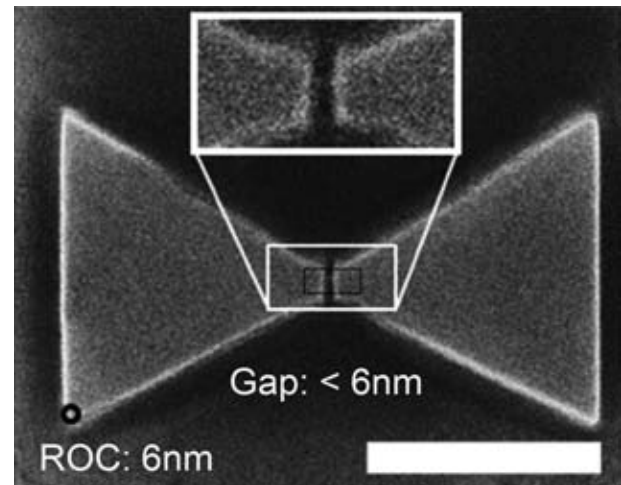


FIG. 38. “Scanning helium ion microscopy image of bowtie nanoantennas fabricated by  $\text{He}^+$ -ion beam milling... milled into a 30 nm thick polycrystalline gold film evaporated onto a glass substrate... Bowtie antenna fabricated by  $\text{He}^+$  milling...”<sup>292</sup> Fig. 1(d) in Ref. 292 (“(d)” removed). Reproduced with permission from Kollmann *et al.*, *Nano Lett.* **14**, 4778 (2014). Copyright 2014 American Chemical Society.

### 5. A x-ray zone plate

The scope is to reproducibly fabricate zone lens plates for X-rays. Here, the challenge is to combine high resolution in the outer rings with pattern placement accuracy requirements, so operating devices can be manufactured. Alternative techniques are electron beam lithography in combination with a suitable pattern transfer technique.

If Ga LMIS FIB milling is applied, the patterning sequence can take many hours (over 15 h with the tool type described under No. 7 in Section V C 1)). Thus, automatic (unattended) drift compensation after partial patterning of the design has been carried out at a mark outside the active area. This has been done in the following sequence: a periodic stop of the patterning process, blank the beam, stage movement away from the device, an automated mark recognition process with a position adjust, driving back to the device and continue patterning at the corrected position. In our example, an operating device (X-ray zone lens), with the desired x-ray focusing

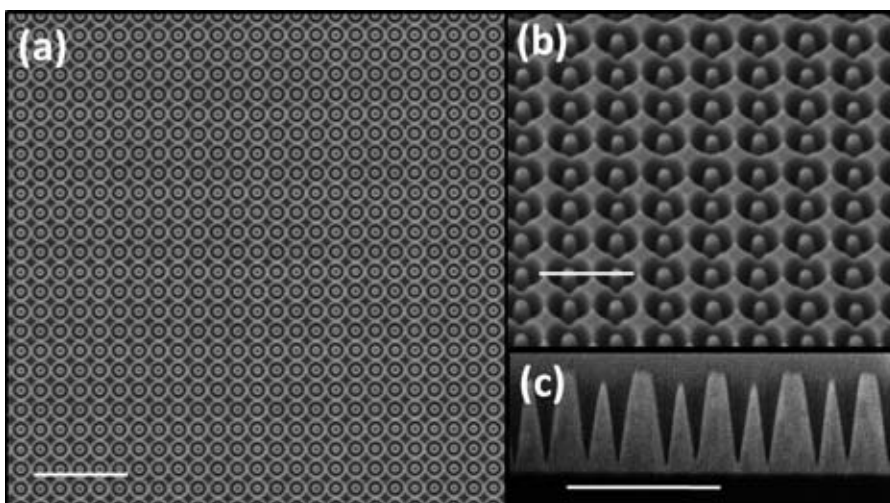


FIG. 37. “SEM images of the combined absorber based on PTCHs... milled in Au” (a) “topview (scale bar: 2  $\mu\text{m}$ ),” (b) “tilted-view (scale bar: 800 nm),” and (c) “cross-section (scale bar: 800 nm),” Fig. 7 in Ref. 291. Reproduced with permission from L. Mo *et al.*, *Opt. Express* **22**, 32233 (2014). Copyright 2014 OSA Publishing.

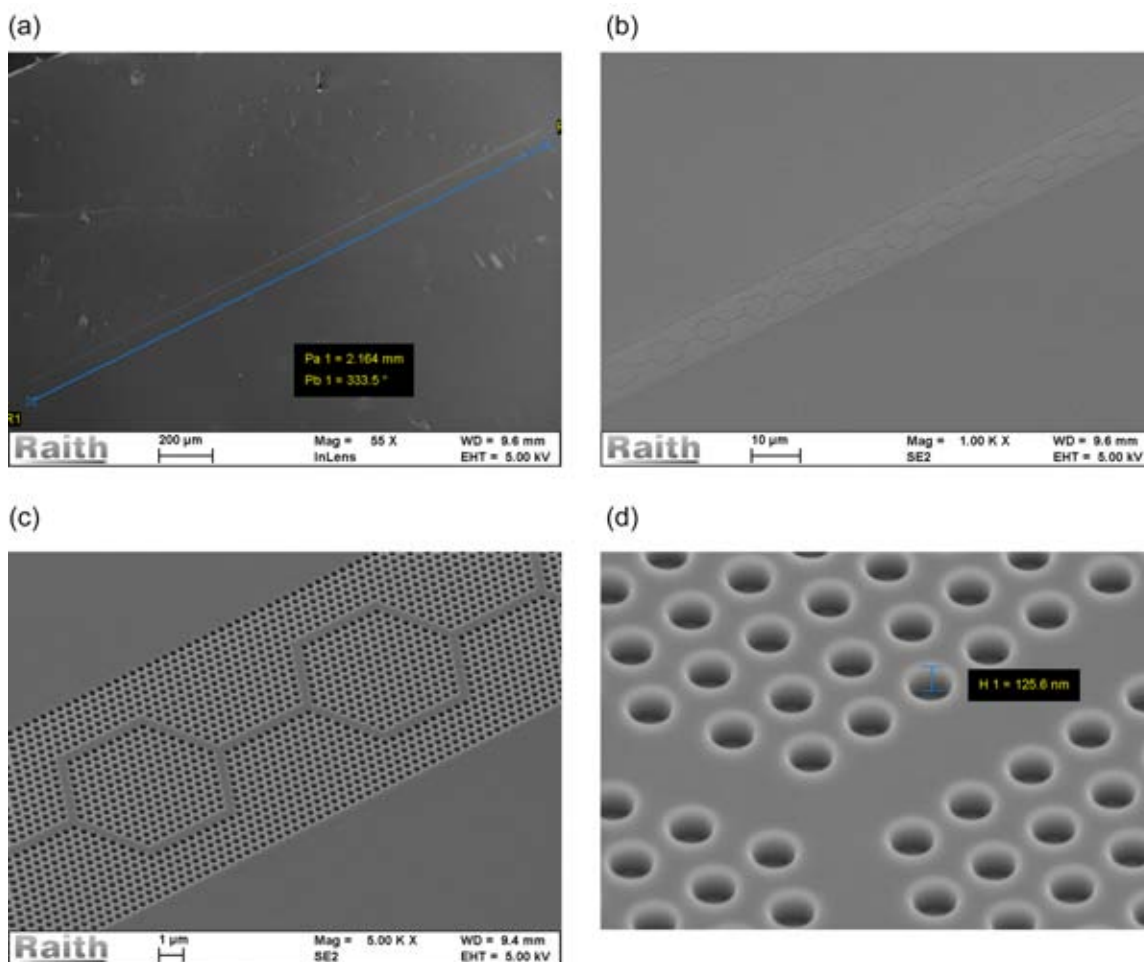


FIG. 39. SEM micrographs of a photonic crystal light guiding devices fabricated by Ga LMIS FIB (35 kV) milled into a Si sample (a) about 2 mm long (blue measurement line) wave guide at an instrument magnification of 55, (b) an instrument magnification of 1000, (c) an instrument magnification of 13 000, and (d) tilted view cut from an instrument magnification of 20 000 to estimate the milling depth all micrographs courtesy and Copyright L.-M. Peng of Peking University and Application Lab Raith GmbH.

capabilities has been manufactured in one process step.<sup>72</sup> It is a milling process, into a 500 nm Au layer on a silicon nitride membrane. Milling is a high dose, thus potentially lower reachable application resolution ion matter interaction regime. The zone plate diameter is 100  $\mu\text{m}$  and the outer rings are 100 nm wide, the procedure and patterned device can be seen in Fig. 30. Fig. 31 shows the device performance of the x-ray zone lens, published under.<sup>31</sup>

### E. Further exemplary applications

Now, an overview about further application fields and other approaches for the already described ones will be given: microfluidics, photonics, nanopores, magnetics, large area milling, classical organic resist exposure, unconventional resists or treatments, feature refinement, local doping, surface functionalization, gas assisted processes, and a form of regular feature self-organization under ion beam bombardment. The application results have been created utilizing 6 out of the 7 mentioned ion source and tool concepts in Section VC 1.

We take a look at the application results with respect to:

- ion matter interaction regimes exploitable for nano patterning
- precision

- process times/(instrument) stability
- resolution
- periodicity

### 1. Fluidics

Nano and micro fluidics have many potential applications in separation science,<sup>287</sup> energy conversion,<sup>287</sup> chemistry and biology taking place on small length scales, e.g., for medical applications.<sup>288</sup> The shown results demonstrate the technologies's feature shape and 3D capabilities as well as versatility. Exemplary devices created partially by milling can be seen in Fig. 32, which is a high dose and thus lower potential application resolution process technology employing Ga LMIS technology.

A first example (displayed in Fig. 32(a)) has been carried out on a Si wafer as a combination of EBL and Ga LMIS FIB (type 6 in Section VC 1) micromachining. A second (shown in Fig. 32(b)) has been patterned on Cr on quartz sample by optical lithography and Ga LMIS FIB (type 7 in Section VC 1).

Fig. 33 shows the result of a combinatory technique using FIB, nano-manipulation and electron beam induced deposition. A single transmembrane boron nitride nanotube

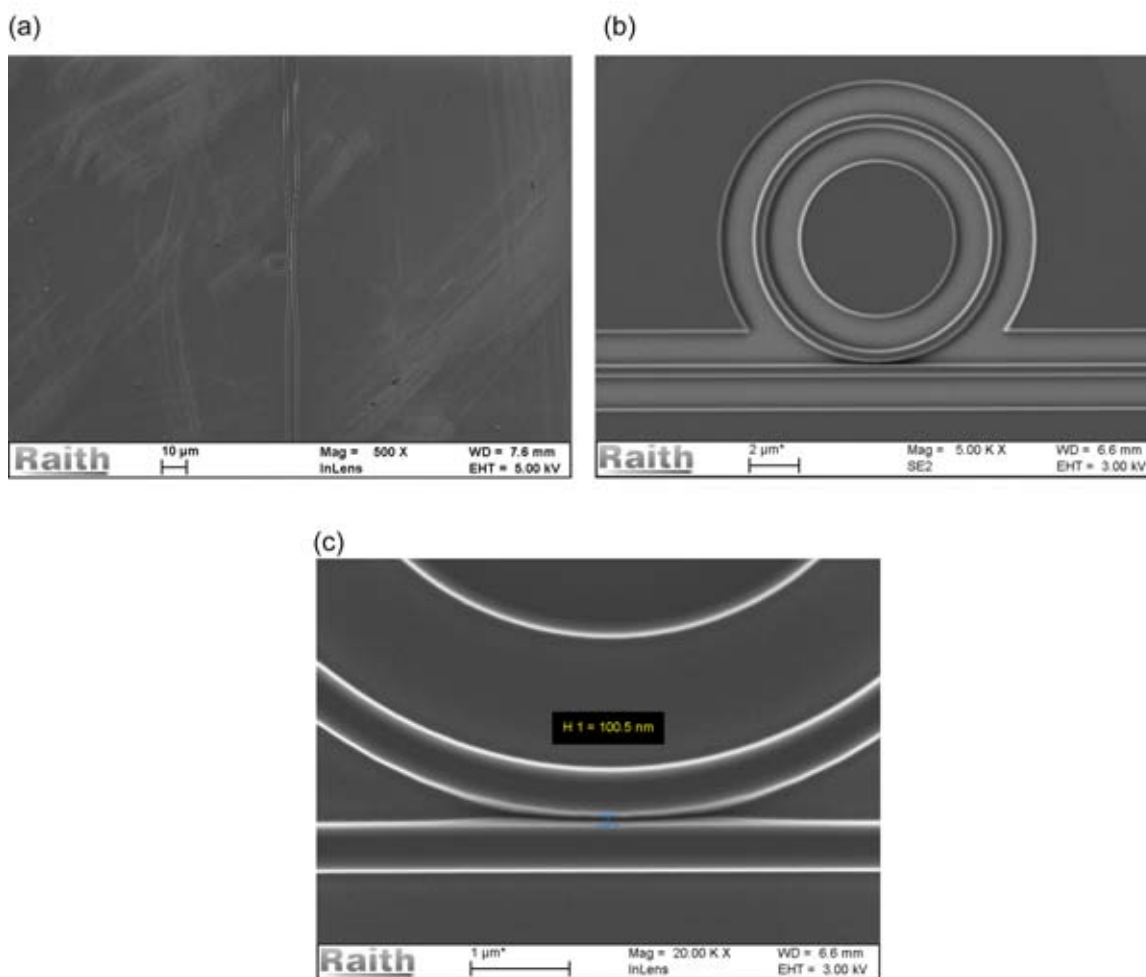


FIG. 40. SEM micrographs of further photonic waveguiding devices milled by Ga LIMS FIB (35 kV) into a (a) Si sample taken at an instrument magnification of 500; (b) Si sample taken at an instrument magnification of 2500; and (c) Si on insulator sample taken at an instrument magnification of 40 000 all micrographs courtesy and Copyright L.-M. Peng of Peking University and Application Lab Raith GmbH.

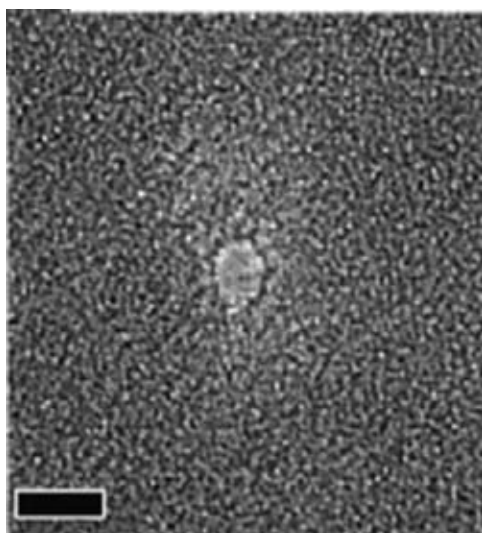


FIG. 41. “Transmission electron micrograph of a 2.5 nm diameter HIM nanopore (scale bar is 5 nm)”<sup>238</sup> (“(c)” removed from image), Fig. 2(c) in Ref. 238. Reproduced with permission from A. R. Hall, *Microsc. Today* 20, 24 (2012). Copyright 2013 Cambridge University Press.

(BNNT) was realized.<sup>290</sup> The displayed hierarchical nano-fluidic device (BNNT) interfuses an ultrathin membrane and links two fluid reservoirs, so fluidic transport can be analyzed through a single nanotube initiated by different forces like: electric fields, pressure drops, and chemical gradients.<sup>290</sup>

## 2. Plasmonics (surface plasmons)

Many different optical devices patterned in Au films for plasmonic applications are nano devices prototyped by ion beam nanopatterning, employing the ion matter interaction regime called milling. The devices can be used to guide light, reflect it, or filter frequencies. Here, reproducible periodicities can be a challenge as well as surface quality and pattern placement accuracy. To achieve the latter, automatic drift correction away from the active device area can be used (as described in Section VD5). Further on, the size of a device is sometimes larger than a field of view, so special patterning techniques or instrument architectures might be required. Figs. 34(a) and 34(b), Fig. 35 and plasmonic tapered coaxial holes (PTCH) Fig. 36 as well as Fig. 37 show exemplary small features repeated in a special way forming an optical

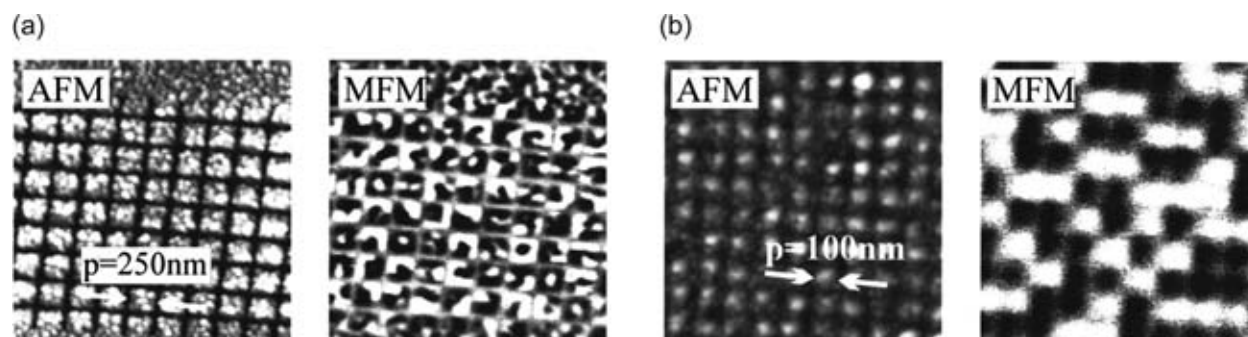


FIG. 42. AFM and MFM images of small single magnetic domain areas, "... of granular perpendicular CoPtCr recording" media, patterned at a period of (a) 250 nm and (b) 100 nm, Fig. 1 in Ref. 293. Reproduced with permission from Appl. Phys. Lett. 78, 990 (2001). Copyright 2001 American Institute of Physics.

device. The results have been realized utilizing a Ga LMIS FIB (type 7 in Section VC 1).

Plasmonic nanoantennas have also successfully patterned by He GFIS milling into a 30 nm thick polycrystalline gold film (instrument type 3 in Section VC 1), an exemplary result is displayed in Fig. 38.<sup>292</sup>

### 3. Photonics devices, larger than one field of view

An exemplary device (Fig. 39), which is significantly larger than one field of view: is an about 2 mm long light guiding one (35 kV, Ga beam, over all patterning time about 4 h). Here, repetitive stitching with dose control at the stitching border has been carried out to create it, utilizing a Ga LMIS FIB instrument (type 7 in Section VC 1).

Another example (Fig. 40) of optical devices extending one field of view is a wave guide with optical resonators. This has been realized by field stitching with the same instrument as described above (35 kV).

### 4. Nanopores II

A further nanopore fabrication example (to the one described in Section VD 3) has been produced by He ion milling (HIM), by an instrument of type 3 in Section VC 1);<sup>238</sup> exemplary results are displayed in Fig. 41. Feature sizes below 3 nm have been achieved applying this technology.

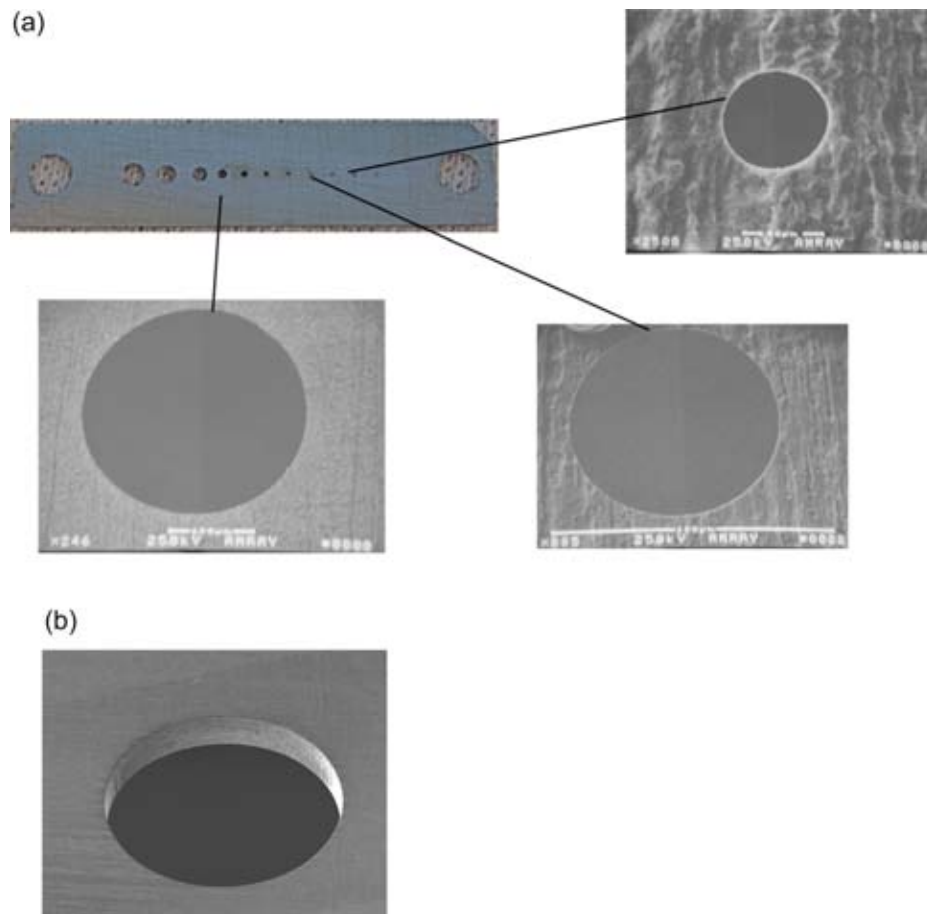


FIG. 43. SEM micrographs of Micromachined holes in FIB aperture strip (molybdenum). Holes machined with Xenon beam currents of 150 nA to 1500 nA beam current.<sup>174</sup> (a) From top (b) an exemplary one tilted, courtesy and Copyright Oregon Physics.

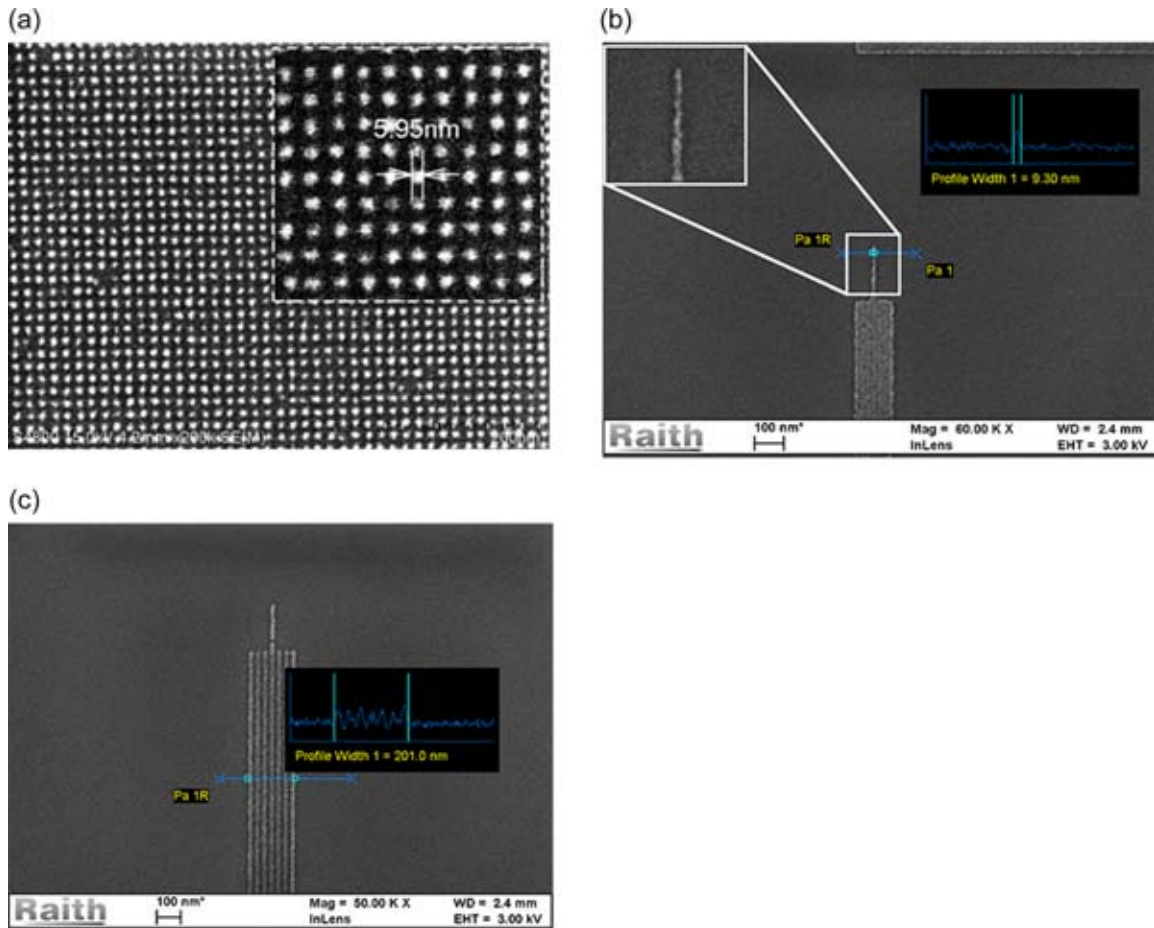


FIG. 44. Micrographs of high resolution and small periodicity experiments in HSQ employing (a) a He GFIS instrument “... arrays of dots written in a 5 nm thick HSQ layer using SHIBL at pitches of... 14 nm. The insets are SEM images at a higher magnification. The average dot size for all pitches is 6.1 nm,” Fig. 1 in Ref. 236 (“(c)” removed). Reproduced with permission from Sidorkin *et al.*, *J. Vac. Sci. Technol. B* 27, L18 (2009). Copyright 2009 American Vacuum Society. (b) Ga LMIS instrument “..., feature size <10 nm (6 nm HSQ on Si, exposed by 40 kV Ga, dose 19.4 pAs/cm” Fig. 1 in Ref. 207. Reproduced with permission from Bruchhaus *et al.*, *Microelectron. Eng.* 97, 48 (2012). Copyright 2012 Elsevier (c) same as (b) but now taking a look at the minimum periodicity of 30 nm (6 nm HSQ on Si, exposed by 40 kV Ga, dose 23.6 pAs/cm, Figure 2 in Ref. 207. Reproduced with permission from Bruchhaus *et al.*, *Microelectron. Eng.* 97, 48 (2012).

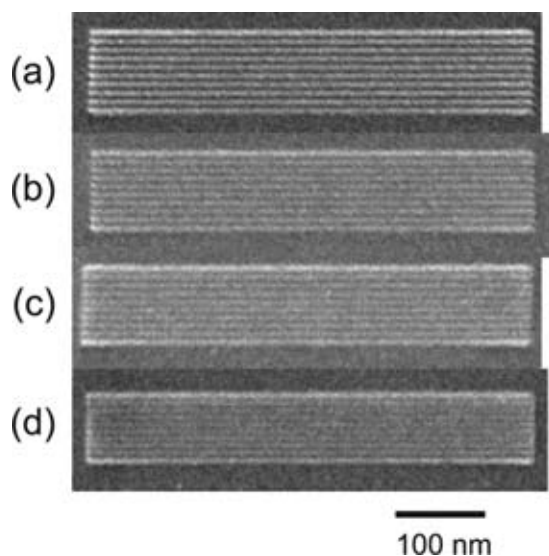


FIG. 45. HIM images of sets of ten parallel lines (with a dose of  $6 \times 10^{10}$  ions  $\text{cm}^{-1}$  for each line) of 500 nm long with half pitch of (a) 5 nm, (b) 4 nm, (c) 3.5 nm, and (d) 3 nm, all patterned with a HIM using swelling for pattern definition, Fig. 1 in Ref. 294. Reproduced with permission Zhang *et al.*, *Nanotechnology* 26, 1 (2015). Copyright IOP Publishing. All rights reserved.

## 5. Magnetism II

Alternatively, to the above described application example, employing ion matter interaction regime of atom intermixing and magnetic smoothing (described in Section VC2), another ion matter interaction regime—milling—has been successfully used to create small single magnetic domain areas (6 nm deep into a 20 nm thin film of  $\text{Co}_{70}\text{Cr}_{18}\text{Pt}_{12}$ ) using a Ga LMIS FIB (type 6 in Section VC1);<sup>283</sup> the exemplary results are displayed in Fig. 42.

## 6. FIB removal of larger amounts of material

If larger volumes than  $\mu\text{m}^3$  shall be milled away, Xe ions—from plasma sources—(type 4 in Section VC1) are a better choice than Ga LMIS. These Xe ions can mill up to 50 times faster, because of the significantly larger accessible beam currents (for example, 1  $\mu\text{A}$  for Xe compared to about 20 nA for Ga LMIS, comp. Section VC1) and the higher mass of Xe about 131 u compared to Ga with about 70 u. Exemplary milling results of different size apertures in an aperture stripe (molybdenum) are

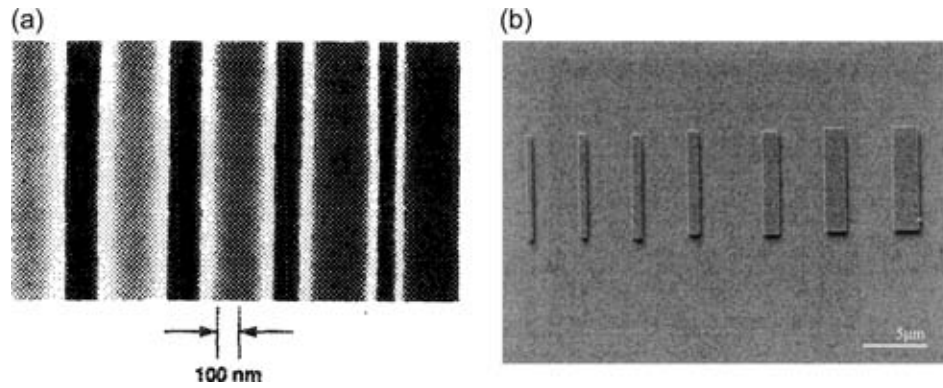


FIG. 46. SEM micrographs of lines where in both LMIS technology has been employed to (a) implant Be, Si, Ga, and Au ions, “Lines ranging in width from 120 to 80 nm patterned with 30-keV  $\text{Ga}^+$  at a dose of  $9 \times 10^{22}$  ions/cm $^2$ ” in SAL 601 resist, Fig. 2 in Ref. 296. Reproduced with permission from Hartney *et al.*, *J. Vac. Sci. Technol. B* 9, 3432 (1991). Copyright 1991 American Vacuum Society. (b) Top-down FIB image of NERIME processed patterns of (right to left) 2, 1.5, 1, 0.75, 0.5, 0.25, and 0.1  $\mu\text{m}$  in a SPR505A resist with thickness of 1.5  $\mu\text{m}$ ; ( $\text{Ga}^+$  beam dose 4700  $\mu\text{C}/\text{cm}^2$ , 1100 s RIE at 16 mTorr, Fig. 7 in Ref. 295. Reproduced with permission from Arshak *et al.*, *J. Vac. Sci. Technol. B* 22, 189 (2004). Copyright 2004 American Vacuum Society.

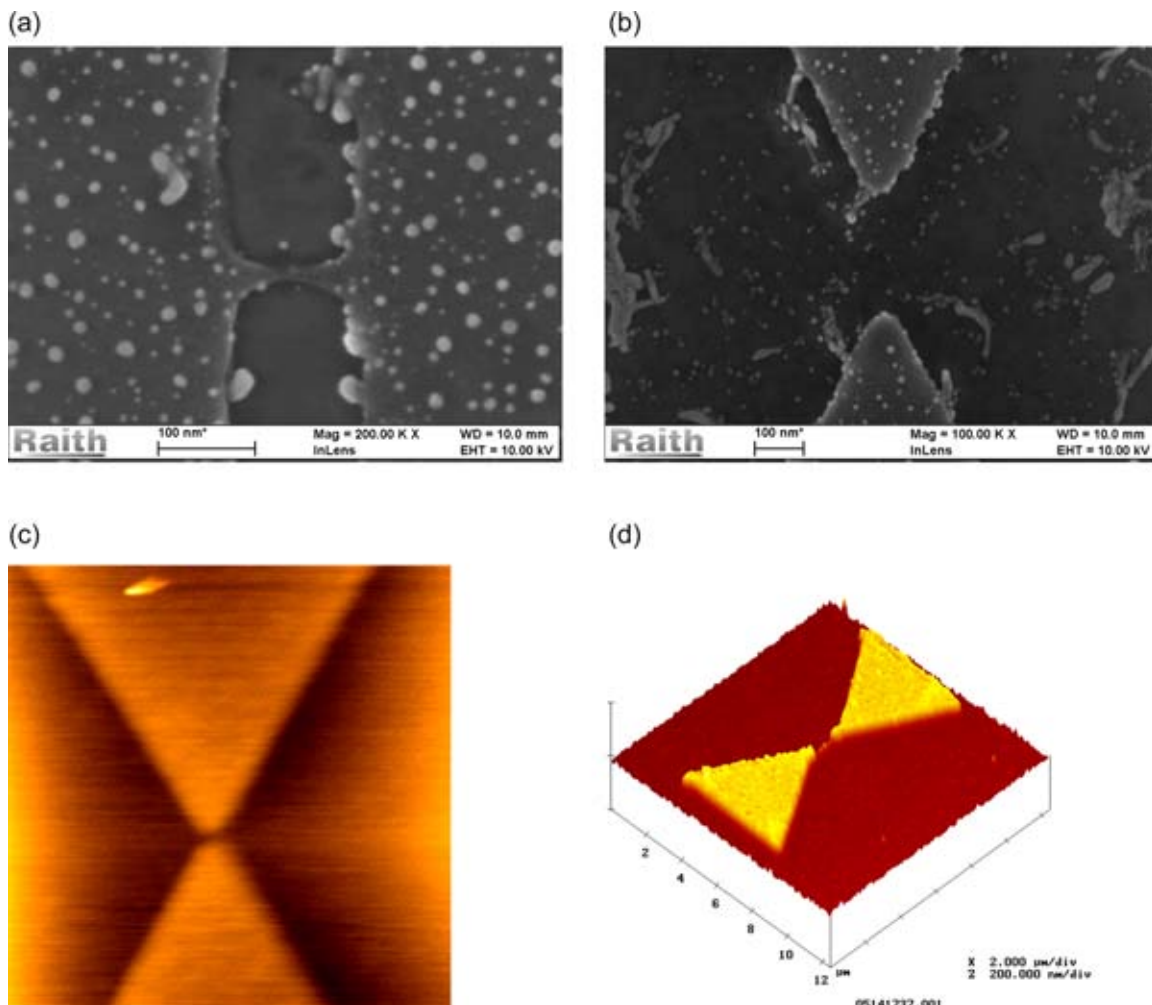


FIG. 47. Nonconventional resist (50 nm  $\text{Au}_{55}(\text{PPh}_3)_{12}\text{Cl}_6$  film) patterned by Ga LMIS, on  $\text{SiO}_2/\text{Si}$  samples (240 nm oxide thickness), SEM micrographs of high resolution results after development (a) thin interconnection ( $<20$  nm) with 100 nm contact pad distance  $<6$  pAs/cm Figure 52(d) in Ref. 41. (b) The inner part of a device, Figure 54(a) in Ref. 41. AFM image (c) of a nanogap realized by FIB irradiation of a single solid  $\text{Au}_{55}(\text{PPh}_3)_{12}\text{Cl}_6$  resist layer (field of view  $3 \mu\text{m} \times 3 \mu\text{m}$ , gap about 35 nm, feature thickness about 1 nm) (d) of a butterfly structure of a single solid  $\text{Au}_{55}(\text{PPh}_3)_{12}\text{Cl}_6$  resist layer Fig. 6 in Ref. 297. Reproduced with permission from Gierak *et al.*, *J. Vac. Sci. Technol. B* 17, 3132 (1999). Copyright 1990 American Vacuum Society.

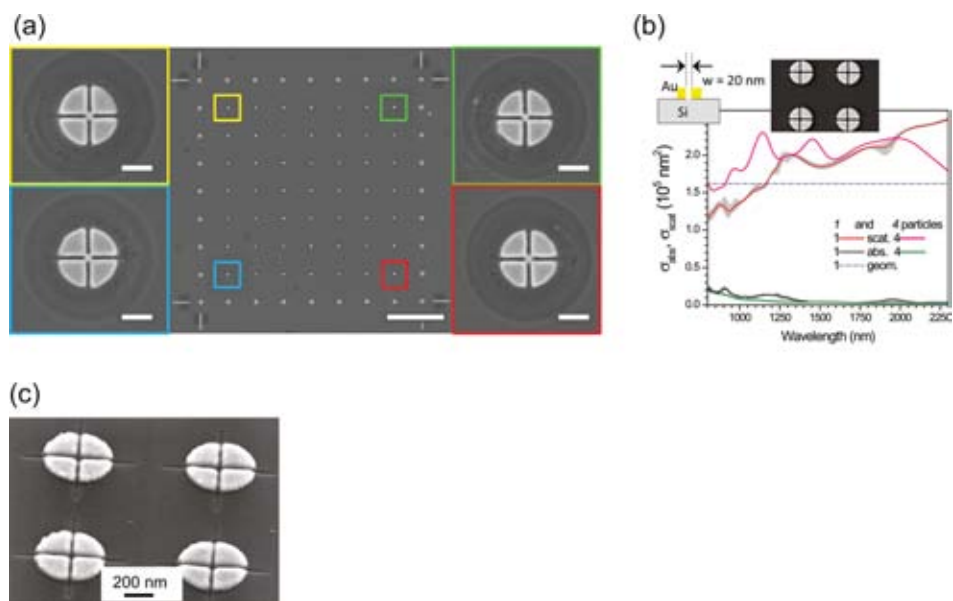


FIG. 48. (a) “SEM image of an array of gold nano-disks manufactured using EBL standard lift-off method and overlay of nanopatterns using our proposed method, colored insets show single nanoparticles in the corresponding corners of pattern. Scale bars are  $10 \mu\text{m}$  for main figure and  $250 \text{ nm}$  for insets,” Fig. 2 in Ref. 300. Gervinskias *et al.*, *Adv. Opt. Mater.* **1**, 456–459 (2013). Copyright 2013 Wiley-VCH Verlag GmbH & Co. KGaA. (b) “The absorption,  $\sigma_{\text{abs}}$ , and scattering,  $\sigma_{\text{cat}}$ , cross sections plotted as average of four single nanoparticles (Figure 2(b)) and the entire assemble of four particles. Calculations were carried out by importing SEM images and extruding them to a height of  $40 \text{ nm}$ . Gray regions depict error range. Numerical simulations of the ideal structures with cuts,” Fig. 3(a) in Ref. 299. Reproduced with permission from Rosa *et al.*, *J. Phys. Chem.* **115**, 5251 (2011). Copyright 2011 American Chemical Society. (c) “SEM images of the through-cuts of Au-nano-particles by lines about  $17 \text{ nm}$  wide with IBL: “a slanted view”  $17 \pm 3 \text{ nm}$  lines cut (about  $10 \text{ nm}$  deep) into Au cylinders” Fig. 2(a) in Ref. 299, Reproduced with permission from Rosa *et al.*, *J. Phys. Chem.* **115**, 5251 (2011). Copyright 2011 American Chemical Society.

displayed in Fig. 43 (aperture diameters of about  $10 \mu\text{m}$  and above).

### 7. Organic resist lithography (EBL resists)

A low-dose, thus high application resolution technique is organic resist exposure. Experiments have been carried out since the historical ion beam patterning start (see Section VB), together with the long tradition of electron beam lithography

employing the same resists (compare Section II) the process know-how is wide spread inside the nanotechnology community. Here, impressive example results are shown in Fig. 44., patterned by a He microscope (type 3 in Section VC 1, GFIS, scanning helium ion beam lithography, SHIBL)<sup>236,237</sup> and a Ga LMIS FIB<sup>207</sup> instrument (type 7 in Section VC 1), using the negative tone resist called hydrogen silsesquioxane (HSQ). The resist process details can be found in Ref. 78.

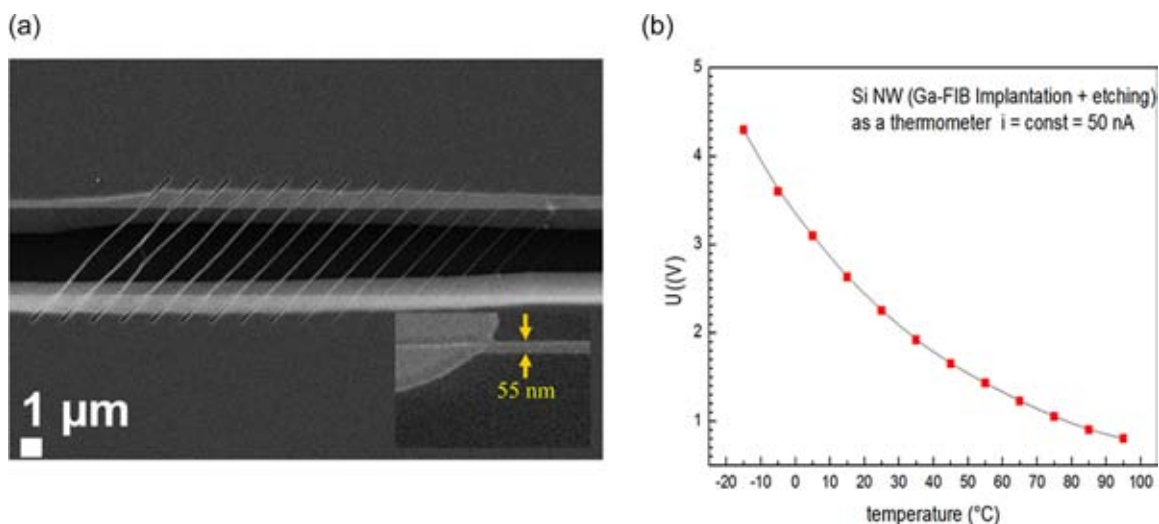


FIG. 49. (a) SEM micrograph of a set of nanowires (NWs) over a gap on top of a SOI wafer. The reduction of the line fluence from  $4 \times 10^{12}$  to  $10^{11} \text{ cm}^{-1}$  (from left to right) leads to a final wire width of  $20 \text{ nm}$ . The etching was performed in a  $30\% \text{ KOH}/\text{H}_2\text{O}$  solution at  $80^{\circ}\text{C}$  for  $3 \text{ min}$ . The inset shows the thickness of the NW corresponding to  $R_p + 3\Delta R_p$  for  $30 \text{ keV Ga}$  in  $\text{Si}$  (SRIM  $54 \text{ nm}$ , SEM  $55 \text{ nm}$ ), Fig. 1 in Ref. 302. Reproduced with permission from Böttger *et al.*, *J. Micromech. Microeng.* **21**, 095025 (2011). Copyright 2011 IOP Publishing. All rights reserved (b) plot of the temperature dependence versus the voltage through the NW ( $w = 90 \text{ nm}$ ) at a constant current of  $50 \text{ nA}$  which can be used for a local temperature control.

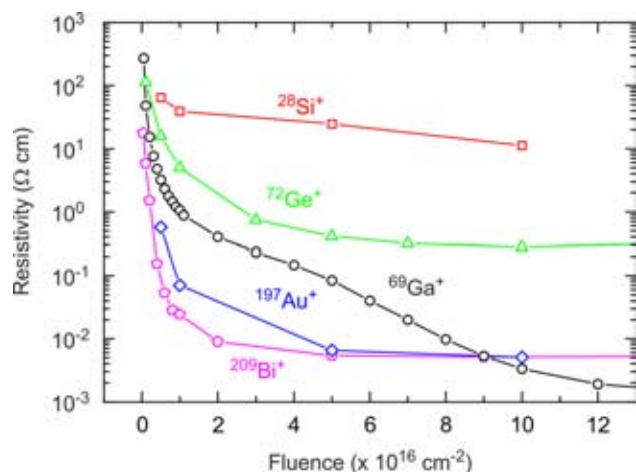


FIG. 50. Resistivity of DLC irradiated with different fluences and ion species (Ion energy = 30 keV; DLC layer thickness = 113 nm), Fig. 3 in Ref. 305. Reproduced with permission from Philipp *et al.*, Carbon **80**, 677 (2014). Copyright 2014 Elsevier.

## 8. Sample surface swelling

Fig. 45 shows even smaller features and periods (3.5 nm half pitch), which have been created by a He GFIS instrument (type 3 in Section VC1). A Si sample surface has been irradiated by the He ions, and then swelling—often unwanted—has been used for pattern definition.<sup>294</sup>

## 9. Alternatives organic resist exposure and development

As classical organic electron beam resist exposure revealed challenges employing ions (described in the history Section VB), alternative routes have been tried, altering locally the reactive ion etching resistance of the ion bombardment patterned organic resist areas, “surface imaged resist,”<sup>208,295</sup> example results are illustrated in Fig. 46. This is a kind of surface functionalization, a low to mid dose regime, thus a potential high application resolution ion matter interaction regime. In two examples, ion irradiation has been carried out on an

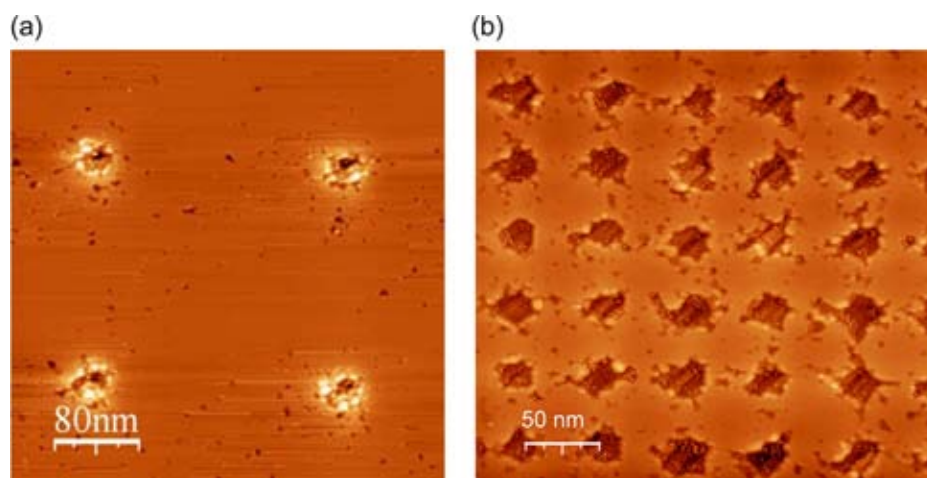


FIG. 51. Surface functionalization of HOPG by Ga LMIS FIB UHV STM micrographs of HOPG patterned by a Ga ion beam, after oxidation, resulting in (a) sub 30 nm resolution (ion dose 1870 ions/point) Figs. 5–34(c) in Ref. 307. (b) 50 nm period (ion dose 1963 ions/point), Figs. 5–32(d) in Ref. 307 and Fig. 4(d) in Ref. 306. Reproduced with permission from J. Appl. Phys. **101**, 044301 (2007). Copyright 2007 American Institute of Physics.

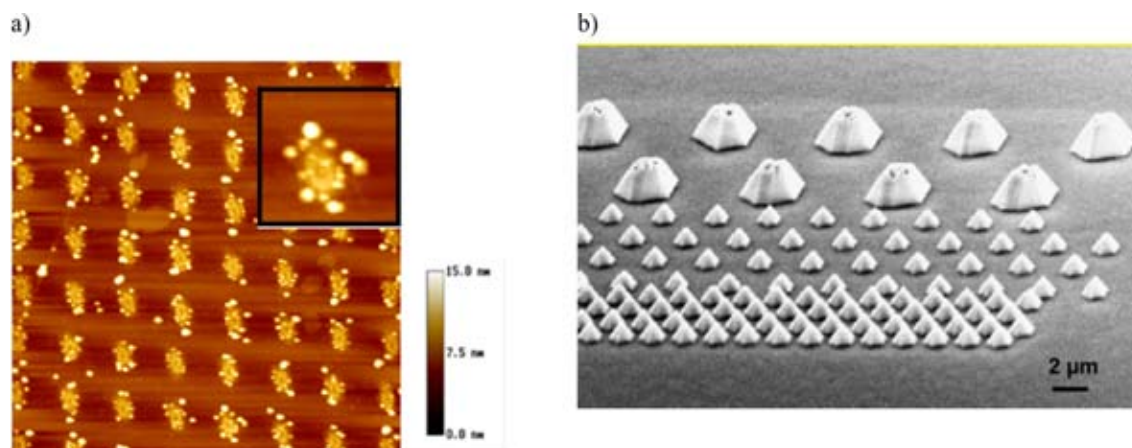


FIG. 52. a) AFM micrograph Surface functionalization of HOPG by Ga LMIS FIB patterned by a Ga ion beam “(2 μm × 2 μm)... of the morphologies of a 10<sup>-2</sup> ML gold film...” (deposited 2.8 nm gold clusters) on HOPG “surfaces patterned with a 30 keV Ga<sup>+</sup>, 8 nm (FWHM) probe size and different ion fluences I<sub>f</sub> and periodicities L<sub>def</sub>. Gold clusters aggregated around etched nano-craters L<sub>def</sub> = 300 nm, N = 37 500 ions/pt, inset (300 nm × 300 nm),” Figure 4(b) in Ref. 183. Reproduced with permission from Gierak *et al.*, Appl. Phys. A **80**, 187 (2005). Copyright 2005 Springer. (b) SEM micrograph “of selectively epitaxially grown GaN on AlN/6H-SiC on 1 and 2 μm openings made on SiN<sub>4</sub> by FIB with a dose of 2.7 × 10<sup>16</sup> ions/cm<sup>2</sup> (Ga<sup>+</sup> 30 keV). Note that for the largest opening, the selective epitaxy is not fully terminated,” Fig. 3 in Ref. 308. Reproduced with permission from Gierak *et al.*, Microelectron. Eng. **73–74**, 610 (2004). Copyright 2004 Elsevier.

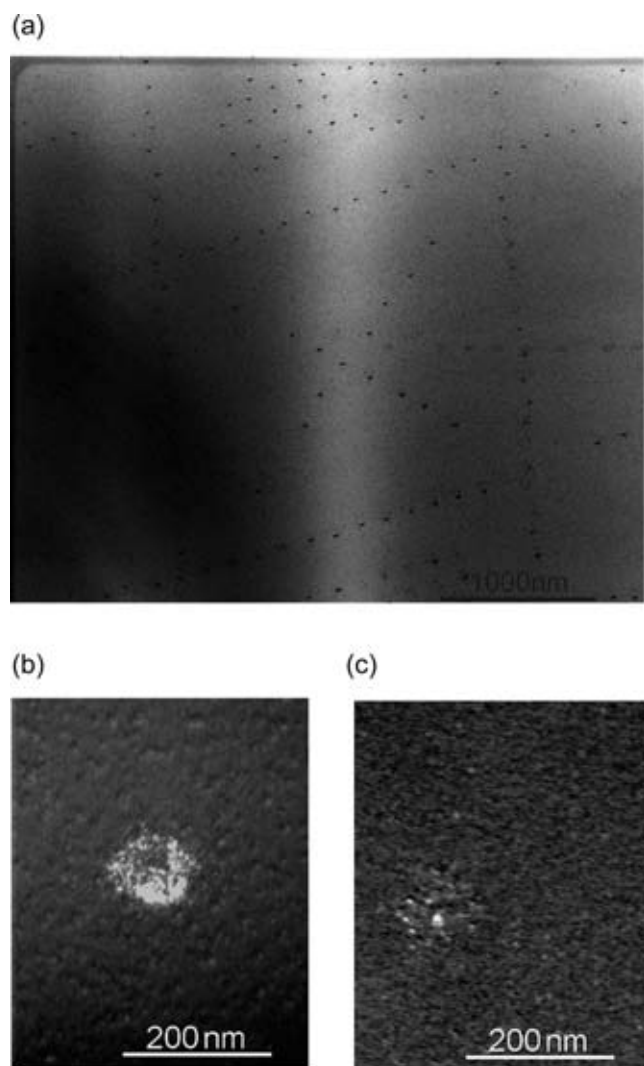


FIG. 53. TEM micrographs of features (a) after Ge cluster growth (precursor digermane, temperature of 650 °C and a digermane partial pressure of  $5 \times 10^{-8}$  Torr), Fig. 3 in Ref. 107. Reproduced with permission from Hull *et al.*, Mater. Sci. Eng. B **101**, 1 (2003). Copyright 2003 Elsevier. (b) A feature “as implanted” and (c) a feature after “annealing at 750 °C for 15 min” Fig. 2 in Ref. 107. Reproduced with permission from Hull *et al.*, Mater. Sci. Eng. B **101**, 1 (2003). Copyright 2003 Elsevier.

organic resist directly followed by a reactive ion etching (RIE) process. An example result from a process called “Silylation” (ions are implanted into SAL 601 resist, oxygen RIE)<sup>296</sup> is shown in Fig. 46(a) and another one called negative resist image by dry etching (NERIME) (SPR505A resist) in Fig. 46(b).<sup>295</sup> Both result in a higher reactive ion etch resistance to subsequent physical etching at the irradiated locations. The combination of silylation or NERIME and FIB lithography decouples the resist film thickness (exposure depth) from the ion penetration depth in the RIE etching process.<sup>182</sup> Experiments have been carried out using Ga LMIS FIB instruments type 6 in Section VC 1).

### 10. Ligand stabilized Au clusters as unconventional resist

In Fig. 47, non classical resist results are shown, containing a metal (50 nm  $\text{Au}_{55}(\text{PPh}_3)_{12}\text{Cl}_6$  film on  $\text{SiO}_2/\text{Si}$

samples).<sup>41,297,298</sup> The results have been patterned using a Ga LMIS nano patterning instrument (NanoFIB as well as the commercialized one, type 7 in Section VC 1). The exposure cuts the link between the metal and the ligand. The ligand gets dissolved during development (broken bonds). 3D capabilities can be tailored by the point ion dose and pixel to pixel spacing, allowing the metal clusters to reorganize on nucleation sites. The impressive 3D capabilities can be seen in Fig. 47(d), where the height of the gate has been purposely reduced. Details about the resist process can be found in Ref. 297. This is a relatively low-dose resist exposure process with potential high application resolution capabilities.

### 11. Nano scale modifications of existing features

A combined technology to create quickly small features is the FIB modification of existing (resist) objects on the sample surface. The initial nano pattern can be realized by any technique. The examples shown in Fig. 48 show Au nano particles, which have been cut by a Ga ion beam final process step, so, for example, an optical prototype device can be quickly (slightly) modified to examine possible improvements of its collection efficiency. Experiments have been carried out employing a Ga LMIS FIB (type 7 in Section VC 1).

### 12. Implantation III

Focused ion beam instruments can also be used for implantation (described in the application examples in Sections VD 2 and VD 3). Implantation can range from low-dose (single ion implantation) to high doses ion matter interaction regimes, depending on the application. In addition, implantation gives the opportunity to introduce a well defined concentration of dopants for other nano-structure fabrication processes. Specifically, mass-separated FIB systems have the advantage of applying a broad spectrum of ion species<sup>301</sup> and being capable to do so at dedicated and intended locations on the sample surface and with almost arbitrary shapes. This potential is shown by the following examples.

Fig. 49 shows a set of nanowires (NWs) over a gap on top of a SOI wafer. The samples have been pre-patterned by optical lithography (contact pads ( $400 \times 400 \mu\text{m}^2$ ) aligned to the  $\langle 110 \rangle$ -orientation) and conventional implantation; then, the NWs have been defined by FIB irradiation ( $\text{Ga}^+$ ,  $E = 30 \text{ keV}$ , Dose =  $3 \times 10^{16} \text{ cm}^{-2}$ ).<sup>302</sup> Fig. 49(b) represents the temperature dependence of the voltage through the NW ( $w = 90 \text{ nm}$ ) at a constant current of 50 nA, which can be used for local temperature control.

Further examples of FIB implantation are the creation of local pn-junctions by Ga into n-Si resulting in low-capacitance point diodes<sup>303</sup> or—a higher dose example—of a well defined concentration of dopants by implanting Co ions into Si at elevated temperatures to form  $\text{CoSi}_2$  nano-structures, after a post-annealing process. They act as ohmic contacts or Schottky-junctions depending on the Si-doping.<sup>304</sup>

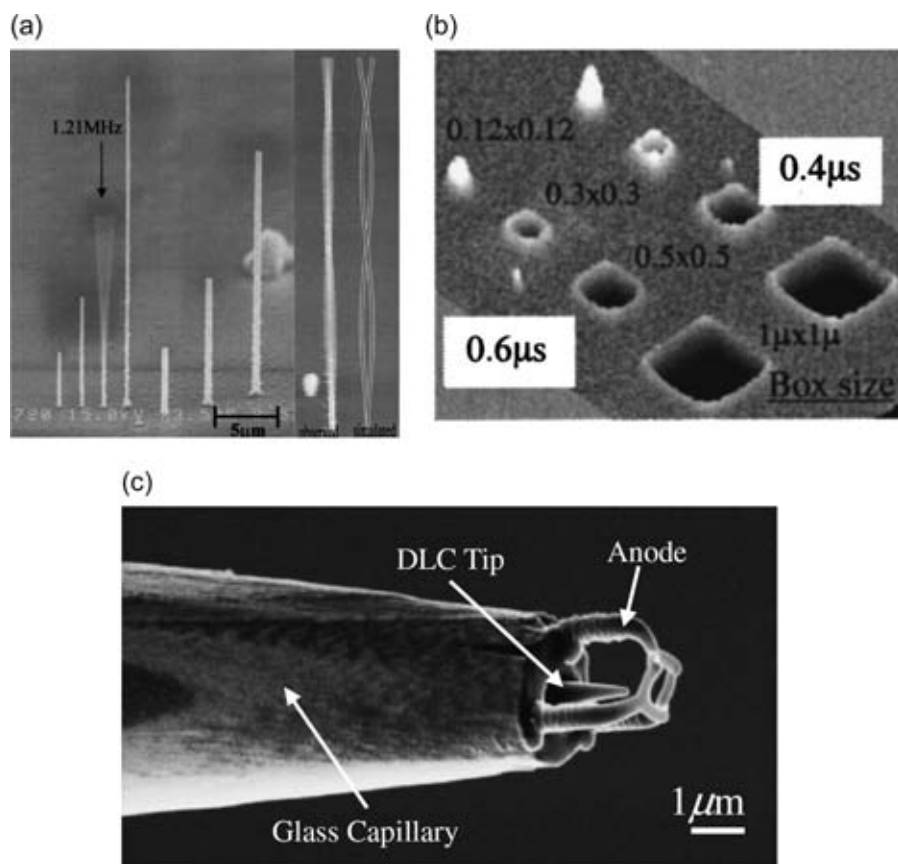


FIG. 54. SEM micrographs (a) “Tilt view of FIB deposited carbon pillars from phenanthrene precursor. Excitation of the fundamental resonance mode left and the second order resonance mode right from Figs. 2 and 5 (merged) in Ref. 310. Reproduced with permission from Fujita *et al.*, *J. Vac. Sci. Technol. B* **19**, 2834 (2001). Copyright 2001 American Vacuum Society. (b) High resolution FIB photomask repair. AFM image of gas assisted FIB etching. Boxes were etched into TiN using Br<sub>2</sub> gas and Ga<sup>+</sup> ions (20 keV, 22 pA), Fig. 3 right side in Ref. 311. Reproduced with permission from Liang *et al.*, *J. Vac. Sci. Technol. B* **18**, 3216 (2000). Copyright 2000 American Vacuum Society. (c) FIB deposited emitter-anode arrangement on glass fiber (“d” removed), Fig. 3 in Ref. 309, adapted from APEX/JJAP.

As<sup>++</sup> ions were implanted at an energy of 220 keV, 25 pA, defocused due to the low-dose of  $1.5 \times 10^{11} \text{ cm}^{-2}$  to increase the clocking frequency of long channel charged coupling devices (CCDs).<sup>296</sup> A 16-fold increase in the maximum clocking frequency of a 26- $\mu\text{m}$ -long-channel CCD has been demonstrated by the focused ion beam implantation of a lateral doping gradient.<sup>296</sup> Since the required doses in the gradient implant are low and high resolution is not needed, the focused-ion-beam implantation time is projected to be short, thus it possesses the potential to be used for volume production.<sup>296</sup> In addition, Fig. 50 shows resistivity changes due to surface functionalization of insulating diamond like carbon (DLC, ion irradiation-induced sp<sup>3</sup>-sp<sup>2</sup> rehybridization) have been observed by Philipp *et al.*<sup>305</sup>

Ion implantation or local amorphization for surface functionalization is also a low-dose ion matter interaction regime with the potential for a high application resolution. This technique allows, in a second process step, such as, etching (oxidation) or epitaxy, the creation of vacancies which can serve as nucleation sites for material growth. In addition, otherwise unreachable dose profiles can be created.

### 13. Surface functionalization

The first example, shown in Fig. 51, is a dot surface functionalization of HOPG (highly oriented pyrolytic graphite) by Ga ions from a Ga LMIS FIB (type 7 in Section VC1), followed by an oxidation process.<sup>306,307</sup>

Two further Ga surface functionalization examples are shown in Fig. 52. The first is a cluster (Au cluster 2.8 nm

diameter) deposition one using a laser vaporization technique,<sup>183</sup> on artificial defects created by FIB employing a HOPG substrate Fig. 52(a). The second is a GaN epitaxy process, on AlN/6H-SiC (1 and 2  $\mu\text{m}$  openings made on SiN<sub>4</sub>) Fig. 52(b). Both FIB local surface functionalizations have been carried out employing a Ga LMIS FIB (NanoFIB, type 7 in Section VC1).

In the following example, nucleation of Ge clusters in regions where Ga has been implanted by focused-ion beam micropatterning is shown.<sup>107</sup> A clean Si (001) surface has been irradiated with a Ga<sup>+</sup> focused ion beam, using a beam energy of 25 keV and a beam current of 10 pA ( $6.2 \times 10^7$  ions/s). After irradiation, the Si (001) was annealed (600 to 750 °C) to recover its crystal orientation, followed by a Ge deposition process. An example is shown in Fig. 53(a). The impact of an annealing process after FIB irradiation can be seen in Figs. 53(b) and 53(c).<sup>107</sup> The Ga FIB has been type 6 in Section VC1.

### 14. Gas assisted growth

In this section, a selection of published gas assisted patterning results is shown, employing FIB instruments. Although not in all dimensions “nanotechnology” (definition in preface, Section I), however, giving access to the 3rd dimension, examples are shown in Figs. 54 and 55. Here, the applied dose and patterning parameters may vary depending on the employed gas, target height, and lateral dimensions of the features, which can influence the potential application resolution.

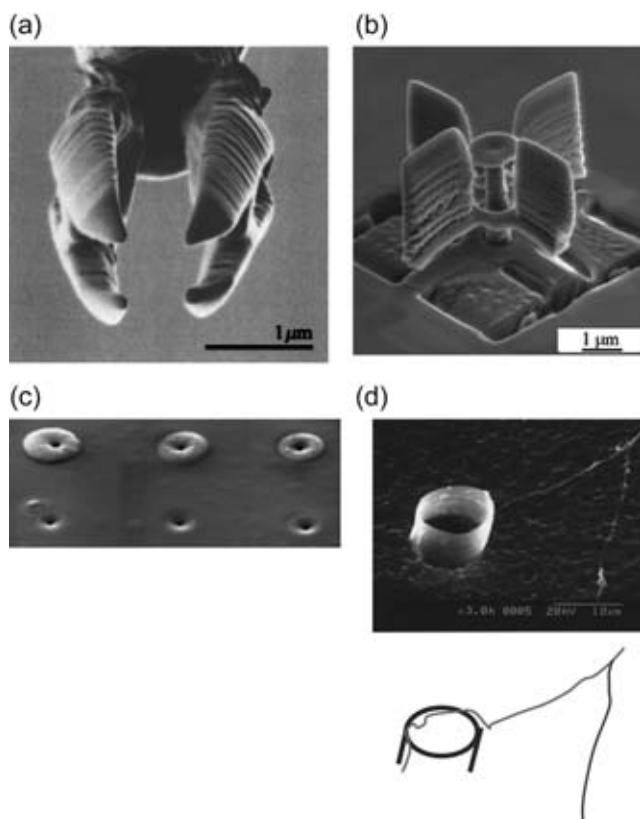


FIG. 55. SEM micrographs (a) FIB deposited electrostatically actuated gripper Fig. 6 in Ref. 312. Reproduced with permission from Kometani *et al.*, *J. Vac. Sci. Technol. B* **23**, 298 (2005). Copyright 2005 American Vacuum Society. (b) SEM micrograph of a FIB deposited four wing rotor (“The rotor diameter, wing-height, wing-width and axis length were  $6\mu\text{m}$ ,  $3\mu\text{m}$ ,  $500\text{nm}$ , and  $2.6\mu\text{m}$ , respectively.”), Fig. 7 in Ref. 313. Reproduced with permission from J. Igaki *et al.*, *Microelectron. Eng.* **83**, 1221 (2006). Copyright 2006 Elsevier. (c) “FIB fabricated biological structures. Nanopore diameter tuning with FIB deposition from tetraethoxysilane (TEOS). Nanopores were FIB milled into membrane,” Fig. 2(c) in Ref. 314. Reproduced with permission from Nilsson *et al.*, *Adv. Mater.* **18**, 427–431 (2006). Copyright 2006 Wiley-VCH Verlag GmbH & Co. KGaA. (d) “Biocompatible FIB deposited diamondlike carbon microtube with an in vitro grown nerve.” “Axon extension on a microtube attached to a polycarbonate membrane.” Top—“SEM image of the microtube and the axon... The axon grew from the upper right...” “... to the microtube, extended along the inner surface of the microtube, and then exited from it...” Process parameters for the DLC growth:  $30\text{keV Ga}^+$  ion beam employing a phenanthrene precursor ( $\text{C}_{14}\text{H}_{10}$ ). Bottom—Schematic for the device concept in the SEM image above (Rem: (a) and (b) removed from original), Fig. 8 in Ref. 315. Hoshino *et al.*, *J. Vac. Sci. Technol. B* **24**, 2538 (2006). Copyright 2006 American Vacuum Society.

First, Fig. 54(a) shows Ga LMIS deposited carbon pillars from a phenanthrene precursor; second, Fig. 54(b) shows etching into TiN using  $\text{Br}_2$  gas; and third Fig. 54(c) diamond like carbon (DLC) field emitters, which have been deposited on a glass fiber with a FIB-CVD instrument.<sup>309</sup> For all three, Ga LMIS FIB instruments (type 6 in Section VC1) have been employed.

Fourth, Fig. 55(a) displays an electrostatic gripper, which has been created with a FIB CVD instrument using a phenanthrene ( $\text{C}_{14}\text{H}_{10}$ ) precursor.<sup>312</sup>

Fifth, diamond like carbon (DLC) 3D rotors have been fabricated by nano-sheets, using a Ga LMIS FIB beam and a phenanthrene ( $\text{C}_{14}\text{H}_{10}$ ) precursor gas injection system (GIS) growth process. In addition, rotation of the rotor (shown in

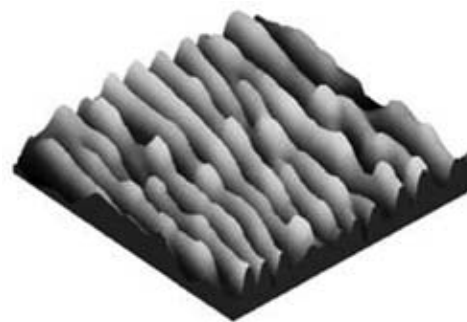


FIG. 56. “Three-dimensional view of the surface morphology resulting after 20 min  $\text{Ne}^+$  bombardment of  $\text{Ag}(110)$  at an ion dose rate of  $\Phi = 5\mu\text{A}/\text{cm}^2$ . Images are taken after grazing incidence milling  $\theta_i = 70^\circ$  at  $T = 180\text{K}$  (erosive regime),” Fig. 5(d) in Ref. 89. Reproduced with permission from Mater. Sci. Eng. C **23**, 201 (2003). Copyright 2003 Elsevier.

Fig. 55(b)) is possible by electrostatic forces or nitrogen gas flow (aerodynamic force).<sup>313</sup>

Sixth, Ga LMIS milling and a mixture of tetraethylorthosilicate (TEOS) gas and  $\text{H}_2\text{O}$  precursor have been used to locally deposit  $\text{SiO}_2$  and form nanopores of the desired size and biocompatible material composition, an example is displayed in Fig. 55(c).

Seventh, growth of diamond like carbon (DLC) has been carried out, to study the biocompatibility and connection possibilities of the human nervous system with external devices, to transfer information between them.<sup>315</sup> A prototype of an electrode’s segment as microtubes has been fabricated using FIB-CVD Fig. 55(d), employing a  $30\text{keV Ga}^+$  ion beam and a phenanthrene precursor ( $\text{C}_{14}\text{H}_{10}$ ).<sup>315</sup>

## 15. Self-organization under ion irradiation

So far, results from 4 kinds of ion source/instrument technologies (described in Section VC1) have been reported, operating in the linear cascade regime ( $5\text{--}50\text{kV}$ , explained in Section VC2):

- GFIS (low beam current, currently highest resolution, type 3 in Section VC1)
- Xe ICP (resolution optimized plasma ion sources, high probe currents, type 4 in Section VC1)
- versatile LMIS (type 6 in Section VC1)
- as well as nano patterning dedicated LM(A)IS instruments (mid beam current, high resolution, maturity, large selection of incident ions, type 7 in Section VC1).

Finally, fascinating self-organized regular structures like dots and ripples can evolve under ion irradiation, employing mainly “...collimated beams of low energy ions...”<sup>316</sup> Atoms are removed from the face of the sputter plate and some accumulate at the nearby target sample surface<sup>111,112</sup> or “...roughening induced by ion milling and smoothing due to surface diffusion...”<sup>124</sup> can be seen in Figs. 56–58.

Fig. 59 shows exemplary results employing a different instrument type: a focused ion beam (FIB, type 6 in Section VC1),<sup>318,319</sup> which allows these regular self-organizing patterns to be positioned at specific locations on the sample and the tailoring of the outer geometries of these regions.

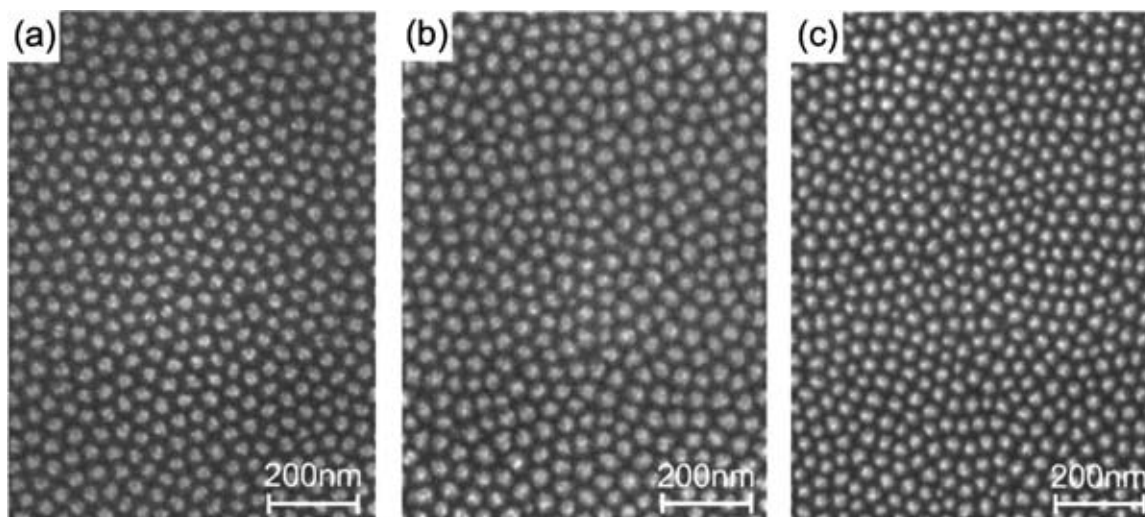


FIG. 57. “Scanning electron micrographs of dot patterns on GaSb films: (a) the initial layer is c-GaSb (100), (b) the initial layer is c-GaSb (111), and (c) the initial layer is amorphous GaSb deposited on Si(111). The patterns are created at an  $\text{Ar}^+$ -ion energy of 500 eV, an ion flux of  $1 \times 10^{16} \text{ cm}^{-2} \text{ s}^{-1}$ , and an erosion time of 200 s,” Fig. 1 in Ref. 259. Reproduced with permission from Facsko *et al.*, Appl. Phys. Lett. **80**, 130 (2002).

### F. Capabilities for nano device prototyping

The examples above prove that feature sizes below 5 nm and periodicities down to 7 nm are accessible for point ion source nano patterning. For some of the examples given for

ion matter interaction regimes used for nano patterning (milling and gas-assisted processing), the process know-how is wide spread; however, other examples given (surface functionalization, atom intermixing,...) are only used by a small number of researchers.

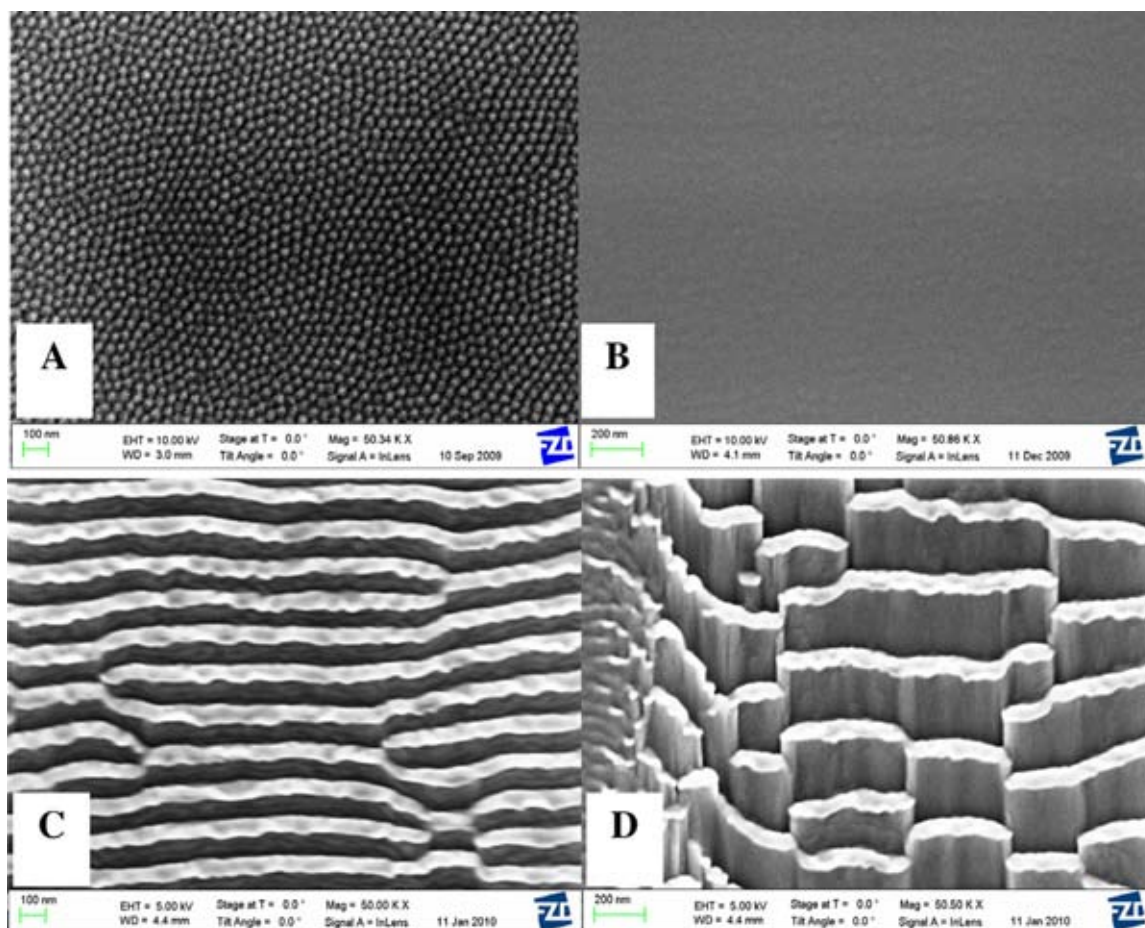


FIG. 58. SEM micrograph “Pattern evolution as a function of angle of incidence: dot pattern at normal incidence (a), smoothing at 45° (b), ripple structures at 75° (c), and shingles at 85° (d)” Fig. 3 in Ref. 317. Reproduced with permission from Bischoff *et al.*, Nucl. Instrum. Methods I. Phys. Res. B **272**, 198 (2012). Copyright 2012 Elsevier.

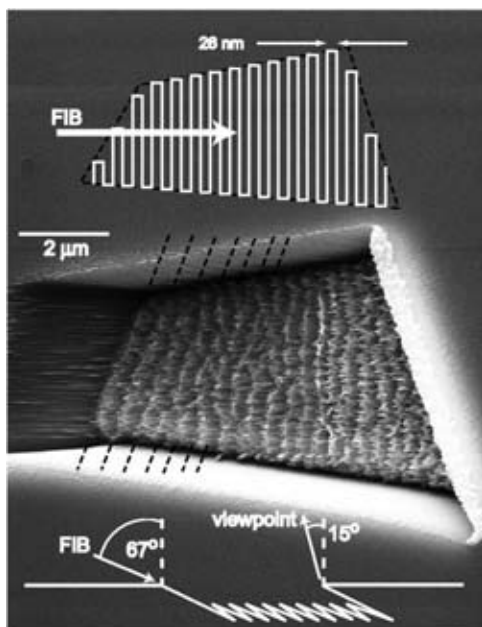


FIG. 59. SEM micrograph example of self-organized regular features with well-defined boundary shape at a dedicated sample location by an FIB instrument. “Ripple alignment with boundary of FIB-milled irregular quadrilateral. SEM image taken at  $15^\circ$  from normal. Ion irradiation  $67^\circ$  from normal, projected ion beam direction shown by arrow: ion dose of  $0.4 \times 10^{18}/\text{cm}^2$ . A schematic cross section is shown at the bottom. Schematic of raster pattern in plane view is shown at the top. Raster path is the white line: left boundary of the raster pattern is inclined by  $10^\circ$ . Note that the actual line pitch of the raster is much smaller than drawn,  $10 \text{ nm}/\cos(67^\circ)$ , or 26 nm. Ripple alignment with boundary near left edge decays over several periods until ripples align normal to the projected ion beam in the center of the milled region. Diagonal lines drawn along the ripples are guides to the eye.” Fig. 2 in Ref. 318. Reproduced with permission from S. Ichim and M. J. Aziz, *J. Vac. Sci. Technol. B* 23, 1068 (2005). Copyright 2005 American Vacuum Society.

Technology costs for FIB vary similarly to that for EBL. Depending on FIB equipment available and patterning requirements, the integrated patterning capabilities of the FIB instrument can be used, or upgraded at moderate cost by patterning attachments. However, for some applications, dedicated equipment might be necessary to facilitate the work, and these are similar in expense to an EBL writer.

Computer controlled FIB nano patterning is a similar serial fabrication process as electron beam lithography and therefore rather slow in volume production respects, compared to parallel techniques like optical projection lithography, nano imprint, or self-organized 3D epitaxy (compare Section III); however, for R&D type rapid nano device prototyping, the overall process time from an idea to an actual working device can be very short.

Some application examples show that a dedicated patterning instrument architecture—similar to dedicated EBL writers—can handle large samples and successfully pattern large areas. In addition, a high pattern placement accuracy and reproducibility can be achieved. Further, focused ion beam techniques give easy access to 3D patterning, especially as the application resolution can be tailored to sub 10 nm in the 3 dimensions. In addition, unique material properties can be locally created at almost arbitrary shapes, “... not obtainable by other techniques...”<sup>165</sup>

Point ion beam nano patterning is a top-down lithography technique employing SW designs, which can be easily and quickly modified. Device design, shape, and position fine tuning is easy and quick as in the SPM and EBL writer techniques.

As the ion beam is a charged beam, the charge has to be removed from the sample surface; thus, charge removal is necessary either by a sufficiently conducting sample/resist surface (adequate to the selected probe current) or by other means. Most applications and material systems can be addressed neglecting this, as many substrates are (semi) conducting and for high resolution small beam currents are required.

The large variety of accessible ions allows unique tailoring of many materials (systems) and interfacing to the surface (for details, see Section III C), where sometimes a subsequent annealing process step is necessary.

The technologies versatility is unique, due to the large variety of exploitable ion matter interaction regimes and incident ions. If the desired ion species is not (yet) available as a source, a thin layer material system might be composed to get the desired atoms into the surface layer by means of atom intermixing (the fundamentals have been described in Section VC 2 and an application example has been given in Section VD 4), where the layer below a thin active layer consists of the desired atoms.

Vector scan “Gaussian” beam nano patterning is well suited for R&D type rapid prototyping, especially with the potential beauty to create operating nano devices in a single process step.

The techniques’ capabilities for nano device prototyping will be summarized and compared with the others—covered in this article—in Table II.

## G. Conclusion

We have presented many successful nano device prototypes created by a variety of ion-matter interaction regimes. They include: intended surface modification, atom intermixing, refining classical milling, gas assisted, and combined processes with other technologies. They can create operating devices in many application fields, for example: microfluidics, photonics, small holes, local doping, or magnetics. This large variety of leading edge application results (examples have been illustrated in Sections VD and VE), representing only a fraction of all published and tested ones, shows that (almost) all challenges or drawbacks reported for ion beam nano patterning in the literature (listed at the end of Section VB) have been successfully resolved by recent process and technical developments.

Finally, the dedicated focused ion beam nanopatterning instrument (developed by us, type 7 in Section VC 1) has been realized on an EBL instrument architecture, thus with long term instrument stability, correction mechanisms and unattended batch process capabilities known from EBL writers. This refutes the previously reported statement: “But, and perhaps most telling, the available tooling for electron beam lithography is much more sophisticated, which is perhaps the single-most reason it is much more widely used.”<sup>82</sup> explained in Section VB.

In addition for some cases, alternative processes have been developed where the drawbacks have no relevance especially as some ion beam technologies possess the versatility to quickly select incident ions, clusters, charge states, acceleration voltage, and dose to easily match the application requirements.

As a result, point ion source vector beam nano patterning is well suited for R&D type rapid nano device prototyping and small scale production. This is because of its high resolution capabilities, software design based patterning and the availability of point ion beam technology in most R&D nanopatterning labs. Thus, they offer a uniquely fast (process time) device creation capability for many applications, some devices can even be created within a single process step or as an all-in-one instrument fabrication. In addition, unique patterning capabilities exist with regard to process simplicity, 3D patterning, and interface quality.

Depending on the instrumentation, the results can be seen immediately, either with an electron beam or the same ion beam employing a lower dose or a different ion species.

Finally, complementary capabilities for ion beam techniques are expected from improvements for the other ion source technologies described above, such as GFIS, ICP, or ECR plasma sources (type 3 and 4 in Section VC1). Additional progress can be expected from promising ion source concepts like: atomic-size metal ion sources,<sup>320</sup> a “super-tip” concept for LMIS,<sup>231</sup> liquid ionic sources,<sup>194,222,321</sup> heavily charged ions,<sup>322</sup> or cold solid state sources.<sup>323</sup>

## VI. SUMMARY AND OUTLOOK

As shown by this collection of nano device prototyped application results from different techniques, there exist many ways to create nano features. We have reviewed processes by four technology families suitable for nano device prototyping: (organic resist) electron beam lithography (EBL), self-organized 3D epitaxy,

atomic probe microscopy (STM/AFM) patterning derivatives and in particular, focused ion beam (FIB) technologies, especially those from liquid metal (alloy) ions sources (LM(A)IS).

On one hand, there exist matured and established technologies with the related process know-how for many applications. On the other hand, new challenges and requirements have evolved beyond well understood processing, and in these instances, clever ways have been found to meet these needs (exemplary application results have been given in Section VD and VE).

We took a look at these techniques with respect to the following criteria for nano device prototyping (NDP): application resolution; minimum periodicities; interfacing to the surface (in a manner realizable like in homoepitaxy, for details see Section III C); freedom for arbitrary geometry and shape; the ability to produce features at dedicated sample positions/locations, with a high accuracy; 3 dimensional objects; large area patterning exceeding a write-field (see Sections IIC1 and IIC2); time required to develop a new process; the process know-how accessibility to the community (“standardization”); process and instrumentation maturity; over all time and efforts necessary to create devices which can be tested and measured (“time to device”); time required for design changes; versatility of the technology for all kind of applications and material systems; costs from idea to device ready for testing, and finally the reproducibility for structuring more than a few devices up to the feasibility to run small scale production lines. Among these criteria, every technique possesses favorable ones. Some of them are uniquely favorable or advanced “★”, others very good “++”, good “+”, some are “variable” depending on the processes as well as the actual pattern definition effect, or their performance to fulfill this criterion is not so developed (yet) “–”, which are summarized in Table II. For details, compare the corresponding capabilities for nano device prototyping sections of each technology family above Sections IIE, III E, IVE, and VF.

TABLE II. R&D type nano device prototyping techniques, detailed definition criteria see text and the detailed explanations inside each technique’s “capabilities for nano device prototyping,” Sections IIE, III E, IVE, and VF.

Criteria	EBL	STM/AFM	Self-organized 3D epitaxy	FIB LM(A)IS
Resolution	++	★	++	++
Periodicity	++	★	++	++
Interfacing to surface	Variable	++	★	++
Free shapes	++	++	–	++
Placement accuracy	++	++	–	++
3D	Variable	Variable	+	++
Large area	++	–	★	+
Overall process complexity	++	++	variable	★
Process standardization	★	–	–	variable
Process and instrumentation maturity	★	Variable	variable	++
Duration (“time to device”)	variable	Variable	variable	★
Little modifications (“design changes/adjustments”)	++	Variable	variable	++
Versatility	++	++	+	★
Costs	variable	Variable	★	variable
Reproducibility suitable for small scale production	++	–	★	++

Electron beam lithography patterning of organic resist possesses more than 50 years of history;<sup>83</sup> thus, the process know-how and instrumentation are wide spread and have reached an incredible level of stability, maturity, precision, and automation. As a result, it is also well suited and regularly used for small scale production jobs.

Self-organized 3D epitaxy is well suited for the creation of regular 3D features with perfect interfaces to the substrate (as described in Section III C). It can be applied at extremely low costs, cover large areas, and possess simple single process step capabilities for nano devices creation, so small times to device are possible.

Atomic probe microscopy (APM) patterning has leading edge single atom placement capabilities, so gives access to very small scale device concepts down to the few atoms level and can give access to good interfaces to the substrate.

EBL, APM, and FIB based technologies all share the beauty of software designs (no need for expensive masks and their sometimes time consuming production period), allowing fast design modifications. In addition arbitrary shapes (limited only by the application resolution) at dedicated sample locations can be created.

Ion beam technologies, especially FIB, possess outstanding capabilities like: good interfacing to the surface (sometimes requiring a subsequent annealing process), 3D patterning, only one process step, thus (for some applications) the quickest time from idea to device and the largest versatility. The large variety of successful application results (Sections V D and V E summarized in Section V G) prove that solutions for almost all reported challenges (end of Section V B) have been found—especially the tooling one, because commercial solutions have become available.<sup>41,183,218,219</sup> In comparison to EBL, the instrument stability, control and feedback mechanisms, as well as dose control and patterning field calibration are available now on the level necessary for many applications, also in dedicated ion beam instruments. As a result, large area patterning (few hundreds of microns) of small features is possible with point ion beams (“FIB instruments”).

In addition, the promising new ion source technologies mentioned in Sections V C 1 and V G can bring additional unique capabilities for ion beam technologies.

A combination of the techniques discussed can provide further nano patterning process alternatives. For example, ions can locally functionalize sample surface areas (also possible by an electron beam<sup>108</sup>) and then another processes step like self-organized 3D epitaxy could follow. This can widen the application space and thus increase the number of successful results of nano device prototyping by more unique or different combinations of the criteria described in Table II above.

In addition, there exist further technologies, which can be combined for similar reasons: Block copolymers;<sup>324–327</sup> lithography and microcontact printing;<sup>12</sup> assisted assembly of nanoparticles using gold nanoparticles stabilized with ligands and self-assembled on irradiation with ultraviolet light;<sup>10</sup> “on wire lithography” a template-directed synthesis of nanowires;<sup>328</sup> electrochemical deposition and wet-

chemical etching; and pre patterning by holographic lithography followed by a MBE Ge deposition.<sup>14,116</sup>

In this article, we have reviewed many powerful nano device prototyping fabrication alternatives, a similar view on nanofabrication can be found in Ref. 329. If an application is limited by conventional processing technologies, exploring one of the described or other non-conventional alternatives with unique capabilities may be an option.

## ACKNOWLEDGMENTS

The authors thank especially: Bill R. Appleton (University of Florida, USA and Co-Editor of APR) for the invitation and advice; J. Fridmann (Raith America, Troy, NY, USA) for proof reading and together with S. Bauerdick (Raith GmbH, Dortmund, Germany) and A. Nadzeyka (Raith GmbH, Dortmund, Germany) for the tremendous application work; J. E. Sanabia (Raith America, Islandia, NY, USA) and R. Jede (Raith GmbH, Dortmund, Germany) for proof reading, discussions, scientific guidance and suggestions; K. E. Burcham, J. Fridmann and J. Klingfus (all Raith America, Islandia, NY, USA) for native speaker proof reading; H. Romijn and M. Butler (Raith BV, the Netherlands) for assisting the EBL history section; R. Schott (Ruhr-Universität Bochum, Germany), as well as M. Olmstead (University of Washington) for advice on the self-organized 3D epitaxy chapter; J. Orloff for assisting the CPO section, our application cooperation partners for providing ideas, samples, final testing of the devices and much more; the European Commission (EC, Contract No. G5RD-CT2000-0034) and BMWI (Contract No. (ZIM) KF2712302DF1) for funding the initial research project and the multispecies option, respectively; all colleagues at Raith for jointly realizing the instrument technology.

<sup>1</sup>See [http://www.nsf.gov/crssprgm/nano/reports/omb\\_nifty50.jsp](http://www.nsf.gov/crssprgm/nano/reports/omb_nifty50.jsp) for Nanotechnology definition, NSET, February 2000; accessed 10 July 2008.

<sup>2</sup>A. A. Tseng, A. Notargiacomo, and T. P. Chen, *J. Vac. Sci. Technol. B* **23**, 877 (2005).

<sup>3</sup>See <https://de.wikipedia.org/wiki/Giraffe> for the original photograph; accessed 28 October 2015.

<sup>4</sup>See <http://county.wsu.edu/king/gardening/mg/factsheets/Fact%20Sheets/Ants%20-%20Household.pdf> for the original photograph; accessed 28 October 2015.

<sup>5</sup>See <http://www.optics.rochester.edu/workgroups/cml/opt307/spr06/xue/project.htm> for “Asian” hair; accessed 28 October 2015.

<sup>6</sup>See <https://en.wikipedia.org/wiki/Lasius> for the original photograph; accessed 28 October 2015.

<sup>7</sup>See <http://science.energy.gov/bes/community-resources/scale-of-things-chart/> for the original photograph; accessed 18 May 2016.

<sup>8</sup>A. T. S. Wee, *Selected Topics in Nanoscience and Nanotechnology* (World Scientific Publishing Co. Pte. Ltd., Singapore, 2009).

<sup>9</sup>S. Srivastava and N. A. Kotov, *Soft Mater.* **5**, 1146 (2009).

<sup>10</sup>Z. Nie, A. Petukhova, and E. Kumacheva, *Nat. Nanotechnol.* **5**(1), 15 (2010).

<sup>11</sup>A. Böker, J. He, T. Emrick, and T. P. Russell, *Soft Mater.* **3**, 1231 (2007).

<sup>12</sup>S. Kinge, M. Credo-Calama, and D. N. Reinhoudt, *ChemPhysChem* **9**, 20 (2008).

<sup>13</sup>A. Singh and K. M. Ryan, *Part. Part. Syst. Charact.* **30**, 624 (2013).

<sup>14</sup>J. Stangl, V. Holý, and G. Bauer, *Rev. Mod. Phys.* **76**, 725 (2004).

<sup>15</sup>Y. Min, M. Akbulut, K. Kristiansen, Y. Golan, and J. Israelachvili, *Nat. Mater.* **7**, 527 (2008).

- <sup>16</sup>See <https://www.bmbf.de/de/die-organisation-des-hauses-192.html> for Abteilung 5 Schlüsseltechnologien; accessed 14 December 2015.
- <sup>17</sup>G. Shalev, S. W. Schmitt, H. Embrechts, G. Brönstrup, and S. Christiansen, *Sci. Rep.* **5**, 8570 (2015).
- <sup>18</sup>M. C. Demirel, M. Cetinkaya, A. Pena-Francesch, and H. Jung, "Recent advances in nanoscale bioinspired materials," *Macromol. Biosci.* **15**, 300 (2015).
- <sup>19</sup>R. Bappert, S. Benner, B. Häcker, U. Klein, and G. Zweckbronner, in *Biologie Technik Bionik: Zukunfts-Technik lernt von der Natur* (SiemensForum, Munich/Berlin, Germany, 1999), ISBN 3980493059.
- <sup>20</sup>J. E. Ayers, in *Heteroepitaxy of Semiconductors: Theory, Growth, and Characterization* (Taylor & Francis Group/CRC Press, Boca Raton, FL, USA, 2007), ISBN 0-8493-7195-3.
- <sup>21</sup>E. V. Shevchenko, D. V. Talapi, N. A. Kotov, S. O'Brien, and C. B. Murray, *Nature* **439**, 55 (2006).
- <sup>22</sup>*Nanolithography: A Borderland Between STM, EB, IB, and X-Ray Lithographies*, Nato ASI Series, Series E: Applied Science Vol 264, edited by M. Gentili and C. Giovannella (Kluwer Academic Publishers, Dordrecht, 1994), ISBN 0-7923-2794-2.
- <sup>23</sup>H. J. Levinson and W. H. Arnold, "Optical lithography," in *Handbook of Microlithography, Micromachining and Microfabrication Volume 1: Microlithography*, edited by P. Rai-Choudhury (SPIE Optical Engineering Press, Bellingham, Washington, USA, 1997), Chap. 1, p. 11, ISBN 978-0852969069.
- <sup>24</sup>C. Wagner and N. Harned, *Nature Photon.* **4**, 24 (2010) and further articles about optical lithography in the same issue.
- <sup>25</sup>S. Y. Chou, P. R. Kraus, and P. J. Renstrom, *Science* **272**, 85 (1996).
- <sup>26</sup>R. F. Pease and S. Y. Chou, *Proc. IEEE* **96**, 248 (2008).
- <sup>27</sup>M. A. McCord and M. J. Rooks, "Electron beam lithography," in *Handbook of Microlithography, Micromachining and Microfabrication Volume 1: Microlithography*, edited by P. Rai-Choudhury (SPIE Optical Engineering Press, Bellingham, Washington, USA, 1997), Chap. 2, pp. 139, ISBN 978-0852969069.
- <sup>28</sup>*Nanofabrication Fundamentals and Applications*, edited by A. A. Tseng (World Scientific Publishing, Singapore, 2008), pp. vii, ISBN 10-981-270-076-5.
- <sup>29</sup>K. Holmberg, in *Tribology of Mechanical Systems: A Guide to Present and Future Technologies*, edited by J. Vizintin, M. Kalin, K. Dohda, and S. Jahanmir (ASME Press, NY, USA, 2004), ISBN 0791802094.
- <sup>30</sup>R. Bennewitz and N. Strobach, *Phys. J.* **14**, 37 (2015).
- <sup>31</sup>K. Keskinbora, C. Grévent, M. Bechtel, M. Weigand, E. Goering, A. Nadzeyka, L. Peto, S. Rehbein, G. Schneider, R. Follath, J. Vila-Comamala, H. Yan, and G. Schütz, *Opt. Express* **21**, 11747 (2013).
- <sup>32</sup>F. K. Men, F. Liu, P. J. Wang, C. H. Chen, D. L. Cheng, J. L. Lin, and F. J. Himpfel, *Appl. Phys. Lett.* **88**, 096105 (2002).
- <sup>33</sup>R. P. Feynman, *Eng. Sci.* **23**, 22 (1960); See <http://calteches.library.caltech.edu/47/02/1960Bottom.pdf> for Caltech; accessed 29 December 1959 or See <http://www.zyvex.com/nanotech/feynman.html> for the text of his speech accessed 14 December 2015.
- <sup>34</sup>S. P. Newberry, in Proceedings of the Fourth SEBT, edited by R. A. Bakish (1962), Vol. 81.
- <sup>35</sup>See <http://www.semiconductor-technology.com/features/feature226/> for SC Technol, 2008; accessed 14 December 2015.
- <sup>36</sup>L. Veneklasen, "Electron beam lithography," in *Handbook of VLSI Microlithography, Principles, Technology and Applications*, edited by W. B. Glendinning and J. N. Helbert (Noyes Publications, Park Ridge New Jersey, USA, 1991), Chap. 5, p. 365, ISBN 0-8155-1281-3.
- <sup>37</sup>G. Owen and J. R. Sheats, in *Microlithography*, edited by J. R. Sheats and B. W. Smith (M. Dekker Inc., New York, USA, 1998), Chap. 6, pp. 367–402, ISBN 0-8247-9953-4.
- <sup>38</sup>R. K. Watts, in *VLSI Technology*, 2nd ed., edited by S. M. Sze (McGraw-Hill Book Company, Singapore, 1988), Chap. 4, p.141, ISBN 0-07-100347-9.
- <sup>39</sup>Raith GmbH, "Technical description pioneer two," Document No. 15-2-1463-1.0, 2015.
- <sup>40</sup>See <http://www.elionix.co.jp/english/products/ELS/ELSF125.html> for Ellionix, 2015; accessed 10 April 2015.
- <sup>41</sup>L. Bruchhaus, Ph.D. thesis, TU Dortmund, Dortmund, Germany (2012).
- <sup>42</sup>J. P. Beasley, *Int. Conf. Electron Ion Beam Sci. Technol.* **4**, 515 (1970).
- <sup>43</sup>See <http://www.computerhistory.org/semiconductor/timeline/1955-Photolithography.html> for further details about adapting photolithography to produce fine designs on silicon wafers; accessed 16 September 2008.
- <sup>44</sup>E. Ruska, *Rev. Mod. Phys.* **59**, 627 (1987).
- <sup>45</sup>L. de Broglie, Ph.D. thesis, Université de Paris, France (1924); *Ann. Phys. Paris* **10**(3), 22 (1925).
- <sup>46</sup>B. Lencová, in *Handbook of Charged Particle Optics*, 2nd ed., edited by J. Loroff (CRC Press, Boca Raton, USA, 2009), Chap. 5, pp. 161–208, ISBN 1-4200-4554-7.
- <sup>47</sup>E. Ruska, *Z. Phys.* **87**, 580 (1934).
- <sup>48</sup>W. Glaser, *Grundlagen der Elektronenoptik* (Springer Verlag, Wien, Austria, 1952), ISBN 978-3662236208.
- <sup>49</sup>P. W. Hawkes and E. Kasper, *Principles of Electron Optics: Volume 1* (Academic Press, London, GB, 1989), ISBN 0-12-333351-2.
- <sup>50</sup>P. Hawkes, *Ann. Fond. Louis Broglie* **29**, 837 (2004).
- <sup>51</sup>M. Knoll and E. Ruska, *Z. Phys.* **78**, 318 (1932).
- <sup>52</sup>M. Haider, S. Uhlemann, E. Schwan, H. Rose, B. Kabius, and K. Urban, *Nature* **392**, 768 (1998).
- <sup>53</sup>H. H. Rose, *Sci. Technol. Adv. Mater.* **9**, 014107 (2008).
- <sup>54</sup>See <http://www.jeol.co.jp/en/products/detail/JEM-1000.html> for Transmission electron microscope JEM-1000; accessed 14 December 2015.
- <sup>55</sup>See <https://www.fei.com/products/tem/titan/> for 300 kV TEM Titan FEI; accessed 29 April 2016.
- <sup>56</sup>M. Schmallenberg, [http://eipbn.org/wp-content/uploads/2015/01/EIPBN\\_history.pdf](http://eipbn.org/wp-content/uploads/2015/01/EIPBN_history.pdf) for a historical view on lateral nanopatterning, 2007, pp. 1–16; accessed 12 December 2015.
- <sup>57</sup>P. H. Carr, *Rev. Sci. Instrum.* **AIP, NY 1**, 711 (1930).
- <sup>58</sup>D. A. Buck and K. Shoulders, in *Proceedings Eastern Joint Computer Conference* (American Institute of Electrical Engineers (AIEE), New York, 1958), pp. 55–59.
- <sup>59</sup>R. F. M. Thornley and M. Hatzakis, in *Record of the IEEE 9th Annual Symposium on Electron, Ion and Laser Beam Technology* (1967), p. 64.
- <sup>60</sup>I. Haller, M. Hatzakis, and S. Srinivasan, *IBM J. Res. Dev.* **12**, 251 (1968).
- <sup>61</sup>A. N. Broers, W. W. Molzen, J. J. Cuomo, and N. D. Wittels, *Appl. Phys. Lett.* **29**, 596 (1976).
- <sup>62</sup>I. Utke, P. Hoffmann, and J. Melngailis, *J. Vac. Sci. Technol. B* **26**, 1197 (2008).
- <sup>63</sup>*Nanofabrication Using Focused Ion and Electron Beams*, edited by I. Utke, S. Moshkalev, and P. Russell (Oxford University Press Inc., New York, NY, USA, 2012), ISBN 9-780-19-973421-4.
- <sup>64</sup>R. M. F. Thornley, A. V. Brown, and A. J. Speth, *IEEE Trans. Electron. Compon. EC-13*, 36 (1964).
- <sup>65</sup>Technical description of Raith 150-TWO. V TD\_RAITH150TWO\_3.2, April 2010.
- <sup>66</sup>See <http://www.elionix.co.jp/english/products/ELS/ELSF125.html> for Ellionix ELS-F125; accessed 5 October 2015.
- <sup>67</sup>See <http://www.jeol.de/electronoptics-en/products/semiconductor-equipment/electron-beam-lithography-systems/jbx-9500fs.php> for Jeol JBX-9500FS; accessed 5 October 2015.
- <sup>68</sup>See <http://www.crestec8.co.jp/englishF/product/newfolder-1/> for Crestec CABL-9000C; accessed 5 October 2015.
- <sup>69</sup>See [http://www.nanobeam.co.uk/index.php?option=com\\_content&view=article&id=26&Itemid=48](http://www.nanobeam.co.uk/index.php?option=com_content&view=article&id=26&Itemid=48) for nanobeam nB4; accessed 5 October 2015.
- <sup>70</sup>L. Reimer, in *Scanning Electron Microscopy*, 2nd ed. (Springer Verlag, Berlin, Germany, 1998), ISBN 3-540-63976-4.
- <sup>71</sup>See <http://www.zeiss.de/c1256c1500431210/Contents-Frame/6531cac4d5c10402c1256df7003f3cbc> for EB Mask Repair 2010 - MeRiT HR 32 Zeiss SMT GmbH; accessed 25 June 2010.
- <sup>72</sup>A. Nadzeyka, L. Peto, S. Bauerdick, M. Mayer, K. Keskinbora, C. Grévent, M. Weigand b, M. Hirscher, and G. Schütz, *Microelectron. Eng.* **98**, 198 (2012).
- <sup>73</sup>W. S. Mackie, PhD thesis, University of Glasgow, Glasgow, Great Britain (1984), p. 7154.
- <sup>74</sup>L. Bruchhaus, Diplomarbeit, BGUH Wuppertal, Wuppertal, Germany (1997).
- <sup>75</sup>R. M. H. New, R. F. W. Pease, and R. L. White, *J. Vac. Sci. Technol. B* **12**, 3196 (1994).
- <sup>76</sup>D. R. S. Cumming, S. Thoms, S. P. Beaumont, and J. M. R. Weaver, *Appl. Phys. Lett.* **68**, 322 (1996).
- <sup>77</sup>J. K. W. Yang, B. Cord, H. Duan, K. K. Berggren, J. Klingfus, S.-W. Nam, K.-B. Kim, and M. J. Rooks, *J. Vac. Sci. Technol. B* **27**, 2622 (2009).
- <sup>78</sup>W. F. van Dorp, C. W. Hagen, P. A. Crozier, and P. Kruit, *Nanotechnology* **19**, 1 (2008).
- <sup>79</sup>Raith info No. 26, September 2005.
- <sup>80</sup>A. Fernández-Pacheco, L. Serrano-Ramón, J. M. Michalik, M. R. Ibarra, J. M. De Teresa, L. O'Brien, D. Petit, J. Lee, and R. P. Cowburn, *Sci. Rep.* **3**, 1492 (2013).

- <sup>81</sup>J. Kretz, private communication (1998).
- <sup>82</sup>C. R. K. Marrian and D. M. Tennant, *J. Vac. Sci. Technol. A* **21**, S207 (2003).
- <sup>83</sup>G. Moellenstedt and R. Speidel, *Phys. Bl.* **16**, 192 (1960).
- <sup>84</sup>See <http://www.amtc-dresden.com/content/index.php?xmlfile=overview.xml> for more details about a optical lithography mask fabrication process; 15 accessed 2015.
- <sup>85</sup>W. P. McCray, *Nat. Nanotechnol.* **2**, 259 (2007).
- <sup>86</sup>M. A. Herman, W. Richter, and H. Sitter, in *Epitaxy Physical Principles, and Technical Implementation*, Springer Series in Material Science (Springer Verlag, Berlin, 2004), ISBN 3-540-67821-2.
- <sup>87</sup>C. W. Pearce, "Epitaxy," in *VLSI Technology*, edited by S. M. Sze, 2nd ed. (Mc-Graw-Hill Book Company/Elsevier, Singapore, 1988), Chap. 2, p. 55, ISBN 0-07-100347-9.
- <sup>88</sup>D. Chrastina, S. Cecchi, J. P. Hague, J. Frigerio, A. Samarelli, L. Ferrellin, D. J. Paul, E. Müller, T. Etzelstorfer, J. Stangl, and G. Isella, *Thin Solid Films* **543**, 153 (2013).
- <sup>89</sup>U. Valbusa, C. Boragno, and F. Buatier de Mongeot, *Mater. Sci. Eng. C* **23**, 201 (2003).
- <sup>90</sup>D. Bimberg, M. Grundmann, N. N. Ledentsov, S. S. Ruvimov, P. Werner, U. Richter, J. Heydenreich, V. M. Ustinov, P. S. Kop'ev, and Zh. I. Alferov, *Thin Solid Films* **267**, 32 (1995).
- <sup>91</sup>D. Reuter, P. Kailuweit, A. D. Wieck, U. Zeitler, O. Wibelhoff, C. Meier, A. Lorke, and J. C. Maan, *Phys. Rev. Lett.* **94**, 26808 (2005).
- <sup>92</sup>M. L. Frankenheim, *Ann. Phys.* **113**, 516 (1836).
- <sup>93</sup>M. Ohring, "Thin-film evaporation processes," in *Materials Science of Thin Films: Deposition and Structure Account* (Academic Press, San Diego, CA, USA, 2002), Chap. 3, p. 95, ISBN 978-0125249751.
- <sup>94</sup>I. N. Stranski and L. Krastanow, *Monatshfte Chem. Verwandte Teile Anderer Wissenschaften* **71**, 351 (1937).
- <sup>95</sup>H. Welker, *Z. Naturforsch.* **7a**, 744 (1952).
- <sup>96</sup>K. Brunner, *Rep. Prog. Phys.* **65**, 27 (2001).
- <sup>97</sup>L. Esakit and R. Tsu, *IBM J. Res. Dev.* **14**, 61 (1970).
- <sup>98</sup>H. Kroemer, *Proc. IEEE* **51**, 1782 (1963).
- <sup>99</sup>Zh. I. Alferov, *ChemPhysChem* **2**, 500 (2001).
- <sup>100</sup>R. Dingle, H. L. Störmer, A. C. Gossard, and W. Wiegmann, *Appl. Phys. Lett.* **33**, 665 (1978).
- <sup>101</sup>A. D. Wieck and D. Reuter, *Compound Semicond.* **166**, 51 (2000).
- <sup>102</sup>K. v. Klitzing, G. Dorda, and M. Pepper, *Phys. Rev. Lett.* **45**, 494 (1980).
- <sup>103</sup>D. C. Tsui, H. L. Stormer, and A. C. Gossard, *Phys. Rev. Lett.* **48**, 1559 (1982).
- <sup>104</sup>R. B. Laughlin, *Phys. Rev. Lett.* **50**, 1395 (1983).
- <sup>105</sup>L. Goldstein, F. Glas, J. Y. Marzin, M. N. Charasse, and G. Le Roux, *Appl. Phys. Lett.* **47**, 1099 (1985).
- <sup>106</sup>V. A. Shchukin and D. Bimberg, *Rev. Mod. Phys.* **71**, 1125 (1999).
- <sup>107</sup>R. Hull, J. L. Gray, M. Kammler, T. Vandervelde, T. Kobayashi, P. Kumar, T. Pernell, J. C. Bean, J. A. Floro, and F. M. Ross, *Mater. Sci. Eng. B* **101**, 1 (2003).
- <sup>108</sup>G. B. Strinifellow, *Rep. Prog. Phys.* **45**, 469 (1982).
- <sup>109</sup>B. A. Grzybowski, C. E. Wilmer, J. Kim, K. P. Browne, and K. J. M. Bishop, "Self-assembly: from crystals to cells," *Soft Mater.* **5**, 1110 (2009).
- <sup>110</sup>R. Schott, private communication (2013).
- <sup>111</sup>*Handbook of Thin-Film Deposition Processes and Techniques Principles, Methods, Equipment and Applications*, 2nd ed., edited by K. Seshan (William Andrew Publishing, Norwich, USA, 2002), ISBN: 0-8155-1442-5.
- <sup>112</sup>D. Reuter, A. D. Wieck, and A. Fischer, *Rev. Sci. Instrum.* **71**, 1125 (1999).
- <sup>113</sup>U. Hillermann, in *Silizium Halbleitertechnologie* (Teubener, Wiesbaden, Germany, 2004), p. 131, ISBN 3-519-30149-0.
- <sup>114</sup>M. Mühlberger, C. Schelling, G. Springholz, and F. Schäffler, *Surf. Sci.* **532–535**, 721 (2003).
- <sup>115</sup>C. Schelling, M. Mühlberger, G. Springholz, and F. Schäffler, *Phys. Rev. B* **64**, 041301(R) (2001).
- <sup>116</sup>N. Hrauda, J. J. Zhang, H. Groiss, T. Etzelstorfer, V. Holý, G. Bauer, C. Deiter, O. H. Seeck, and J. Stangl, *Nanotechnology* **24**, 1 (2013).
- <sup>117</sup>T. O. Menteş, A. Locatelli, L. Aballe, M. A. Niño, and E. Bauer, *Ultramicroscopy* **130**, 82 (2013).
- <sup>118</sup>E. V. Shevchenko, D. V. Talapi, N. A. Kotov, S. O'Brien, and C. B. Murray, *Nature* **439**, 55 (2006).
- <sup>119</sup>P. Gambardella and K. Kern, *Surf. Sci. Lett.* **475**, L229 (2001).
- <sup>120</sup>S. Rohart, G. Baudot, V. Repain, Y. Girard, S. Rousset, H. Bulou, C. Goyhenex, and L. Proville, *Surf. Sci.* **559**, 47 (2004).
- <sup>121</sup>C. E. ViolBarbosa, J. Fujii, G. Panaccione, and G. Rossi, *New J. Phys.* **11**, 113046 (2009).
- <sup>122</sup>A. Greilich, D. R. Yakovlev, A. Shabaev, A. L. Efros, I. A. Yugova, R. Oulton, V. Stavarache, D. Reuter, A. Wieck, and M. Bayer, *Science* **313**, 341 (2006).
- <sup>123</sup>W. Cheng, M. J. Campolongo, J. J. Cha, S. J. Tan, C. C. Umbach, D. A. Muller, and D. Luo, *Nat. Mater.* **8**, 519 (2009).
- <sup>124</sup>S. Facsko, T. Dekorsy, C. Koerdt, C. Trappe, H. Kurz, A. Vogt, and H. L. Hartnagel, *Science* **285**, 1551 (1999).
- <sup>125</sup>J. Huang, F. Kim, A. R. Tao, S. Connor, and P. Yang, *Nat. Mater.* **4**, 896 (2005).
- <sup>126</sup>S. C. Glotzer and M. J. Solomon, *Nat. Mater.* **6**, 557 (2007).
- <sup>127</sup>W.-Q. Wu, B.-X. Lei, H.-S. Rao, Y.-F. Xu, Y.-F. Wang, C.-Y. Su, and D.-B. Kuang, *Sci. Rep.* **3**, 1 (2013).
- <sup>128</sup>J. Kretz, Ph.D. thesis, TU Dresden, Dresden, Germany (2001).
- <sup>129</sup>U. Staufer, "Surface modifications with a scanning proximity probe microscope," in *Scanning Tunneling Microscopy II*, 2nd ed., edited by R. Wiesendanger and H.-G. Güntherodt (Springer, Berlin, Germany, 1995), Chap. 8, p. 273, ISBN 978-3540585893.
- <sup>130</sup>X. N. Xie and H. J. Chung, "Scanning probe microscopy based nanoscale patterning and fabrication," in *Selected Topics in Nanoscience and Nanotechnology*, edited by A. T. S. Wee (World Scientific Publishing Co. Pte. Ltd., Singapore, 2009), Chap. 1, ISBN 978-981-283-955-8.
- <sup>131</sup>See <http://www.azom.com/article.aspx?ArticleID=3249> for the historical details of scanning tunneling and atomic force microscopes; accessed 15 December 2015.
- <sup>132</sup>R. Young, J. Ward, and F. Scire, *Rev. Sci. Instrum.* **43**, 999 (1972).
- <sup>133</sup>G. Binnig, H. Rohrer, C. Gerber, and E. Weibel, *Phys. Rev. Lett.* **49**, 57 (1982).
- <sup>134</sup>G. Binnig and C. F. Quate, *Phys. Rev. Lett.* **56**, 930 (1986).
- <sup>135</sup>K. Ivanova, Y. Sarov, T. Ivanov, A. Frank, J. Zöllner, C. Bitterlich, U. Wenzel, B. E. Volland, S. Klett, I. W. Rangelow, P. Zawierucha, M. Zielony, T. Gotszalk, D. Dontzov, W. Schott, N. Nikolov, M. Zier, B. Schmidt, W. Engl, T. Sulzbach, and I. Kostic, *J. Vac. Sci. Technol. B* **26**, 2367 (2008).
- <sup>136</sup>*Scanning Probe Microscopy Atomic Scale Engineering by Forces and Currents*, edited by A. Foster and W. Hofer (Springer New York, NY, USA, 2006), ISBN 0-387-40090-7.
- <sup>137</sup>F. J. Giessibl, *Science* **267**, 68 (1995).
- <sup>138</sup>N. W. Ashcroft and N. D. Mermin, "Cohesive energy," in *Solid State Physics* (Cengage Learning, Inc., New York, 1976), Chap. 20, p. 395, ISBN 0-03-083993-9.
- <sup>139</sup>A. A. Tseng, S. D. Sartale, M. F. Luo, and C. C. Kuo, in *Nanofabrication*, edited by A. A. Tseng (World Scientific Publishing Co. Pte. Ltd., Singapore, 2008), Chap. 1, pp. 1–32.
- <sup>140</sup>N. Kawasegi, D. W. Lee, N. Morita, and J. W. Park, in *Nanofabrication*, edited by A. A. Tseng (World Scientific Publishing Co. Pte. Ltd., Singapore, 2008), Chap. 2, pp.33–64, ISBN 981-270-076-5.
- <sup>141</sup>C. Santschi, J. Polesel-Maris, J. Brugger, and H. Heinzelmann, in *Nanofabrication*, edited by A. A. Tseng (World Scientific Publishing Co. Pte. Ltd., Singapore, 2008), Chap. 3, pp. 65–126, ISBN 981-270-076-5.
- <sup>142</sup>E. E. Moon and H. I. Smith, *J. Vac. Sci. Technol. B* **24**, 3083 (2006).
- <sup>143</sup>M. Kaestner and I. W. Rangelow, *J. Vac. Sci. Technol. B* **29**, 06FD02 (2011).
- <sup>144</sup>E. E. Moon, J. Kupec, M. K. Mondol, H. I. Smith, and K. K. Berggren, *J. Vac. Sci. Technol. B* **25**, 2284 (2007).
- <sup>145</sup>K. Wilder, C. F. Quate, B. Singh, and D. F. Kyser, *J. Vac. Sci. Technol. B* **16**, 3864 (1998).
- <sup>146</sup>M. Fuechsle, J. A. Miwa, S. Mahapatra, H. Ryu, S. Lee, O. Warschkow, L. C. L. Hollenberg, G. Klimeck, and M. Y. Simmons, *Nat. Nanotechnol.* **5**, 502 (2010).
- <sup>147</sup>J. W. Lyding, T. C. Shen, J. S. Hubacek, J. R. Tucker, and G. C. Abeln, *Appl. Phys. Lett.* **64**, 2010 (1994).
- <sup>148</sup>I.-W. Lyo and P. Avouris, *Science* **253**, 173 (1991).
- <sup>149</sup>S. R. Schofield, N. J. Curson, M. Y. Simmons, F. J. Rueß, T. Hallam, L. Oberbeck, and R. G. Clark, *Phys. Rev. Lett.* **91**, 136104 (2003).
- <sup>150</sup>M. Fuechsle, S. Mahapatra, F. A. Zwanenburg, M. Friesen, M. A. Eriksson, and M. Y. Simmons, *Nat. Nanotechnol.* **5**, 502 (2010).
- <sup>151</sup>D. M. Eigler and E. K. Schweizer, *Nature* **344**, 524 (1990).
- <sup>152</sup>S. W. Hla, K.-F. Braun, and K.-H. Rieder, *Phys. Rev. B* **67**, 201402(R) (2003).
- <sup>153</sup>L. Bartels, G. Meyer, and K.-H. Rieder, *Phys. Rev. Lett.* **79**, 697 (1997).
- <sup>154</sup>A. J. Heinrich, C. P. Lutz, J. A. Gupta, and D. M. Eigler, *Science* **298**, 1381 (2002).

- <sup>155</sup>Z. Durrani, M. Kaestner, M. Hofer, T. Ivanov, and I. Rangelow, "Scanning probe lithography for electronics at the 5 nm scale," *SPIE* (published online).
- <sup>156</sup>I.-W. Lyo and P. Avouris, *Science* **253**, 173 (1991).
- <sup>157</sup>T. A. Jung, R. R. Schlittler, J. K. Gimzewski, H. Tang, and C. Joachim, *Science* **271**, 181 (1996).
- <sup>158</sup>H. T. Soh, K. Wilder Guarini, and C. F. Quate, in *Scanning Probe Lithography* (Kluwer Academic Publishers, Norwell, MA, USA, 2001), ISBN 0-7923-7361-8.
- <sup>159</sup>S. Rusponi, G. Costantini, F. Buatier de Mongeot, C. Boragno, and U. Valbusa, *Appl. Phys. Lett.* **75**, 3318 (1999).
- <sup>160</sup>P. Vettiger, G. Cross, M. Despont, U. Drechsler, U. Dürig, B. Gotsmann, W. Häberle, M. A. Lantz, H. E. Rothuizen, R. Stutz, and G. K. Binnig, *IEEE Trans. Nanotechnol.* **1**, 39 (2002).
- <sup>161</sup>R. D. Piner, J. Zhu, F. Xu, S. Hong, and C. A. Mirkin, "Dip pen nanolithography," *Science* **283**, 661 (1999).
- <sup>162</sup>See <http://www.zyvexlabs.com/Products/STMLithoControlSystem.html> for an exemplary STM lithography system; accessed 30 November 2015.
- <sup>163</sup>See <https://swisslitho.com/nanofrazor-explore/> for an exemplary further lithography tool based on the atomic probe microscope technology; accessed 30 November 2015.
- <sup>164</sup>M. D. Giles, in *VLSI Technology*, edited by S. M. Sze, 2nd ed. (McGraw-Hill Book Company, Singapore, 1988), p. 327, ISBN 0-07-100347-9.
- <sup>165</sup>P. D. Townsend, J. C. Kelly, and N. E. W. Hartley, in *Ion Implantation, Sputtering and Their Applications* (Academic Press, London, GB, 1976), ISBN 0-12-696950-7.
- <sup>166</sup>F. A. Stevie, L. A. Giannuzzi, and B. I. Prentner, in *Introduction to Focused Ion Beams*, edited by L. A. Giannuzzi and F. A. Stevie (Springer, NY, USA, 2005), Chap. 1, pp. 1–12, ISBN 0-387-23116-1.
- <sup>167</sup>N. Yao, in *Introduction to Focused Ion Beams*, edited by L. A. Giannuzzi and F. A. Stevie (Springer, NY, USA, 2005), Chap. 1, pp. 1–30, ISBN 0-387-23116-1.
- <sup>168</sup>T. Fujii, T. Asahata, and T. Kaito, in *Introduction to Focused Ion Beams*, edited by L. A. Giannuzzi and F. A. Stevie (Springer, NY, USA, 2005), Chap. 14, pp. 355–390, ISBN 0-387-23116-1.
- <sup>169</sup>R. M. Langford, S. O'Reilly, and I. J. McEwen, Richard, *Application of a Focused Ion Beam System to Nanolithography* (Mater. Res Soc. Proc., 2002), Vol. 739, p. H7.2.
- <sup>170</sup>J. Mayer, L. A. Giannuzzi, T. Kamino, and J. Michael, "TEM sample preparation and fib-induced damage," *MRS Bull.* **32**, 400 (2007).
- <sup>171</sup>J. J. Van Es, J. Gierak, R. G. Forbes, V. G. Suvorov, T. Van den Berghe, Ph. Dubuisson, I. Monnet, and A. Septier, *Microelectron. Eng.* **73–74**, 132 (2004).
- <sup>172</sup>B. W. Ward, J. A. Notte, and N. P. Economou, *J. Vac. Sci. Technol. B* **24**, 2871 (2006).
- <sup>173</sup>N. S. Smith, D. E. Kinion, P. P. Tesch, and R. W. Boswell, *Microsc. Microanal.* **13**, 180 (2007).
- <sup>174</sup>P. Tesch, N. Smith, N. Martin, and N. Kinion, "Nanoscale to millimeter scale milling with a focused ion beam instrument," in EIPBN Conference Poster (2008).
- <sup>175</sup>T. Shinada, H. Koyama, C. Hinoshita, K. Imamura, and I. Ohdomari, *Jpn. J. Appl. Phys.* **41**(3A), L287 (2002).
- <sup>176</sup>T. Shinada, S. Okamoto, T. Kobayashi, and I. Ohdomari, *Nature* **437**, 1128 (2005).
- <sup>177</sup>S. Tongay, M. Lemaitre, J. Fridmann, A. F. Hebard, B. P. Gila, and B. R. Appleton, *Appl. Phys. Lett.* **100**, 73501 (2012).
- <sup>178</sup>M. G. Lemaitre, S. Tongay, X. Wang, D. K. Venkatachalam, J. Fridmann, B. P. Gila, A. F. Hebard, F. Ren, R. G. Elliman, and B. R. Appleton, *Appl. Phys. Lett.* **100**, 193105 (2012).
- <sup>179</sup>T. Hiramoto, K. Hirakawa, and T. Ikoma, *J. Vac. Sci. Technol. B* **6**, 1014 (1988).
- <sup>180</sup>B. Schmidt, L. Bischoff, and J. Teichert, *Sens. Actuators A* **61**, 369 (1997).
- <sup>181</sup>H. Loeschner, G. Stengl, R. Kaesmaier, and A. Wolter, *J. Vac. Sci. Technol. B* **19**, 2520 (2001).
- <sup>182</sup>M. A. Hartney, D. C. Shaver, M. I. Shepard, J. Melngailis, V. Medvedev, and W. P. Robinson, *J. Vac. Sci. B* **9**, 3432 (1991).
- <sup>183</sup>J. Gierak, D. Mailly, P. Hawkes, R. Jede, L. Bruchhaus, P. Mélinon, A. Perez, R. Hyndman, J.-P. Jamet, J. Ferre, A. Mougin, C. Chappert, V. Mathet, P. Warin, and J. Chapman, *Appl. Phys. A* **80**, 187 (2005).
- <sup>184</sup>E. W. Müller, *Adv. Electron. Phys.* **13**, 83 (1960).
- <sup>185</sup>I. W. Drummond and J. V. P. Long, *Nature* **215**, 950 (1967).
- <sup>186</sup>R. L. Seliger, R. L. Kubena, R. D. Olney, J. W. Ward, and V. Wang, *J. Vac. Sci. Technol.* **16**, 1610 (1979).
- <sup>187</sup>R. G. Wilson and G. R. Brewer, in *ION BEAMS With Applications to Ion Implantation* (Robert E. Krieger Publishing Company, Huntington, New York, USA, 1979), ISBN 0-88275-899-3.
- <sup>188</sup>R. L. Seliger, J. W. Ward, V. Wang, and R. L. Kubena, *Appl. Phys. Lett.* **34**, 310 (1978).
- <sup>189</sup>W. H. Escovitz, T. R. Fox, and R. Levi-Setti, *Proc. Nat. Acad. Sci.* **72**, 1826 (1975).
- <sup>190</sup>K. Kanaya, H. Kawakatsu, S. Matsui, H. Yomazaki, I. Okazaki, and K. Tanaka, in *Proceedings of the ELBS*, edited by A. B. El-Kareh (1965), p. 489.
- <sup>191</sup>M. Gabby, R. Goute, C. Guillard, and C. Monllor, *C. R. Acad. Sci.* **261**, 3325 (1965).
- <sup>192</sup>R. Forbes, "LMIS," in *Handbook of Charged Particle Optics*, edited by J. Orloff, 2nd ed. (CRC Press, Boca Raton, USA, 2009), Chap. 2, p. 29, ISBN 1-4200-4554-7.
- <sup>193</sup>P. D. Prewett and G. L. R. Mair, in *Focused Ion Beams from Liquid Metal Ion Sources*, No. 1 Electronic & Electrical Engineering Research Studies, Microengineering Series, edited by P. S. Walsh (Research Studies Press Ltd., Taunton, Somerset, GB, 1991), ISBN 978-0471930884.
- <sup>194</sup>L. Bischoff, P. Mazarov, L. Bruchhaus, and J. Gierak, *Appl. Phys. Rev.* **3**, 021101 (2016).
- <sup>195</sup>R. Clampitt and D. K. Jeffries, *Nucl. Instrum. Methods* **149**, 739 (1978).
- <sup>196</sup>J. Melngailis, *J. Vac. Sci. Technol. B* **5**, 469 (1987).
- <sup>197</sup>Y. Ochiai, Y. Kojima, and S. Matsui, *J. Vac. Sci. Technol. B* **6**, 1055 (1988).
- <sup>198</sup>R. L. Kubena and J. W. Ward, *Appl. Phys. Lett.* **51**, 1960 (1987).
- <sup>199</sup>P. H. LaMarche, R. Levi-Setti, and Y. L. Wang, *J. Vac. Sci. Technol. B* **1**, 1056 (1983).
- <sup>200</sup>L. Bischoff, B. Schmidt, H. Lange, and D. Donzev, *Nucl. Instrum. Methods B* **267**, 1372 (2009).
- <sup>201</sup>R. L. Seliger and W. P. Flemming, *J. Vac. Sci. Technol.* **10**, 1127 (1973).
- <sup>202</sup>R. L. Seliger and W. P. Fleming, *J. Appl. Phys.* **45**, 1416 (1974).
- <sup>203</sup>J. H. Orloff and L. W. Swanson, *J. Vac. Sci. Technol.* **12**, 1209 (1975).
- <sup>204</sup>R. L. Kubena, J. W. Ward, F. P. Stratton, R. J. Joyce, and G. M. Atkinson, *J. Vac. Sci. Technol. B* **9**, 3079 (1991).
- <sup>205</sup>H. Ryssel, K. Habberger, and H. Kranz, *J. Vac. Sci. Technol.* **19**, 1358 (1981).
- <sup>206</sup>S. Matsui, K. Mori, K. Saigo, T. Shiokawa, K. Toyoda, and S. Namba, *J. Vac. Sci. Technol. B* **4**, 845 (1986).
- <sup>207</sup>L. Bruchhaus, S. Bauerdick, L. Peto, U. Barth, A. Rudzinski, J. Musmann, J. Gierak, and H. Hövel, *Microelectron. Eng.* **97**, 48 (2012).
- <sup>208</sup>J. Melngailis, *Nucl. Instrum. Methods Phys. Res. B* **80/81**, 1271 (1993).
- <sup>209</sup>S. Rejntjens and R. Puers, *Micromech. Microeng.* **11**, 287 (2001).
- <sup>210</sup>C. Lehrer, L. Frey, S. Petersen, H. Ryssel, M. Schäfer, and T. Sulzbach, *J. Vac. Sci. Technol. B* **22**, 1402 (2004).
- <sup>211</sup>N. S. Smith, P. P. Tesch, N. P. Martin, and R. W. Boswell, *Microsc. Today* **17**, 18 (2009).
- <sup>212</sup>W. J. MoberlyChan, D. P. Adams, M. J. Aziz, G. Hobler, and T. Schenkel, *MRS Bull.* **32**, 424 (2007).
- <sup>213</sup>R. Forbes, "GFIS," in *Handbook of Charged Particle Optics*, edited by J. Orloff, 2nd ed. (CRC Press, Boca Raton, USA, 2009), Chap. 3, pp. 87–128, ISBN 1-4200-4554-7.
- <sup>214</sup>N. S. Smith, J. A. Notte, and A. V. Steele, *MRS Bull.* **39**, 329 (2014).
- <sup>215</sup>G. Hlawacek, V. Veligura, R. V. Gastel, and B. Poelsema, *J. Vac. Sci. Technol. B* **32**, 020801 (2014).
- <sup>216</sup>N. S. Smith, W. P. Skoczylas, S. M. Kellogg, D. E. Kinion, P. P. Tesch, O. Sutherland, A. Aanesland, and R. W. Boswell, *J. Vac. Sci. Technol. B* **24**, 2902 (2006).
- <sup>217</sup>N. S. Smith, P. P. Tesch, N. P. Martin, and R. W. Boswell, *Microsc. Today* **17**, 18 (2009).
- <sup>218</sup>J. Gierak, *Nanofabrication* **1**, 35 (2014).
- <sup>219</sup>A. Joshi-Imre and S. Bauerdick, *J. Nanotechnol.* **2014**, 170415 (2014).
- <sup>220</sup>Raith ionLiNE 2015 - <http://www.raith.de/products/ionline.html> (22.05.2015).
- <sup>221</sup><http://www.ruhr-uni-bochum.de/afp/downloads/ausstattung/ionen.pdf> (22.05.2015).
- <sup>222</sup>A. B. Tolstogousov, S. F. Belykh, V. S. Gurov, A. A. Lozovan, A. I. Taganov, O. M. N. D. Teodoro, A. A. Trubitsyn, and S. P. Chenakin, *Instrum. Exp. Tech.* **58**, 1 (2015).
- <sup>223</sup>B. Knuffman, A. V. Steele, J. Orloff, and J. J. McClelland, "Nanoscale focused ion beam from laser-cooled lithium atoms," *New J. Phys.* **13**, 103035 (2011).

- <sup>224</sup>A. Delobbe, O. Salord, and P. Sudraud, "The ECR-FIB," in The European Focused Ion Beam Users Group (EFUG) Annual Meeting (2011).
- <sup>225</sup>R. Kelley, K. Song, B. Van Leer, D. Wall, and L. Kwakman, *Microsc. Microanal.* **19**, 862 (2013).
- <sup>226</sup>M. Nastasi, J. W. Mayer, and J. K. Hirvonen, in *Ion-Solid Interactions: Fundamentals and Applications* (Cambridge University Press, GB, 1996), ISBN 0521 37376.
- <sup>227</sup>N. Imanishi, in *Focused Ion Beam Systems*, edited by N. Yao (Cambridge University Press, 2007), Chap. 2, p. 31, ISBN 978-0521-83199-4.
- <sup>228</sup>L. A. Giannuzzi, B. I. Prentner, and B. W. Kempshall, in *Introduction to Focused Ion Beams*, edited by L. A. Giannuzzi and F. A. Stevie (Springer, NY, USA, 2005), Chap. 2, p. 13, ISBN 0-387-23116-1.
- <sup>229</sup>S. Tan, R. Livengood, D. Shima, J. Notte, and S. McVey, *JVST B* **28**, C6F15 (2010).
- <sup>230</sup>S. Bauerdick, L. Bruchhaus, P. Mazarov, A. Nadzeyka, R. Jede, J. Fridmann, J. E. Sanabia, B. Gila, and B. R. Appleton, *J. Vac. Sci. Technol.* **31**, 06F404 (2013).
- <sup>231</sup>V. N. Tondare, *J. Vac. Sci. Technol. A* **23**, 1498 (2005).
- <sup>232</sup>A. V. Steele, B. Knuffmann, J. J. McClelland, and J. Orloff, *J. Vac. Sci. Technol. B* **28**, C6F1 (2010).
- <sup>233</sup>C. Perez-Martinez, S. Guilet, N. Gogneau, P. Jegou, J. Gierak, and P. Lozano, *J. Vac. Sci. Technol. B* **28**, L25 (2010).
- <sup>234</sup>C. Perez-Martinez, S. Guilet, J. Gierak, and P. Lozano, *Microelectron. Eng.* **88**, 2088 (2011).
- <sup>235</sup>S. Guilet, C. Perez-Martinez, P. Jegou, P. Lozano, and J. Gierak, *Microelectron. Eng.* **88**, 1968 (2011).
- <sup>236</sup>V. Sidorkin, E. Veldhoven, E. Drift, P. Alkemade, H. Salemkink, and D. Maas, *J. Vac. Sci. Technol. B* **27**, L18 (2009).
- <sup>237</sup>D. Winston, B. M. Cord, B. Ming, D. C. Bell, W. F. DiNatale, L. A. Stern, A. E. Vladar, M. T. Postek, M. K. Mondol, J. K. W. Yang, and K. K. Breggren, *J. Vac. Sci. Technol. B* **27**, 2702 (2009).
- <sup>238</sup>A. R. Hall, *Microsc. Today* **20**, 24 (2012).
- <sup>239</sup>See <https://www.zeiss.de/mikroskopie/produkte/multi-ionenstrahl/orion-nanofab-fuer-materialien.html> for details about usable ions in this instrument type; accessed 30 November 2015.
- <sup>240</sup>A. Delobbe, O. Salord, and P. Sudraud, "The ECR-FIB," in The European Focused Ion Beam Users Group (EFUG) Annual Meeting (2011).
- <sup>241</sup>P. Kruit and G. H. Jansen, in *Handbook of Charged Particle Optics*, edited by J. Orloff, 2nd ed. (CRC Press, Boca Raton, USA, 2009), Chap. 7, p. 341, ISBN 1-4200-4554-7.
- <sup>242</sup>G. L. R. Mair, D. C. Grindrod, M. S. Mousa, and R. V. Latham, *J. Physica D* **16**, L209 (1983).
- <sup>243</sup>J. Gierak, E. Bourhis, G. Faini, G. Patriarche, A. Madouri, R. Jede, L. Bruchhaus, S. Bauerdick, B. Schiedt, A. L. Biance, and L. Auvray, *Ultramicroscopy* **109**, 457 (2009).
- <sup>244</sup>R. Livengood, S. Tana, P. Hacka, M. Kanea, and Y. Greenzweig, *Microsc. Microanal.* **17**, 672 (2011).
- <sup>245</sup>"Focused ion beam technology and applications," *MRS Bull.* **39** (2014); see <https://www.cambridge.org/core/journals/mrs-bulletin/issue/6A8F0F6DD3958E6D8898EE9B539074CB>.
- <sup>246</sup>EC Growth Project Contract No. G5RD-CT2000-0034.
- <sup>247</sup>J. Gierak, A. Madouri, A. L. Biance, E. Bourhis, G. Patriarche, C. Ulysse, D. Lucot, X. Lafosse, L. Auvray, L. Bruchhaus, and R. Jede, *Microelectron. Eng.* **84**, 779 (2007).
- <sup>248</sup>B. R. Appleton, S. Tongay, M. Lemaitre, B. Gila, J. Fridmann, P. Mazarov, J. E. Sanabia, S. Bauerdick, L. Bruchhaus, R. Mimura, and R. Jede, *Nucl. Instrum. Methods B* **272**, 153 (2012).
- <sup>249</sup>A. A. Tseng, in *Focused Ion Beam Systems*, edited by N. Yao (Cambridge University Press, 2007), Chap. 7, p. 187, ISBN 978-0521-83199-4.
- <sup>250</sup>G. Hakvoort and C. M. Hol, *J. Therm. Anal.* **52**, 195 (1998).
- <sup>251</sup>J. C. Beckman, T. H. P. Chang, A. Wagner, and R. F. W. Pease, *J. Vac. Sci. Technol. B* **15**, 2332 (1997).
- <sup>252</sup>J. Orloff, J.-L. Li, and M. Sato, *J. Vac. Sci. Technol. B* **9**, 2609 (1991).
- <sup>253</sup>A. Benninghoven, R. D. Rüdenauer, and H. W. Werner, in *Secondary Ion Mass Spectroscopy* (John Wiley and Sons, New York, USA, 1987), ISBN 0-471-01056-1.
- <sup>254</sup>J. F. Ziegler, J. P. Biersack, and M. D. Ziegler, [www.LuLu.com](http://www.LuLu.com) for SRIM, 2008.
- <sup>255</sup>J. F. Ziegler, M. D. Ziegler, and J. P. Biersack, <http://www.srim.org.com> for SRIM 2008—SRIM software, the stopping and range of ions in matter, Chester, MD, USA.
- <sup>256</sup>F. Watt, A. A. Bettiol, J. A. van Kan, E. J. Teo, and M. B. Breese, *Int. J. Nanosci.* **4**, 269 (2005).
- <sup>257</sup>L. E. Ocola, C. Rue, and D. Maas, *MRS Bull.* **39**, 336 (2014).
- <sup>258</sup>O. Bobes, K. Zhang, and H. Hofsäss, *Phys. Rev. B* **86**, 235414 (2012).
- <sup>259</sup>S. Facsko, T. Bobek, H. Kurz, T. Dekorsy, S. Kyrsta, and R. Cremer, *Appl. Phys. Lett.* **80**, 130 (2002).
- <sup>260</sup>J. Orloff, M. Utlaut, and L. Swanson, in *High Resolution Focused Ion Beams* (Kluwer Academic Plenum Publishers, New York, USA, 2003), ISBN 0-306-47350-X.
- <sup>261</sup>M. Utlaut, in *Handbook of Charged Particle Optics*, edited by J. Orloff, 2nd ed. (CRC Press, Boca Raton, USA, 2009), Chap. 11, p. 523, ISBN 1-4200-4554-7.
- <sup>262</sup>B. Basnar, A. Lugstein, H. Wanzenboeck, H. Langfischer, E. Bertagnolli, and E. Gornik, *J. Vac. Sci. Technol. B* **21**, 927 (2003).
- <sup>263</sup>E. Abbe, "Beiträge zur theorie des mikroskops und der mikroskopischen wahrnehmung," *Arch. Mikrosk. Anat.* **9**, 456 (1873).
- <sup>264</sup>J. E. Barth and P. Kruit, *Optik* **101**, 101 (1996).
- <sup>265</sup>*Electron Optics: Part 1 Optics*, 2nd ed., edited by P. Grivet, P. W. Hawkes, and A. Septier (Pergamon Press, Oxford, GB, 1972).
- <sup>266</sup>P. W. Hawkes and E. Kasper, in *Principles of Electron Optics: Volume 2* (Academic Press, London, GB, 1989), ISBN 0-12-333352-0.
- <sup>267</sup>J. Großer, in *Einführung in die Teilchenoptik* (Teubener Studienbücher, B. G. Steubener, Stuttgart, Germany, 1983), ISBN 3-519-03050-0.
- <sup>268</sup>J. Orloff, private communication (23 March 2016).
- <sup>269</sup>J. Gierak, R. Jede, and P. Hawkes, *Nanofabrication Handbook*, edited by S. Cabrini and S. Kawata (CRC Press, 2012), pp. 41–84.
- <sup>270</sup>See <http://www.ilp.physik.uni-essen.de/wucher/movies/movies.html> for example molecular dynamics simulation results; accessed 15 December 2015.
- <sup>271</sup>F. G. Rudenauer and W. Steiger, *Microchem. Akta* **76**, 375 (1981).
- <sup>272</sup>Z. Malamud, Y. Greenzweig, and A. Raveh, *Microsc. Microanal.* **21**, 90 (2015).
- <sup>273</sup>T. Shinada, Y. Kumura, J. Okabe, T. Matsukawa, and I. Ohdomari, *J. Vac. Sci. Technol. B* **16**, 2489 (1998).
- <sup>274</sup>A.-L. Biance, J. Gierak, E. Bourhis, A. Madouri, X. Lafosse, G. Patriarche, G. Oukhaled, C. Ulysse, J.-C. Galas, Y. Chen, and L. Auvray, *Microelectron. Eng.* **83**, 1474 (2006).
- <sup>275</sup>B. Schiedt, L. Auvray, L. Bacri, G. Oukhaled, A. Madouri, E. Bourhis, G. Patriarche, J. Pelta, R. Jede, and J. Gierak, *Microelectron. Eng.* **87**, 1300 (2010).
- <sup>276</sup>G. Oukhaled, L. Bacri, E. Bourhis, B. Schiedt, A. Madouri, G. Patriarche, R. Jede, J. M. Betton, P. Guegan, L. Auvray, J. Pelta, and J. Gierak, *MRS Proc.* **1253** (2011).
- <sup>277</sup>A. N. Boers, A. C. F. Hoole, and J. M. Ryan, *Microelectron. Eng.* **32**, 131 (1996).
- <sup>278</sup>C. Dekker, *Nat. Nanotechnol.* **2**, 209 (2007).
- <sup>279</sup>J. Li, D. Stein, C. McMullan, D. Branton, M. Aziz, and J. A. Golovchenko, *Nature* **412**, 166 (2001).
- <sup>280</sup>T. Schenkel, V. Radmilovic, E. A. Stach, S.-J. Park, and A. Persaud, *J. Vac. Sci. Technol. B* **21**, 2720 (2003).
- <sup>281</sup>K. Healy, B. Schiedt, and A. P. Morrison, *Nanomedicine* **2**, 875 (2007).
- <sup>282</sup>J.-P. Adam, J.-P. Jamet, J. Ferré, A. Mougín, S. Rohart, R. Weil, E. Bourhis, and J. Gierak, *Nanotechnology* **21**, 1 (2010).
- <sup>283</sup>C. T. Rettner, M. E. Best, and B. D. Terris, *IEEE Trans. Magn.* **37**, 1649 (2001).
- <sup>284</sup>S. Y. Chou, M. S. Wei, P. R. Krauss, and P. B. Fischer, *J. App. Phys.* **76**, 6673 (1994).
- <sup>285</sup>S. Sun, C. B. Murray, D. Weller, L. Folks, and A. Moser, *Science* **287**, 1989 (2000).
- <sup>286</sup>R. Hyndman, A. Mougín, L. C. Sampaio, J. Ferre, J. P. Jamet, P. Meyer, V. Mathet, C. Chappert, D. Mailly, and J. Gierak, *J. Magnetism Magn. Mater.* **240**, 34 (2002).
- <sup>287</sup>W. Sparreboom, A. van den Ber, and J. C. T. Eijkel, *Nat. Nanotechnol.* **4**, 713 (2009).
- <sup>288</sup>L. E. Ocola and E. Palacios, *J. Vac. Sci. Technol. B* **31**, 06F401 (2013).
- <sup>289</sup>E. Palacios, L. E. Ocola, A. Joshi-Imre, S. Bauerdick, M. Berse, and L. Peto, *J. Vac. Sci. Technol. B* **28**, C6I1 (2010).
- <sup>290</sup>A. Siria, P. Poncharal, A.-L. Biance, R. Fulcrand, and X. Blasé, *Nature* **494**, 455 (2013).
- <sup>291</sup>L. Mo, L. Yang, A. Nadzeyka, S. Bauerdick, and S. He, *Opt. Express* **22**, 32233 (2014).
- <sup>292</sup>H. Kollmann, X. Piao, M. Esmann, S. F. Becker, D. Hou, C. Huynh, L.-O. Kautschor, G. Boušker, H. Vieker, A. Beyer, A. Göulzhäuser, N. Park, R. Vogelgesang, M. Silies, and C. Lienau, *Nano Lett.* **14**, 4778 (2014).

- <sup>293</sup>J. Lohau, A. Moser, C. T. Rettner, M. E. Best, and B. D. Terris, *Appl. Phys. Lett.* **78**, 990 (2001).
- <sup>294</sup>L. Zhang, N. F. Heinig, S. Bazargan, M. Abd-Ellah, N. Moghimi, and K. T. Leung, *Nanotechnology* **26**, 1 (2015).
- <sup>295</sup>K. Arshak, M. Mihov, S. Nakahara, A. Arshak, and D. McDonagh, *J. Vac. Sci. Technol. B* **22**, 189 (2004).
- <sup>296</sup>M. A. Hartney, D. C. Shaver, M. I. Shepard, J. Melngailis, V. Medvedev, and W. P. Robinson, *J. Vac. Sci. Technol. B* **9**, 3432 (1991).
- <sup>297</sup>J. Gierak, E. Cambril, M. Schneider, C. David, D. Maily, J. Flicstein, and G. Schmid, *J. Vac. Sci. Technol. B* **17**, 3132 (1999).
- <sup>298</sup>P. Hoffmann, G. BenAssayag, J. Gierak, J. Flicstein, M. Maar-Stumm, and H. van Bergh, *J. Appl. Phys.* **74**, 7588 (1993).
- <sup>299</sup>L. Rosa, K. Sun, V. Mizeikis, S. Bauerdick, L. Peto, and S. Juodkazis, *J. Phys. Chem.* **115**, 5251 (2011).
- <sup>300</sup>G. Gervinskas, G. Seniutinas, L. Rosa, and S. Juodkazis, *Adv. Opt. Mater.* **1**, 456 (2013).
- <sup>301</sup>L. Bischoff, *Nucl. Instrum. Methods Phys. Res. B* **266**, 1846 (2008).
- <sup>302</sup>R. Böttger, L. Bischoff, B. Schmidt, and M. Krause, "Characterization of Si nanowires fabricated by Ga<sup>+</sup> FIB implantation and subsequent selective wet etching," *J. Micromech. Microeng.* **21**, 095025 (2011).
- <sup>303</sup>L. Bischoff and B. Schmidt, *Solid State Electron.* **47**, 989 (2003).
- <sup>304</sup>Ch. Akhmalaliev, L. Bischoff, and B. Schmidt, *Mater. Sci. Eng. C* **26**, 818 (2006).
- <sup>305</sup>P. Philipp, L. Bischoff, U. Treske, B. Schmidt, J. Fiedler, R. Hübner, F. Klein, A. Koitzsch, and T. Mühl, "The origin of conductivity in ion-irradiated diamond-like carbon—Phase transformation and atomic ordering," *Carbon* **80**, 677 (2014).
- <sup>306</sup>F. Ghaleh, R. Köster, H. Hövel, L. Bruchhaus, S. Bauerdick, J. Thiel, and R. Jede, *J. Appl. Phys.* **101**, 044301 (2007).
- <sup>307</sup>F. Ghaleh, Ph.D. thesis, TU Dortmund (2008).
- <sup>308</sup>J. Gierak, E. Bourhis, R. Jede, L. Bruchhaus, B. Beaumont, and P. Gibart, *Microelectron. Eng.* **73–74**, 610 (2004).
- <sup>309</sup>R. Kometani, K. Kanada, Y. Haruyama, T. Kaito, and S. Matsui, *Jpn. J. Appl. Phys.* **45**, L711 (2006).
- <sup>310</sup>J. Fujita, M. Ishida, T. Sakamoto, Y. Ochiai, T. Kaito, and S. Matsui, *J. Vac. Sci. Technol. B* **19**, 2834 (2001).
- <sup>311</sup>T. Liang, A. Stivers, R. Livengood, P.-Y. Yan, G. Zhang, and F.-C. Lo, *J. Vac. Sci. Technol. B* **18**, 3216 (2000).
- <sup>312</sup>R. Kometani, T. Hoshino, K. Kondo, K. Kanda, Y. Haruyama, T. Kaito, J. Fujita, M. Ishida, Y. Ochiai, and S. Matsui, *J. Vac. Sci. Technol. B* **23**, 298 (2005).
- <sup>313</sup>J. Igaki, R. Kometani, K. Nakamatsu, K. Kanda, Y. Haruyama, Y. Ochiai, J. Fujita, T. Kaito, and S. Matsui, *Microelectron. Eng.* **83**, 1221 (2006).
- <sup>314</sup>J. Nilsson, J. R. I. Lee, T. V. Ratto, and S. E. Létant, *Adv. Mater.* **18**, 427 (2006).
- <sup>315</sup>T. Hoshino, A. Ozasa, R. Kometani, T. Suzuki, S. Matsui, and K. Mabuchi, *J. Vac. Sci. Technol. B* **24**, 2538 (2006).
- <sup>316</sup>W. L. Chan and E. Chason, *J. Appl. Phys.* **101**, 121301 (2007).
- <sup>317</sup>L. Bischoff, K.-H. Heinig, B. Schmidt, S. Facsko, and W. Pilz, *Nucl. Instrum. Methods I. Phys. Res. B* **272**, 198 (2012).
- <sup>318</sup>S. Ichim and M. J. Aziz, *J. Vac. Sci. Technol. B* **23**, 1068 (2005).
- <sup>319</sup>Q. Wei, X. Zhou, B. Joshi, Y. Chen, K.-D. Li, Qihuo Wei, K. Sun, and L. Wang, *Adv. Mater.* **21**, 2865 (2009).
- <sup>320</sup>S. T. Purcell, Y. T. Binh, and P. Thevenard, *Nanotechnology* **12**, 168 (2001).
- <sup>321</sup>C. Perez-Martinez, S. Guilet, N. Gogneau, P. Jegou, J. Gierak, and P. Lozano, *J. Vac. Sci. Technol. B* **28**, L25 (2010).
- <sup>322</sup>F. Ullmann, F. Großmann, V. P. Ovsyannikov, J. Gierak, and G. Zschornack, *Appl. Phys. Lett.* **90**, 083112 (2007).
- <sup>323</sup>B. Knuffman, A. V. Steele, and J. J. McClelland, *J. Appl. Phys.* **114**, 044303 (2013).
- <sup>324</sup>V. Z.-H. Chan, J. Hoffman, V. Y. Lee, H. Iatrou, A. Avgeropoulos, N. Hadjichristidis, R. D. Miller, and E. L. Thomas, *Science* **286**, 1716 (1999).
- <sup>325</sup>J. Y. Cheng, A. M. Mayes, and C. A. Ross, *Nat. Mater.* **3**, 823 (2004).
- <sup>326</sup>A. F. Hannon, K. W. Gotrik, C. A. Ross, and A. Alexander-Katz, *ACS Macro Lett.* **2**, 251 (2013).
- <sup>327</sup>R. A. Mickiewicz, J. K. W. Yang, A. F. Hannon, Y.-S. Jung, A. Alexander-Katz, K. K. Berggren, and C. A. Ross, *Macromolecules* **43**, 8290 (2010).
- <sup>328</sup>L. Qin, S. Park, L. Huang, and C. A. Mirkin, *Science* **309**, 113 (2005).
- <sup>329</sup>Z. Cui, in *Nanofabrication - Principles Capabilities and Limits* (Springer Science Business Media, LLC, New York, NY 10013, USA, 2008).